Research Grants 2018

APPLICANT	AFFILIATION	TITLE OF PROGRAMME	FUND	AMOUNT (£)
Billy ANDREWS	Strathclyde	The effect of sedimentary structures on fracture attributes within the UK Carboniferous Coal measures	Gloyne Outdoor	876
Anna BIDGOOD	Oxford	Oxford University Liverpool Land Expedition: the geological history of a subducted continent	Mike Coward	2000
Sarah BOULTON	Plymouth	The role of lithology on catchment average erosion rates in the Gediz Graben, Turkey	Elspeth Matthews	1000
Samuel BROOKE-BARNETT	Imperial	The effects of salt tectonics in the evolution of a fold and thrust belt	Mike Coward	840
Daniel COLLINS	Japan Society for the Promotion of Science	Holocene mangrove carbon sequestration in the Northern Mekong delta	Daniel Pidgeon	1000
Patrick DOWEY	Manchester	Trace element productivity and redox proxies in the Bowland-Hodder Shale, UK	Edmund Johnson Garwood	950
Finley GILCHRIST	Bristol	A petrological investigation into the evolution of the 1902 eruption of Santa Maria, Guatemala	Daniel Pidgeon	363
Catherine GODDARD	Oxford	What is the strength of the lower crust as determined by examining the roots of exhumed fault zones?	Mike Coward	1000
Joshua GRINHAM	St Andrews	Out-of-Phase Magnetic Susceptibility as a Tool in Mineral Exploration	Daniel Pidgeon	1050
Daniella GUY	Imperial	Utilising outcrop analogue data from the Ebro Basin, Spain for forward modelling in South Lokichar, Kenya	Elspeth Matthews	1165
Julie HARRALD	Open	Use of an unmanned aerial vehicle as a tool for mapping complex foreshore deposits	Annie Greenly	1323
Chris HOLDSWORTH	Glasgow	Ecotoxic metal distribution, mobility and flux in steel slag-derived alkaline leachate environments	William George Fearnsides	900
Joshua JONES	Plymouth	Investigating the spatial distributions and susceptibility of co-seismic landslide in a glacial environment, Langtang Valley, Nepal	Elspeth Matthews	1100
James Logan KING	Bristol	Brain Anatomy in Transitional Asian Sauropods and Ankylosaurs: Mapping Sensory Evolution and Perception in Non-Avian Dinosaurs	Daniel Pidgeon	2700
Brendan McCORMICK KILBRIDE	Cambridge	A geochemical survey of volcanic unrest at Rabaul caldera, Papua New Guinea	Elspeth Matthews	1276
Susannah MAIDMENT	NHM	Palaeobiology of north Africa's first stegosaur: implications for herbivorous dinosaur evolution and biogeography	Edmund Johnson Garwood	1980
Catherine MASCORD	Hull	Worms on film: How, where and when did metazoans begin bioturbating microbial substrates	Elspeth Matthews	997

Research Grants 2018

Zoe MILDON	Plymouth	Measuring Holocene throw of normal faults to improve models of Coulomb stress transfer in the central Italian Apennines for assessing seismic hazard	Jeremy Willson Charitable Trust & Mike Coward	1220
Hannah MOORE	Bristol	Investigating the triggers of the regular paroxysms observed at Volcan de Fuego, Guatemala	William George Fearnsides	363
Aodhan O'GOGAIN	Trinity College Dublin	Micro-computed tomography of tetrapods from the Langsettian (Pennsylvanian) Jarrow assemblage: implications for early tetrapod evolution and ecology	William George Fearnsides	400
David PEACOCK	University of Bergen	Detailed mapping of damage zones around intersecting faults on Gozo, Maltese Islands	Annie Greenly	900
Carla PONT	Imperial	Field constraints on lithological controls on landscape response times to active faulting in Calabria, Italy	Elspeth Matthews	1498
Pamela RATTIGAN	Glasgow	The stratigraphy and emplacement of lava-like ignimbrites on the southern flank of the Las Cañadas Caldera, Tenerife: implications for volcanological hazards in the Canary Islands	William George Fearnsides	1530
Tom RAVEN	Brighton	Evolution and palaeobiology of North American armoured dinosaurs	Daniel Pidgeon	1105
Michael STEVENTON	Imperial	Mass-transport complexes (MTCs) as seals: a case study from the Magnus Field, Northern North Sea	Daniel Pidgeon	1000
Mark STILLINGS	Strathclyde	What happens to groundwater chemistry during fault slip?	Daniel Pidgeon	1200
James WHEELEY	Birmingham	Deciphering the palaeoceanography and temperature structure of Iapetus using conodont oxygen isotopes: temporal variability across the Cambro-Ordovician boundary, Newfoundland, Canada	Joseph Burr Tyrrell	1990
Esty WILLCOX	Aberystwyth	Using high resolution thermal imaging and stereo-photography to quantify calving law controls	Robert Scott Memorial Fund	2000
Julia WOITISCHEK	Cambridge	Understanding the persistent outgassing of open vent volcanoes	Elspeth Matthews	2000
Ying ZHOU	UCL	Tracing silicate weathering during the early Tonian using Lithium isotopes	William George Fearnsides	1800

PROGRESS REPORT

"The effect of sedimentary structures on fracture attributes within the UK coal measures."

by Billy Andrews

Geological Society Research Grant of the value: £875.95

1. Scope and purpose

This project aims to quantify the impact of lithology and sedimentary heterogeneity on fracture attributes in the UK Carboniferous Coal Measures. Fracture networks often provide important subsurface pathways for fluid flow which is relevant to several sectors. In recent years there has been a resurgence of interest in the UK Carboniferous coal measures. For example, the BGS are championing a £9 million UK Geo-energy observatory for geothermal energy in flooded mine working below Glasgow. The field site is also a good field analogue for the Westphalian B and C fluvial-deltaic deposits of the Southern North Sea which host gas source rocks along with local siliciclastic reservoirs.

During the summer of 2017 a tangible link between sub-bed scale heterogeneities (e.g. mud draped ripples) and fracture attributes (e.g. termination, aperture and trace length) was identified, but not quantified. While links between fracture spacing and fault properties (Soden et al. 2013) and bed thickness (e.g. Wennburg et al. 2006) have been reported, to our knowledge the controls of specific sedimentary features on fracture attributes remains unclear. This work aims to investigate if there is a *statistically significant* correlation between any depositional properties and fracture attributes. Initially we wanted to investigate the strength of sedimentary interfaces using shear box experiments, however, permission to sample was not provided prior to undertaking the work. The ability to predict fracture propagation and connectivity based on sedimentary structures will improve predictions of fracture networks by using large-scale sedimentary information available during basin modelling.

2. Progress & initial results

Fieldwork in the summer of 2018 enabled the following data to be collected for both bed and sub-bed scales; 1) sedimentary logs; 2) mechanical stratigraphy; 3) fracture maps combined with topological sampling (following Sanderson and Nixon, 2015) and 4) common sedimentary features which impact fracture terminations. Based of field observations seven sedimentary facies were identified and used as a basis for bed-scale fracture observations. For observations on sub-bed scale heterogeneity, individual horizons were traced across the fracture map based on the cm-scale sedimentary logs. For both scales a strong correlation between grain size and mechanical strength, measured using an N-type Schmidt hammer (following the methodology of Morris et al., 2009), was observed. This section reports initial results and is separated into how lithology and sub-bed scale heterogeneity impact A) fractures and B) faults. These findings were presented as a poster at Young Researchers in Structural Geology and Tectonics Conference (YORSGET 2018) in July 2018.

A. The impact of lithology and sub-bed scale heterogeneity on fractures

At the bed scale all sedimentary facies, with the exception of coal, when observed in cliff section displayed low connectivity away from fault zones. Heterolithic facies, with a large degree of heterogeneity (e.g. ripple horizons or channel coals) tended to have an increased percentage of y-nodes, with fractures branching at strength interfaces. For all sedimentary facies fracture connectivity in map view was considerably greater than that in cliff section. These findings have important consequences for fluid flow suggesting bed-parallel flow, which in the case of the field site is horizontal, likely to be more important than flow across the sequence. While facies such as channelised sand-bodies have bed-bound fracture networks, heterolithic

facies behaved differently with no clear link between fracture attributes and bed thickness. Cm-scale sedimentary logs and fracture maps enabled the investigation of heterolithic facies in more detail, in particular which sedimentary features impacted how fractures branch or terminate. Thin (0.5 to 2 cm) shale horizons and the presence of coalified organics, which may or may not occur in conjunction with ripples, had a strong control on fracture termination. In beds which displayed ripples, but lacked organics, fractures typically terminated at the top or base of the bed, however, when organics or shale horizons were present fractures terminated or branched within the bed at these levels.

B. ***The impact of lithology and sub-bed scale heterogeneity on faults***

The field observations suggest small scale sedimentary heterogeneity has a large control on both fault zone thickness and growth. In all cases the connectivity, and hence the number of y- and x- nodes is higher than background levels near faults and increases as displacement increases. Similarly to other studies the hanging wall damage zone displayed a wider and more connected damage zone compared to the footwall (Fig. 1). Heterolithic sequences, where faults and fractures in the damage zones branch at sedimentary interfaces accentuate this effect and can either cause the fault to branch or for a wide damage zone to develop in these lithologies.

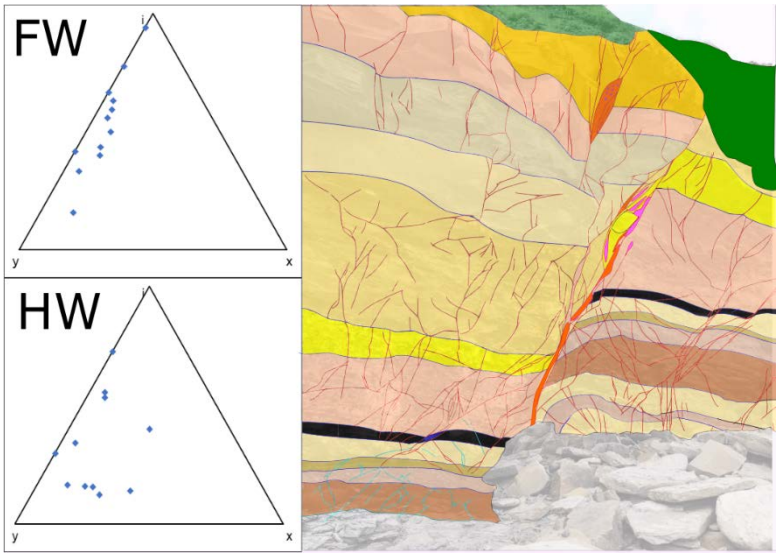

Figure 1: Fault zone fracture and fault map for a 3 m offset fault in the field site. The footwall (FW) and hanging wall (HW) node triangles are shown where each point represents a specific bed.

Small (<10 cm) offset faults investigated in heterolithic units highlight the effect of small scale strength contrasts. For example, thin (<2 cm) discontinuous sand bodies are often transported as lenses bounded by sharp boundaries at right angles to the bedding, possibly due to pre-existing fractures. Coalified organics often lined fault slip planes and clay rich horizons enter the fault as shale smears. The same trends are seen in major faults in the area and I suggest that observations made at this scale can be used as an analogue for processes occurring at a larger scale.

Initial results

a) Sedimentary facies have a weak, but consistent, control on the ratio of fracture node types (i-, y- and x-nodes) and grain size correlates with the mechanical strength.
b) Coalified organics strongly influence how fractures terminate, deflect and branch.
c) The thickness and connectivity of fault damage zones increases with displacement for heterolithic units, however, in channelised sand bodies or clay rich lithology's the fault zone is often thinner and fault rock development (e.g. cataclasite and gouge) is favoured.

3. Additional work and remaining questions

Fracture work

When working up the data it was found that fracture topology notation (i-, y-, and x- nodes) did not sufficiently classify how sedimentary features or horizons impacted fracture terminations and branches. To solve this, i- and y- nodes were further classified as to whether they terminated at the top, within or at the base of a sedimentary layer (e.g. lamination or bed). The ratio of these terminations enabled the relative importance of sedimentary features to be investigated in a quantitative manner and correlated to the mechanical stratigraphy. In my other PhD work it was found that in order to understand and limit subjective bias in fracture data collection, and enable our findings to be used by other authors, it is vital that trace length distributions are also investigated (Andrews et al, *in review*), which is yet to be completed.

Fault work

It was found that to fully understand the impact of lithology and sub-bed scale heterogeneity on faults, it was important to first fully understand how the fractures are impacted. Due to this only limited work has been done and this work will be combined with other data from my PhD to investigate how the underlying sedimentology influences fault thickness and fault growth in the UK Carboniferous Coal Measures.

Expected results and outputs

Our work to date suggests that a statistically significant zones within the node, i-node and y-node triangles exists which are characteristic of specific sedimentary facies. This is important because it can be used as a predictive tool in understanding subsurface connectivity on a bed and sub-bed scale in typical sandstone-siltstone-shale-coal sequences. I also expect to find unique trends in the trace length distributions, which are not only a function of bed thickness (which would indicate bed-bound fractures) but also indicative of typical spacing of sedimentary features (e.g, coal drapes). All findings originating from this study are at a sub-seismic scale and represent important field observations which can be implemented to improve fluid flow predictions. These findings are currently being written up with the aim of submitting a manuscript co-authored by myself and Zoe Cumberpatch, with the support of our respective PhD supervisors, investigating *"the role of lithology and sub-bed scale heterogeneity in fracture topology".*

I also expect lithology and small scale heterogeneity to strongly control both fault zone width and the way in which faults grow. The work into the impact that lithology and sedimentology has on fault development will be combined with other work completed as part of my PhD and form the basis of future publications investigating faults in coal measures.

References

Andrews, B.J., *in review.* How do we see fractures? Subjective bias in fracture data collection. Solid Earth.

Morris, A.P., Ferrill, D.A. and McGinnis, R.N., 2009. Mechanical stratigraphy and faulting in Cretaceous carbonates. AAPG bulletin, 93(11), pp.1459-1470.

Sanderson, D.J. and Nixon, C.W., 2015. The use of topology in fracture network characterization. Journal of Structural Geology, 72, pp.55-66.

Soden, A.M. and Shipton, Z.K., 2013. Dilational fault zone architecture in a welded ignimbrite: The importance of mechanical stratigraphy. Journal of Structural Geology, 51, pp.156-166.

Wennberg, O.P., Svånå, T., Azizzadeh, M., Aqrawi, A.M.M., Brockbank, P., Lyslo, K.B. and Ogilvie, S., 2006. Fracture intensity vs. mechanical stratigraphy in platform top carbonates: the Aquitanian of the Asmari Formation, Khaviz Anticline, Zagros, SW Iran. Petroleum Geoscience, 12(3), pp.235-246.

Oxford University Liverpool Land expedition

Surrounding the settlement of Ittoqqortoormiit, at the mouth of Scoresby Sund in North-East Greenland, is a geological terrain that records evidence of subduction to ultra-high pressures (depths of over 100km). These so called 'ultra-high-pressure terrains', typically found within mountain belts, provide a direct record of a poorly understood process: the subduction of continental crust. The Liverpool Land terrain, located in a steeply mountainous area within the Arctic Circle, is inaccessible even by the standards of ultra-high-pressure terrains and is therefore particularly understudied. The combination of excellent geology combined with a mountaineering challenge was part of the motivation for organising an Oxford University expedition during the summer of 2018.

The aim of this expedition was to understand the metamorphic and structural history of this geological unit and collect samples for further petrological work, to archive with the geological survey of Denmark. As per any expedition plan, it was modified and changed on arrival into Greenland to account for weather, terrain and polar bears. The boat journey from Constable point across Hurry Inlet was relatively short and was reliant on my navigation skills using a 1:250,000 scale map whilst trying not to get sea sick or lose any maps to the wind. We were set down on the western side of the field area with a plan to back pack east onto the 'plateau' where we be in an ideal position to move around the area. As soon as we landed, many of the team members looked at the terrain sloping quite steeply to the east up to a high point of 700m, the incised rivers forming deep canyons filled with snow, the long, frozen lakes which feed these rivers and force you on a huge detour, and the miles of boulder fields with few or no campsites. We soon realised that tackling this terrain with 30-35kg backpacks was out of the question. Our new plan involved following the coastline and approaching the field area from the south, on a 4 day detour.

This route turned out to be an amazing backpacking route with a view of the mountains and Scoresby Sund, the largest fjord in the world. During the first night, many icebergs were blown into the fjord which, combined with the midnight sun, made the night watches magical. The journey along the coast, as well as introducing us to the variation in the geology in the boulders and some interesting outcrops, took us along sandy beaches at the bottom of cliffs of snow and littered with icebergs. At the mouth of the glacial Jaettadal river, we turned inland and painfully crossed a muddy (Triassic) bog where the difference between the solid ground and the sinking ground, to this day, leave me baffled.

After our 4 day detour, we arrived at the Tvaerdal river, which runs down from the southernmost of the frozen Tvaerdal lake and the entrance to our field area. The terrain dramatically changed to the almost barren boulder fields with small arctic flowers and birch peeping out between the boulders or forming small arctic meadows, the steep sided, snow covered mountains and glacial landscape. Access to the plateau every day involved crossing the boulders and rivers which was slow progress. However, the amazing geology displayed in the boulders made up for this. Over the next few days we saw migmatites (melted rocks), eclogites (high pressure, red and green rocks), gneisses (these are stripy rocks which were originally a granite in this case) and peridotites (mantle rocks which weather a horrible crumbly brown but have glassy purple garnets). Our ascent of Kronen (1100m) took us up a steeply inclined boulder field onto a wide, gently sloping summit ridge covered in periglacial stone circles.

The geology by our basecamp and eastward across the braided Jaettadal river was different from up by the Tvaedal lakes because the original rock was a sediment rather than a granite. However, it was strongly metamorphosed into marbles, amphibolites (basalts), and quartzites, layered together and then sheared at high temperatures, smearing it all together. There is no evidence of high pressure

rocks and the melting here is more extensive. The samples that I have collected show a huge range in rock types, pressures and temperatures and could provide some interesting information petrologically if studied under the microscope. Their relationship in the field provides the crucial context for this type of study. The limited time and difficult terrain meant that we were unable to study the contact between these rocks types in detail and were also unable to access the northern end of the field area. However, the preliminary results from this field season provide us with a good building point for future trips.

Figure 1 Photo of the field area looking north from the Plane. The deep incised valley is the Tvaerdal valley and the snow covered glacier on the right the Jaettadal.

Figure 2 The journey along the coast

Figure 3 The discovery of an abandoned Inuit settlement, Kap Hope, across the fjord from the inhabited settlement of Scoresby Sund

Figure 4 The view of the Tvaerdal valley from our basecamp

Figure52 Polar watch and the midnight sun

Figure 3

Granite dykes in the cliffs

Figure 7 Crossing the Jaettadal river

The role of lithology on catchment average erosion rates in the Gediz Graben, Turkey.

Dr Sarah J. Boulton

School of Geography, Earth and Environmental Sciences, University of Plymouth

Amount received: £1000

Introduction

How fast is the landscape response to active faulting? What modulating effect does the rock strength have on the time of response? Questions that until recently have been difficult to answer. In the last ~ 20 years much progress has been made in our ability to interrogate landscapes and extract quantitative geomorphic information both in regions where uplift and erosion are balanced and in locations where the landscape is responding to a change in relative base-level. Combined with advances in dating techniques allowing ages of landforms and rates of erosion or accumulation to de explicitly determined, we can now exploit landscape archives to identify hidden faults, estimate rates of fault motion and determine long term trends in crustal motion. However, few studies have explicitly investigated the role of bedrock strength on landscape response times and this factor remains poorly constrained in many landscape evolution models.

The Gediz Graben in Western Turkey is a half-graben developed upon the Menderes Massif and an ideal location to further our understanding of landscape response to active faulting. In this region, a metamorphic core complex was exhumed along a low angle detachment fault that stopped slipping ~ 2.6 Ma (Buscher et al., 2013). Subsequently high angle normal faulting initiated forming the present topographic graben. Since that time, Miocene sandstones and conglomerates have been uplifted in the southern footwall of the graben bounding fault, along with the metamorphic basement rocks creating a bipartite division in the footwall lithology.

Kent et al., (2016, 2017) suggested that the younger high-angle fault evolved from three initial fault strands through fault linkage into a single active fault, with a maximum slip rate over the 2 Ma of 1.5 mm/yr and the potential to generate an earthquake in the range of Mw = 6.3 – 7.6. The timing of fault linkage was determined to have occurred at ~ 0.75 Ma resulting in a maximum post-linkage throw rate of 2 mm/yr. This acceleration in the rate of fault motion resulted in the tectonic perturbation of the landscape, forcing a transient wave of incision through the river network recorded as a series of slope break knickpoints along the range front. A knickpoint is a distinct geomorphic feature separating areas of the landscape that are incised due to recent incision from areas of relict low-relief landscape. Knickpoint elevation, rate of knickpoint migration and the steepness of the river above and below the knickpoint positively correlate with relief and fault throw rate. In addition, Kent (2015) presents detailed river geometry and stream power calculations for six catchments spanning different uplift rates and with different proportions of metamorphic and sedimentary rocks along the river channel. Kent (2015) demonstrates that these different lithologies have profound effects on the stream power and hydraulic response of the rivers to the uplift on the boundary fault.

This detailed structural and geomorphic framework makes this region ideal to investigate the relationship between uplift rates and erosion rate, and constrain the influence of lithology on erosion and geomorphic development.

These aims will be achieved through the following objectives:

1. River sand samples to be collected for six river systems that cross the active Gediz Graben Fault (Fig. 1), previously investigated by Kent (2015) and additional samples on four rivers investigated by Buscher et al., (2013).
2. *In situ* ^{10}Be cosmogenic nuclide analysis will be undertaken to determine present day rates of catchment average erosion for different slip rates and bedrock lithology.
3. Compare erosion rates to a range of field and DEM-derived topographic and geological variables to characterise the landscape response to active faulting and to different lithologies.

Fieldwork and further work

The funding received from the Geological Society of London allowed me to undertake a visit to Turkey in May 2018 to collect 18 sediment samples (Fig. 1) from identified target rivers from the study area. Samples were collected with the help of local collaborator Dr Cihat Alçiçek (Pamukkale University) from upstream of the active normal fault, at the sediment metamorphic boundary and, where possible, upstream of previously identified knickpoints. Sand was sieved in the field to collect ~ 5-10 kg of sediment < 1 mm in size. A total of 112 kg of sand was collected during this field trip!

The samples were posted to Plymouth and arrived around a month later. Ongoing laboratory work aims to extract the quartz fraction of the collected sediment. This involves firstly sieving the sand into a number of different size fractions (<125μm; 125 - 250μm; 250 - 500μm; > 500 μm). The 125 - 250μm size fraction is then passed through a Franz magnetic separator to isolate the quartz grains from the other minerals (mica, feldspar, lithic fragments etc.) present in the river sand.

Once each sample has been processed mechanically, further separation (if required), acid digestion and AMS analysis will be undertaken at SUERC (pending the award of a NERC facilities grant) to determine the ^{10}Be content of each sample. ^{10}Be cosmogenic nuclide analysis allows the catchment average denudation rates for the river systems to be constrained, thus the role of slip rate and

lithology on denudation rates can be explicitly determined. These data will form pilot data for future research grants but will also be written up as a high-impact journal publication.

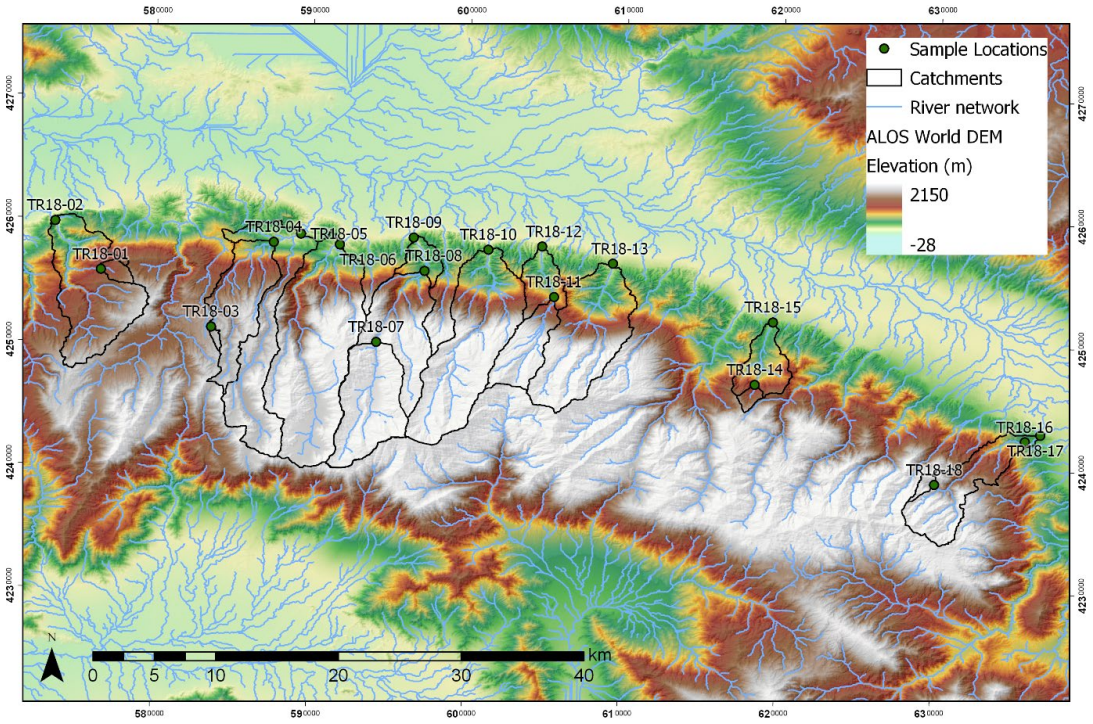

Figure 1. 30 m DEM showing the topography, river network, catchment areas and sample collection sites.

References

Kent, E. 2015. The relationship between active tectonics and fluvial geomorphology: A case study in the Gediz Graben, Turkey. PhD Thesis, University of Plymouth. 397 pp.

Kent, E., Boulton, S. J., Whittaker, A.C., Stewart, I.S., & Alçiçek, M.C. 2017. Normal fault growth and linkage in the Gediz (Alaşehir) Graben, Western Turkey, revealed by transient river long-profiles and slope-break knickpoints. Earth Surface Process and Landforms, 42, 836-852. Doi: 10.1002/esp.4049.

Kent, E., Boulton, S. J., Stewart, I.S., Alçiçek, M.C., Whittaker, A.C., 2016. Geomorphic and geological constraints on the active normal faulting of the Gediz (Alasehir) Graben, Western Turkey. Journal of the Geological Society, London, 173, 666-678. doi: 10.1144/jgs2015-121

Buscher, J. T., Hampel, A., Hetzel, R., Dunkl, I., Glotzbach, C., Struffert, A., ... & Rätz, M. (2013). Quantifying rates of detachment faulting and erosion in the central Menderes Massif (western Turkey) by thermochronology and cosmogenic 10Be. Journal of the Geological Society, 170(4), 669-683.

Salt tectonics; a condiment to French Alpine tectonics since the Triassic.

Samuel Brooke-Barnett (beneficiary of the Mike Coward Fund, £840.00)
Supervisors: Lidia Lonergan, Rodney Graham.

French Alpine geology is a well-trodden, thoroughly studied field, and for good reason; the French Alps are a spectacularly exposed, beautiful, and easily accessible laboratory within which much of our current understanding of structural geology and tectonics has been developed. Consequently, field geology in the Subalpine Chains of southeast France is supported by excellent geological maps and volumes upon volumes of accompanying literature. The tectonic history of the Subalpine Chains since the Triassic is understood in the context of multiple plate scale processes; in particular the rifting of the European plate margin during the opening of the Alpine Tethys ocean from the late Triassic to middle Jurassic, a passive margin phase as the Tethys ocean spread, and a subsequent Alpine shortening phase as Africa collided with Europe from the Late Cretaceous to the Miocene. Whilst this account is well documented and constrained, various peculiar observations suggest there is more to the story; Triassic age evaporites vary significantly in thickness across the area and appear anomalously out of place within the Cretaceous geological section. Additionally, onlap relationships and thickness changes within the passive margin section suggest phases of dynamic topography in an ostensibly tectonically benign period, long before Alpine compression began.

Over the past two decades, understanding of the evolution of passive margin settings has progressed considerably thanks to advances in seismic acquisition and interpretation in the North Sea, Gulf of Mexico, offshore Africa and Brazil. These case studies have all highlighted the importance of salt migration and diapirism in passive margin settings. The passive margin sequence within the Subalpine Chains contains the same essential ingredients as the aforementioned modern day analogues for salt migration, namely an abundant Triassic evaporite section overlain by considerably thick passive infill sequence which serves as a driving load for diapirism. However while the importance of the Triassic evaporites have been acknowledged as an important decollement for compressional deformation, the effect of passive salt deformation in the French Alps has been relatively overlooked. This is primarily due to the fact that the signs of salt migration are not immediately evident; halite simply isn't present in outcrop due to its easily soluble nature, and the subtle, local scale effects of salt body deformation are difficult to untangle from approximately 80 Ma of regional compressional deformation. This begs the question, could

the migration of large evaporite bodies have played a more prominent role in the evolution of the French Alps than previously recognized?

It was with this question in mind that I travelled to the town of Saint Andre les Alpes last summer in search of the filed-down fingerprints of long gone salt, alongside fellow PhD student Adam Csicsek and a number of highly valued field assistants. My field area is situated approximately 130 km to the northeast of Marseille, across the lavender fields of the Valensole Plateau, and deep within Pastis, patou and patisserie country. The area has high geological pedigree, hosting the Annot Sandstone in which turbidite sequences were described by Arnold Bouma in 1962. But my focus of field study was the Rouaine-Daluis Fault System, a series of strike-slip faults with net sinsitral offset which demarcate a significant regional structural boundary. In outcrop, these faults are accessible between the towns of Castellane to the southeast, and Guillaumes to the northwest, flanking local mountains, including Sommet du Teillon, Sommet de la Bernarde, and the Plateau d'Educh, and running parallel to the Var River and the Gorges de Daluis.

Travelling southwest from Guillaumes along strike of the fault system conveniently takes one on tour through time from the Late Permian to the early Oligocene. The tour begins with the sinuous route along the Gorge de Daluis, through the burgundy coloured Permian pelites of the Dôme de Barrot considered the "Basement" of the area. The gorge itself trends parallel to a large normal fault which cuts through the Permian and Triassic rocks. On approach to the town of Daluis, one passes through an anomalously thickened Triassic section, and the verdant fields dotted around the mountainsides helpfully demarcate the extent of the relatively soft gypsum. This thick gypsum is locally onlapped by Liassic to middle Jurassic limestones implying this gypsum body was growing during Tethyan ocean rifting, but had ceased growth (at least temporarily) by the Late Jurassic when it was covered by marine shales.

Southeast of Daluis we see further evidence of evaporite growth during the Late Jurassic to Middle Cretaceous. Between Daluis and the town of Sausses, the Var River broadens out into a number of braided streams, and the riverside section takes one through a spectacular overturned fold composed of Tithonian Limestone, with the overlying Early Cretaceous limestones and marls pinching out into the folded section. Southwest, near Sausses, the Early Cretaceous beds gradually flatten out, and we encounter yet again a thick body of Triassic gypsum, this time overlying Aptian to Albian black shales. Could the Daluis diapir have risen again during sediment loading of the passive margin phase, reaching the sea surface as a canopy in the Aptian-Albian when the sediment rate was low?

The story of salt migration does not end in the Middle Cretaceous however, as more pieces of the puzzle are observable in the Eocene to Oligocene foreland basin units to the southeast of Sausses. The Rouaine-Daluis Fault System has exposed the northwestern face of the Plateau d'Educh, revealing a spectacular section of Lutetian to Priabonian aged nummulitic limestone, draped like stage curtains into a series of growth folds. Furthermore, the town of St. Benoît sits upon an incredibly thickened section of Late Eocene to Oligocene marls associated with syn-depositional extension. While these structures have been attributed to transpression along the Rouaine-Daluis Fault System coinciding with Alpine shortening, the geometries of these structures also hint at deposition on an unstable surface, presumably salt, which was extruded as shortening progressed. This hypothesis is bolstered if corrections for post-Oligocene strike-slip movements are taken into account, whereby it becomes evident that these Eocene to Oligocene aged structures were formed in close proximity to the out-of-section Triassic evaporites at Sausses.

The first field season was enlightening and puzzling in equal measures, and whilst I have trained my eye towards recognizing weird and wonderful salt structures, I still have a lot to learn. Significant headway was made in understanding the story of salt migration in the Subalpine Chains, telling a story beginning with evaporite deposition on the Triassic, followed by the reactive rise of a salt wall during Tethyan rifting, the growth and emergence of said salt during passive margin development in the Cretaceous, and the sinistral offset of the wall and progressive salt evacuation during Alpine compression. My next field seasons will take me north of Guillaumes, where the Rouaine-Daluis Fault System meets significant regional extensional faulting, and southwest of St Benoit, where the fault system hits a restraining bend. But it only took one season to appreciate that a pinch of salt adds a lot of flavor to the tectonic history of the Subalpine Chains.

This project was made possible by valued contributions from the Mike Coward Fund, the CASP Fieldwork Award, and the Imperial College London President's Scholarship. I would like to thank my supervisors Lidia Lonergan and Rodney Graham for their expertise, advice and support, and my colleague Adam Csicsek for his great ideas and field assistance. This project is in partnership with Pau university and while out in the field, Adam and I also benefitted from the input of Jean-Paul Callot, Jean-Claude Ringenbach and Naïm Célini. Adam and I are also grateful to our ten field assistants for volunteering their time and energy to follow us around the French countryside and stare at every outcrop along the way.

Daniel Collins – Daniel Pidgeon Fund - £1,000

Sedimentological, stratigraphic and geomorphological evolution of mangrove-influenced deposition in the northern Mekong River delta, Vietnam

D.S. Collins[1], T. Tamura[1], V.L. Nguyen[2], T.K.O. Ta[2], L. Mao[3], Y. Ishii[1], H. Kitagawa[4], R. Nakashima[1]

[1] *Geological Survey of Japan, AIST, Central 7, Higashi 1-1-1, Tsukuba 305-8567, Japan*

[2] *HCMC Institute of Resources Geography, VAST, Ho Chi Minh City, Vietnam*

[3] *State Key Laboratory of Palaeobiology and Stratigraphy, Nanjing Institute of Geology and Palaeontology, Chinese Academy of Sciences, Nanjing, China*

[4] *Solar-Terrestrial Environment Laboratory, Nagoya University, Nagoya, Japan*

Mangroves are sensitive indicators of climate, sea level, salinity and the balance of river, tide and fluvial processes (e.g. Woodroffe et al., 1985; Ellison & Stoddart, 1991; Woodroffe et al., 1992; Wolanski et al., 1992; Woodroffe et al., 2016). In the present-day northern Mekong delta, extensive mangroves occur in a relatively embayed, wave-protected and tide-influenced, back-barrier setting (Can Gio; Fig. 1) (e.g. Hong et al., 1996; Woodroffe et al., 2016), but the development of this mangrove system during the Holocene is poorly constrained. The objectives of this study were to combine detailed sedimentary facies and stratigraphic analyses, including soft x-ray imaging and palynology, of two Pleistocene–Modern sediment cores and four shorter auger cores (Fig. 2) with radiocarbon and optically stimulated luminescence (OSL) dating (34 samples in total) to interpret and discuss the (1) depositional facies characteristics of mangrove-influenced sedimentation, (2) local palaeo-environmental and geomorphological evolution, and (3) larger-scale controls on sedimentary processes and dynamics impacting mangrove development in the Holocene Mekong River delta.

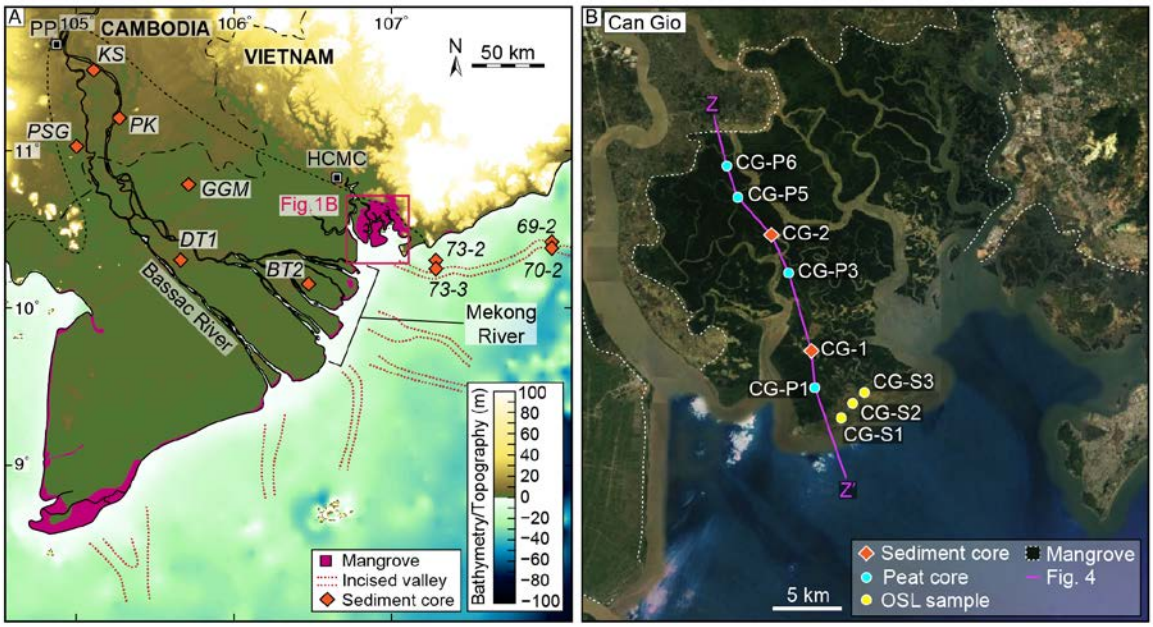

Fig. 1. (A) GEBCO topographic-bathymetric map of the Mekong River delta. Cores KS, PK, and PSG are from Tamura et al. (2009); core GGM is from Proske et al. (2010); cores DT1 and BT2 are from Ta et al. (2002, 2005); cores 69–2, 70–2, 72–2, and 72–3 are from Tjallingii et al. (2010); interpreted incised valleys are from Tjallingii et al., 2012 (after Tjallingii et al., 2010); and mangrove distribution is from Giri et al. (2011). HCMC—Ho Chi Minh City; PP—Phnom Penh.(B) Google Earth map of study area in Can Gio, northern Mekong delta (refer to Fig. 1A), Vietnam, showing the positions of sediment and peat cores, OSL samples and approximate north–south stratigraphic transect (Fig. 4).

The Can Gio geomorphological system comprises a subaerial sandy barrier and back-barrier mangroves with an extensive tidal channel network (Fig. 2). The c. 44,700 ha of mangrove forest in Can Gio were restored after the Vietnam War, primarily with the species *Rhizophora apiculate*, and are highly susceptible to typhoons during wet season (mid-April to October) (Hong 1996; Singh et al., 2003). Sedimentary cores all display a downward transition from interpreted intertidal–upper subtidal facies, which comprise completely bioturbated carbonaceous mudstones with mangrove root and litter with abundant mangrove palynomorphs, to interpreted subtidal facies, which variably comprise bioturbated mudstones, sandy bioturbated mudstones, and more sporadically bioturbated, wavy to lenticular bedded heterolithics (Fig. 3). A north–south stratigraphic transect indicates thinning of the Holocene succession and increased sand content towards the south and present-day subaerial sandy barrier (Fig. 4). Radiocarbon dates indicate the consistent occurrence of very recent mangrove material in the uppermost 6–9 m of sediment, suggesting deep penetration and mixing by mangrove roots (Fig. 4). The OSL dating indicates initial formation of a subaqueous sandy barrier by 3.21 ± 0.19 ka that subsequently accreted towards the south-

west (Figs 2 and 5). Leeching of sand from the developing barrier is suggested by the higher sand content of contemporaneous subtidal sediments between c. 5–3 ka in the closest adjacent core. The mixed sediment zone (<3 ka) succeeding initial barrier development indicates a significant increase in mangrove-influenced deposition, and continued sand supply from the barrier is evidenced by sandy carbonaceous mudstones in adjacent mangroves.

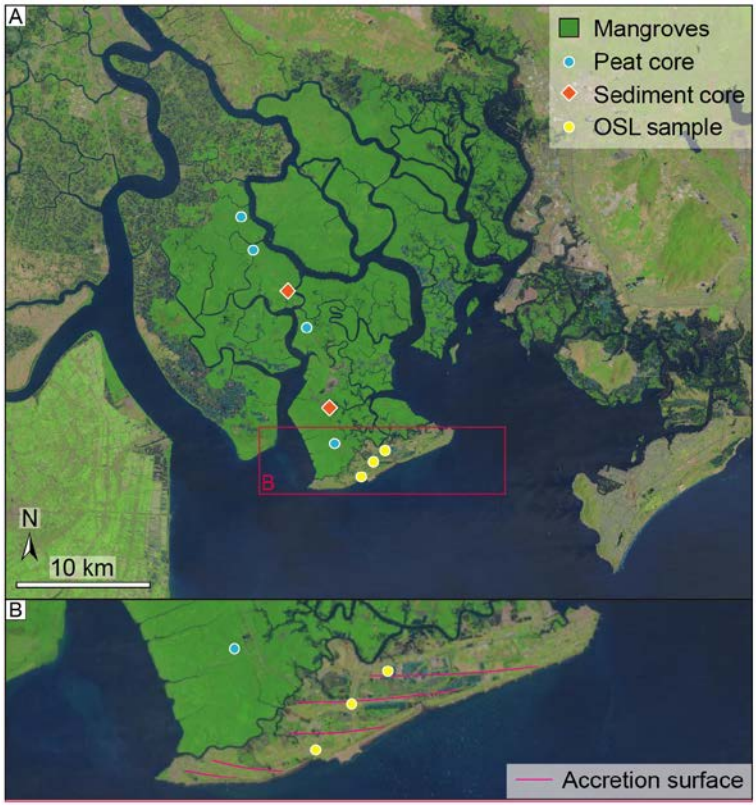

Fig. 2. (A) Sentinel-2 multispectral satellite image of the Can Gio system showing the locations of peat and sediment cores, and OSL samples (refer to Fig. 1). (B) Detailed image of the sandy subaerial barrier with interpreted accretion surfaces indicating migration and expansion towards the south-west.

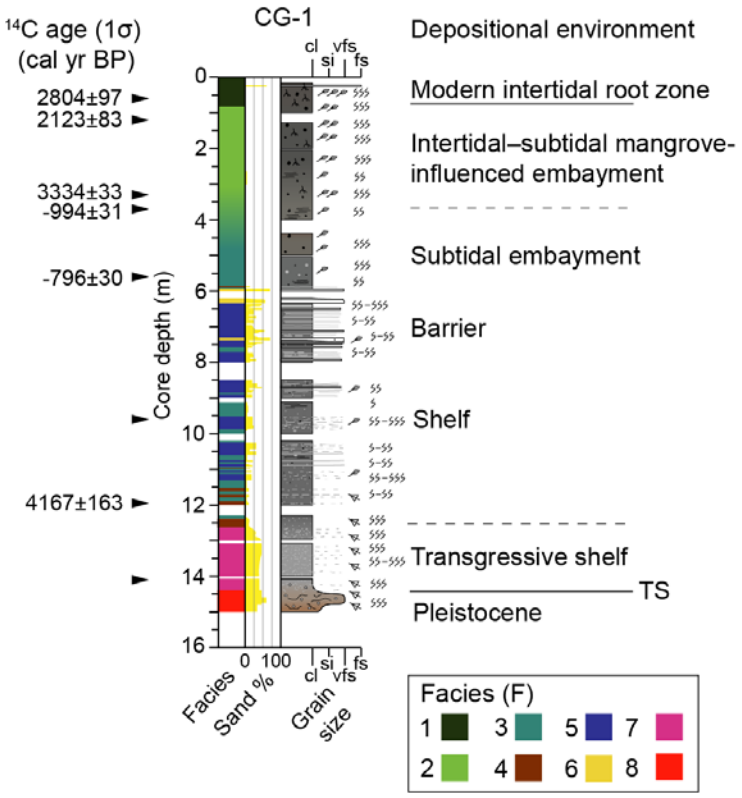

Fig. 3. Stratigraphic log of sedimentary core CG-1 (see Fig. 1B for location) including facies, radiocarbon (^{14}C) age dates (relative to A.D. 2018) and interpreted depositional environment. Negative ^{14}C ages indicate modern samples after A.D. 1950.

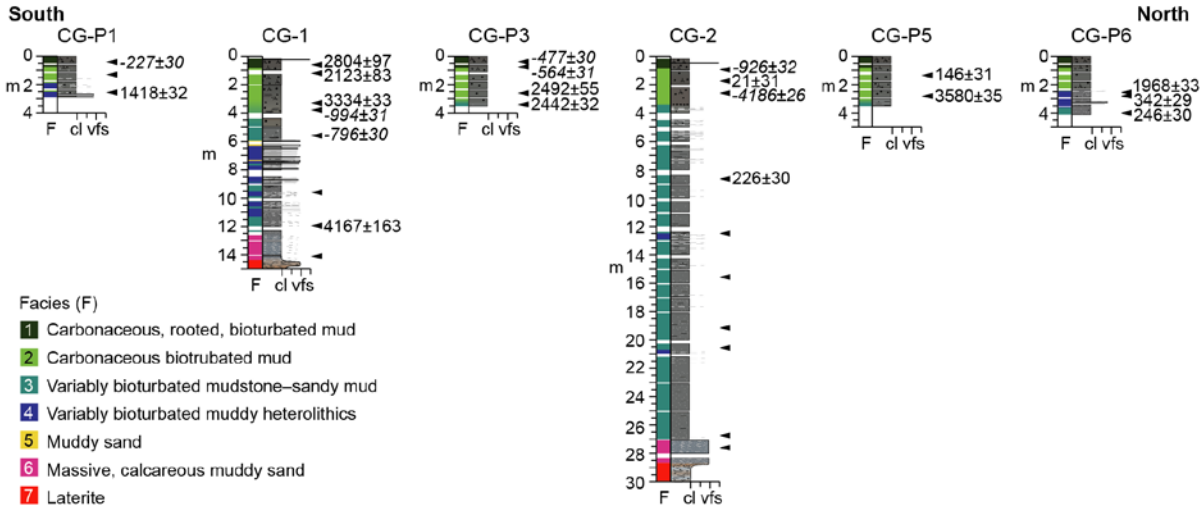

Fig. 4. Simplified north–south correlation of sedimentary facies core data (see Fig. 1B for location). Radiocarbon (^{14}C) age dates (relative to A.D. 2018) are for presently analysed organic material; remaining shell samples are being finalised. Negative ^{14}C ages (italics) indicate modern samples after A.D. 1950.

Thinning of the Pleistocene basement towards the present-day barrier suggests that the position of barrier development was predetermined by existing topography. Direct sand

supply from the developing Mekong delta during barrier development (c. 5–3 ka) was limited due to the relatively lateral and distal position of Can Gio (e.g. Nguyen et al., 2000; Ta et al., 2005; Hanebuth et al., 2012). Instead, the proposed model for barrier development involves the gradual supply of suspended sediment with a small fraction of silt–sand, preferential deposition across a subtly shallower 'basement high', and subsequent winnowing of mud to form a sandier mud-dominated deposit. Suspended sediment was most likely supplied by local, small-scale rivers eroding sandy Pleistocene outcrops (e.g. Saigon and Dong Nai systems; Fujimoto et al., 2008), south-westward alongshore currents during the winter monsoon from sandy shoreline and barriers to the north-east, and subordinate north-eastward alongshore currents during the summer monsoon from the active Mekong delta. The proposed geomorphological model accounts for the early barrier development compared to closely adjacent barriers (e.g. Tamura et al., 2012; Fig. 5) and the subsequent expansion of mangroves in the northern Mekong River delta.

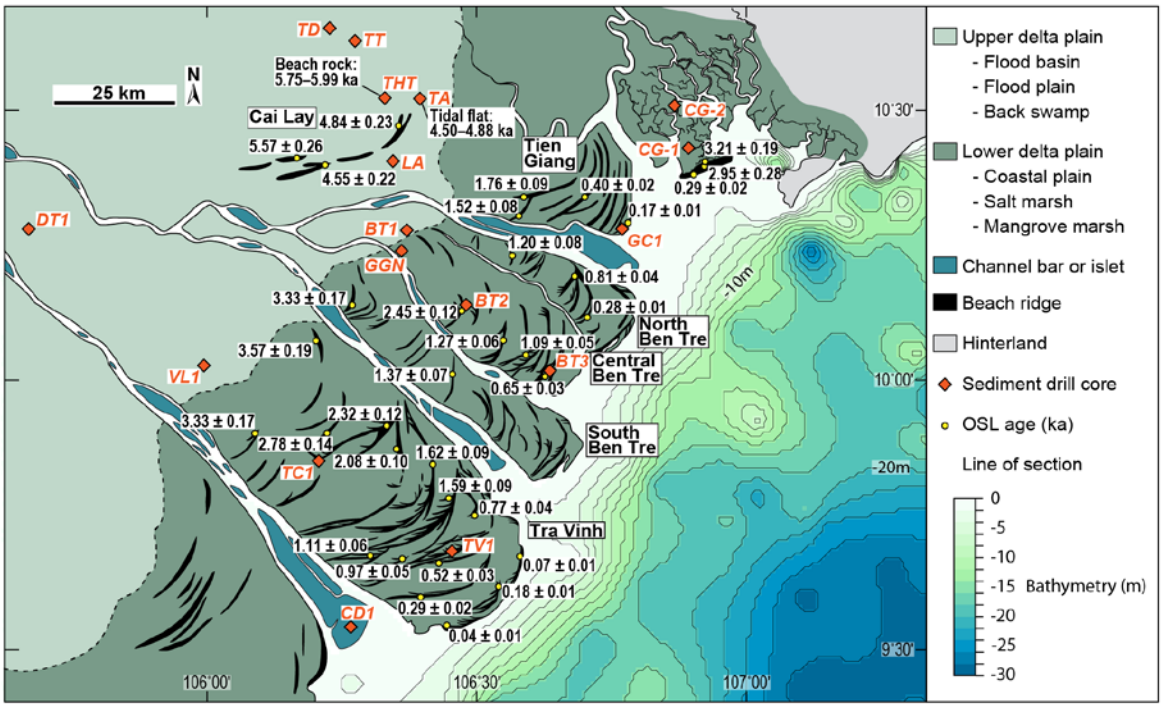

Fig. 5. Geomorphology of the Mekong River delta (after Nguyen et al., 2000) and nearshore bathymetry relative to mean sea level (GEBCO) (after Tamura et al., 2012). Beach ridges were re-interpreted using Landsat imagery from 1989 by Tamura et al., (2012) (after Gagliano and McIntire, 1968; Nguyen et al., 2000). The delta-front platform extends from 0 m to c. 4 m water depths, the delta-front slope from c. 4–20 m, and further offshore is the prodelta–slope. Additional sediment core locations (cf. Fig. 1A) are TA and GGN (Proske et al., 2011) and other cores from Ta et al. (2002, 2005). Optically stimulated luminescence (OSL) and radiocarbon ages, including data from the present study, are expressed relative to A.D. 2010.

References

Ellison, J.C. and Stoddart, D.R. (1991) Mangrove ecosystem collapse during predicted sea-level rise: Holocene analogues and implications. Journal of Coastal Research, v. 7, p. 151–165.

Fujimoto, K., Umitsu, M., Kawase, K., Nguyen, V.L., Ta, T.K.O. and Huynh, D.H., 2008. Geomorphological evolution and mangrove habitat dynamics of the Northern Mekong River Delta and the Dong Nai River Delta. Geomorphological Comparative Research on Natural Disaster Mitigation in the Coastal Regions of Tropical Asia, Phuket, Ho Chi Minh, Pattaya. Department of Geography, Nagoya University, p. 75–83.

Nguyen, V.L., Ta, T.K.O. and Tateishi, M. (2000) Late Holocene depositional environments and coastal evolution of the Mekong River Delta, Southern Vietnam. Journal of Asian Earth Sciences, v. 18, p. 427–439.

Gagliano, S.M., and McIntire, M.G. (1968) Report on the Mekong Delta: Louisiana University Coastal Studies Institute Technical Report 57, 143 p.

Giri, C., Ochieng, E., Tieszen, L.L., Zhu, Z., Singh, A., Loveland, T., Masek, J. and Duke, N. (2011). Status and distribution of mangrove forests of the world using earth observation satellite data. Global Ecology and Biogeography, v. 20, p. 154–159.

Hanebuth, T.J., Proske, U. Saito, Y., Nguyen, V.L. and Thi, K.O.T. (2012) Early growth stage of a large delta: Transformation from estuarine-platform to deltaic-progradational conditions (the northeastern Mekong River Delta, Vietnam). Sedimentary Geology, v. 261, p. 108–119.

Proske, U., Hanebuth, T.J.J., Gröger, J., and Diem, B.P. (2011) Late Holocene sedimentary and environmental development of the northern Mekong River Delta, Vietnam: Quaternary International, v. 230, p. 57–66.

Singh, S., Luong, N.V. and Binh, T.T.H. (2013) Monitoring mangrove forest reclamation using geospatial tools in Can Gio Mangrove Biosphere Reserve, Vietnam. International Journal of Ecology and Environmental Sciences, v. 39, p. 147–157.

Ta, T.K.O., Nguyen, V.L., Tateishi, M., Kobayashi, I., and Saito, Y. (2002) Holocene delta evolution and sediment discharge of the Mekong River, southern Vietnam: Quaternary Science Reviews, v. 21, p. 1807–1819,

Ta, T.K.O., Nguyen, V.L., Tateishi, M., Kobayashi, I. and Saito, Y. (2005) Holocene delta evolution and depositional models of the Mekong River Delta, southern Vietnam. In: River Deltas—Concepts, Models, and Examples (eds Giosan, L. and Bhattacharya, J.P.), SEPM Special Publication 83, p. 453–466.

Tamura, T., Saito, Y., Sieng, S., Ben, B., Kong, M., Sim, I., Choup, S., and Akiba, F., 2009, Initiation of the Mekong River delta at 8 ka: Evidence from the sedimentary succession in the Cambodian lowland: Quaternary Science Reviews, v. 28, p. 327–344.

Tamura, T., Saito, Y., Nguyen, V.L., Ta, T.O., Bateman, M.D., Matsumoto, D., Yamashita, S., 2012. Origin and evolution of interdistributary delta plains: insights from Mekong River delta. Geology, v. 40, p. 303–306.

Tjallingii, R., Stattegger, K., Wetzel, A., and Phach, P.V., 2010, Infilling and flooding of the Mekong River incised valley during deglacial sea-level rise: Quaternary Science Reviews, v. 29, p. 1432–1444.

Tjallingii, R., Stattegger, K., Stocchi, P., Saito, Y., and Wetzel, A. (2014). Rapid flooding of the southern Vietnam shelf during the early to mid-Holocene. Journal of Quaternary Science, v. 29, p. 581–588.

Wolanski, E.E., Mazda, Y.Y. and Ridd, P.P. (1992) Mangrove hydrodynamics. In: Tropical Mangrove Ecosystems (eds Robertson, A. I. & Alongi, D. M.) p. 43–62 (American Geophysical Union).

Woodroffe, C. D., Thom, B.G. and Chappell, J. (1985) Development of Widespread Mangrove Swamps in Mid- Holocene Times in Northern Australia. Nature, v. 317, p. 711–713.

Woodroffe, C. D., Rogers, K., McKee, K.L., Lovelock, C.E., Mendelssohn, I.A. and Saintilan, N. (2016) Mangrove sedimentation and response to relative sea-level rise. Annual Review of Marine Science, v. 8, p. 243–266.

Woodroffe, C.D. (1992) Mangrove sediments and geomorphology. In: Tropical Mangrove Ecosystems (eds Robertson, A.I. & Alongi, D.M.) p. 7–41 (American Geophysical Union).

Trace element productivity and redox proxies in the Bowland-Hodder Shale, UK

Patrick J Dowey, University of Manchester

Amount awarded: £949.79

Background

The formation of organic-rich marine sediments is controlled by organic matter productivity from the euphotic zone or land sources, organic matter preservation due to low oxygen (redox) conditions within the sediment (Tribovillard *et al.*, 2006), and the rates of sediment supply and burial. The Bowland-Hodder Shale, an organic-rich marine sediment in Northern England, has recently been subject to significant academic and industrial interest (Andrews, 2013). The Carboniferous basins in which the Bowland-Hodder Shale formed are structurally complex (Fraser & Gawthorpe, 1990). Recent studies of Bowland-Hodder Shale cores from the Cleveland and Widmerpool Gulf Basins (Figure 1) using organic biomarkers have identified fluctuating anoxia as a control on organic matter concentrations (Gross *et al.*, 2015; Słowakiewicz *et al.*, 2015). The structural complexity of the basins is likely to have resulted in significant variations in sediment supply, basin restriction and organic matter productivity across the North of England at this time (Fraser & Gawthorpe, 1990; Sageman *et al.*, 2003). Identifying how structurally complex marine basins control the preservation of organic matter is of value in understanding climate change, element cycling and characterising variability in a potential shale gas resource. Presently there is no published research on the paleoproductivity and paleoredox conditions in the Bowland and Pennine Basins.

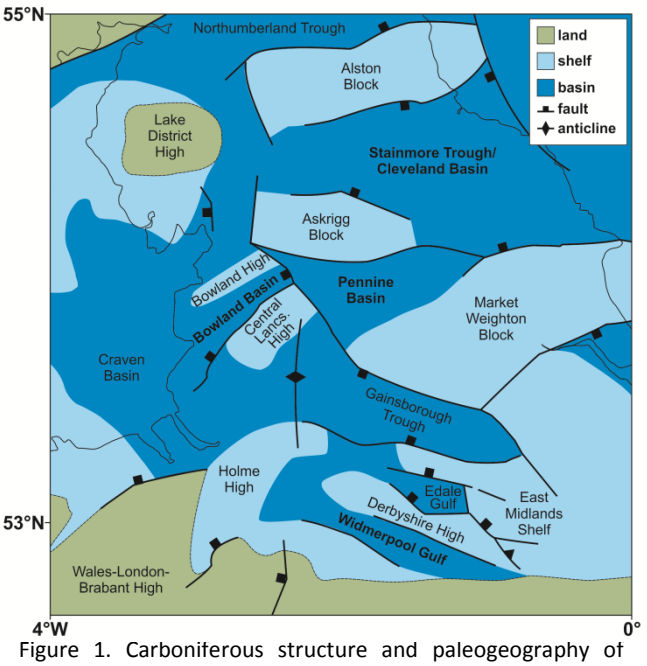

Figure 1. Carboniferous structure and paleogeography of Northern England. (After: Newport et al., 2018).

In the rock record, paleoproductivity and paleoredox conditions in marine settings can be recorded by trace element concentrations (those below 1000 ppm) within sedimentary rocks (Tribovillard *et al.*, 2006). Trace elements are micronutrients for plankton, and organic matter concentrations in sediments are directly proportional to planktonic surface water productivity (Chester, 2009). Certain trace elements, such as Ni, Cu, Zn and Cd, can therefore be used as proxies for productivity. These elements can be retained in the sediment through sulfate mineral formation (Tribovillard et al., 2006). Furthermore, certain trace elements (such as U, V and Mo) are sensitive to oxygen conditions, and can be used as proxies for the redox state of the sediment (Algeo & Maynard, 2004). These redox proxies may be incorporated into clay minerals, or authigenic mineral phases. The preservation of organic matter and the development of early authigenic minerals are recorded in the textural and compositional features within the sediment. Sedimentological and petrographic observations of textural and compositional variability in sediments can provide significant value when coupled with quantitative geochemical datasets (Rimmer *et al.*, 2004).

Research question & objectives

What were the paleoproductivity and paleoredox conditions in the Bowland and Pennine Basins during the Carboniferous, and how did the conditions vary spatially and temporally?

The study has three aims:

1. What are the textural and compositional variations in the Bowland-Hodder Shales from the Bowland and Pennine Basins?
2. Which redox and productivity proxy trace elements are present and how do they vary spatially and temporally?
3. How do redox and productivity proxies relate to textural and compositional variations, and can these be related to basinal controls?

Work to date

Study samples were chosen to provide data from a broad a range of Bowland sub-basins. I visited the BGS core store to log five cores and collect samples; these included cores from several Carboniferous Bowland sub-basins (figure 2). A further three samples were collected from outcrops in the Bowland Basin. Thin sections of thirteen samples were prepared and the textural and mineralogical variability characterised using optical microscopy techniques. Initial geochemical data was collected using X-ray fluorescence analysis (XRF). Assessment of publicly available geochemistry data (BGS) yielded several major and minor trace element datasets which have been utilised to compliment the initial XRF data collected. This data has been combined to provide preliminary data for focused future work.

Uranium and molybdenum enrichment factors (figure 3) can be used to identify trends in water conditions at the time of sediment deposition. The data demonstrates significant variability in the relative concentrations of uranium and molybdenum across the Bowland Shale sub-basins The enrichment factors are also interpreted to largely indicate partially restrictive, suboxic conditions during the deposition of the Bowland Shale (Algeo & Lyons, 2006).

Figure 2. Core photos of lithologies from Bowland Shale Formation. Demonstrates the range of samples collected during visit the BGS core store.

Future work

Then next phase of the work is to return to the BGS core store and collect data from a few focused cores. Fifty samples will be collected, and from these thin sections will be prepared and total organic carbon analyses undertaken. Quantitative geochemical data will be collected using inductively coupled plasma atomic-emission spectrometry anal (ICP-MS) at the University of Manchester. Combining these datasets, the variability in organic richness will be tied to bulk geochemistry data and elemental mapping techniques to identify variations in the concentrations of productivity and redox sensitive elements. Using geological data and interpretations the geological controls on these elements will be defined.

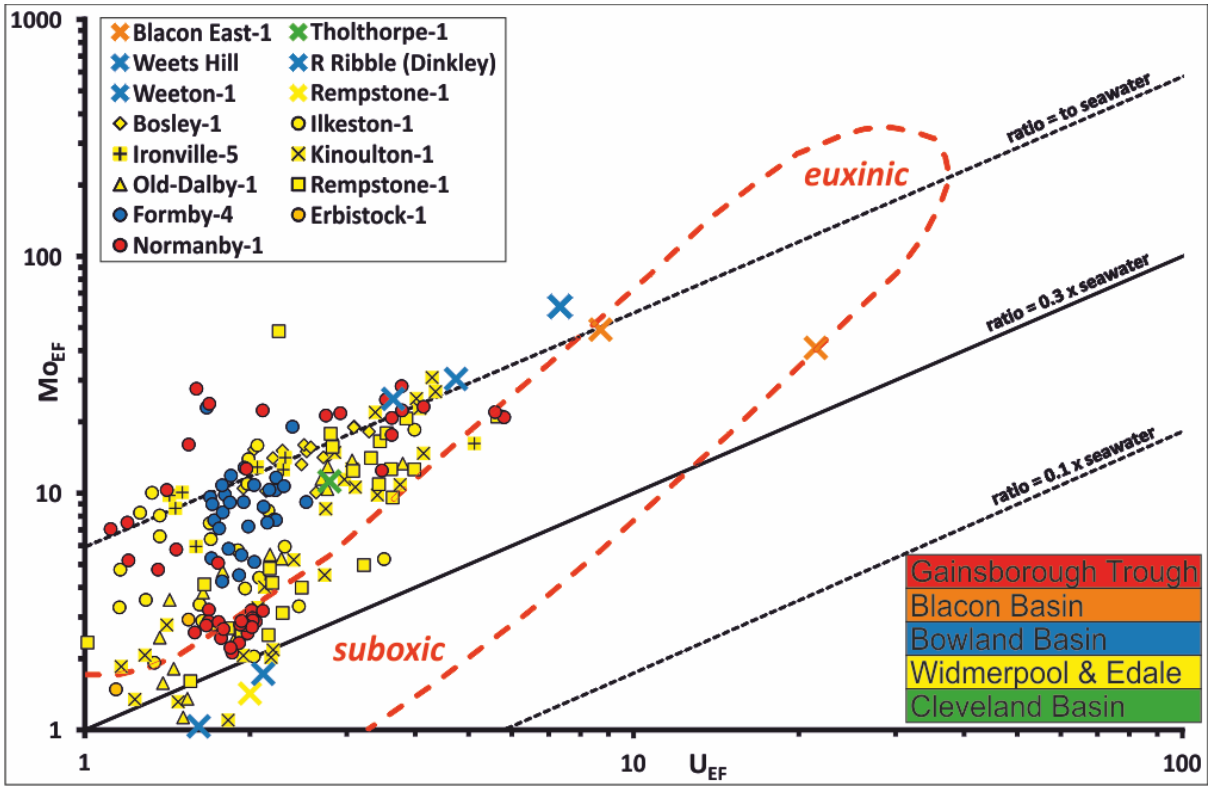

Figure 3. Uranium vs. Molybdenum enrichment factors for collected Bowland Shale samples and public data. Colours relate to different sub-basins (inset).

Bibliography

Algeo, T.J. and **Lyons, T.W.** (2006) Mo–total organic carbon covariation in modern anoxic marine environments: Implications for analysis of paleoredox and paleohydrographic conditions. *Paleoceanography*, **21**, n/a-n/a.

Algeo, T.J. and **Maynard, J.B.** (2004) Trace-element behavior and redox facies in core shales of Upper Pennsylvanian Kansas-type cyclothems. *Chem. Geol.*, **206**, 289–318.

Andrews, I.J. (2013) The Carboniferous Bowland Shale gas study: geology and resource estimation. 64 pp.

Fraser, A.J. and **Gawthorpe, R.L.** (1990) Tectono-stratigraphic development and hydrocarbon habitat of the Carboniferous in northern England. *Geol. Soc. London, Spec. Publ.*, **55**, 49–86.

Gross, D., **Sachsenhofer, R.F.**, **Bechtel, A.**, **Pytlak, L.**, **Rupprecht, B.** and **Wegerer, E.** (2015) Organic geochemistry of Mississippian shales (Bowland Shale Formation) in central Britain: Implications for depositional environment, source rock and gas shale potential. *Mar. Pet. Geol.*, **59**, 1–21.

Rimmer, S.M., **Thompson, J.A.**, **Goodnight, S.A.** and **Robl, T.L.** (2004) Multiple controls on the preservation of organic matter in Devonian–Mississippian marine black shales: geochemical and petrographic evidence. *Palaeogeogr. Palaeoclimatol. Palaeoecol.*, **215**, 125–154.

Sageman, B.B., **Murphy, A.E.**, **Werne, J.P.**, **Ver Straeten, C.A.**, **Hollander, D.J.** and **Lyons, T.W.** (2003) A tale of shales: the relative roles of production, decomposition, and dilution in the accumulation of organic-rich strata, Middle–Upper Devonian, Appalachian basin. *Chem. Geol.*, **195**, 229–273.

Słowakiewicz, M., **Tucker, M.E.**, **Vane, C.H.**, **Harding, R.**, **Collins, A.** and **Pancost, R.D.** (2015) Shale-gas potential of the mid-Carboniferous Bowland-Hodder Unit in the Cleveland Basin (Yorkshire), Central Britain. *J. Pet. Geol.*, **38**, 59–75.

Tribovillard, N., **Algeo, T.J.**, **Lyons, T.** and **Riboulleau, A.** (2006) Trace metals as paleoredox and paleoproductivity proxies: An update. *Chem. Geol.*, **232**, 12–32.

Investigating the petrogenesis of the magmas ejected during the 1902 eruption of Santa María, Guatemala

Author:
Finley Gilchrist

Amount of funding received:
£363

1 Background and introduction

On the 25 October 1902, after months of unrest, Santa María volcano in southwestern Guatemala erupted in a catastrophic event which killed an estimated 5,000 people. Over 8km^3 of dacite magma and a minor amount of basaltic-andesite scoria was produced. This was the first time that the volcano had erupted in recorded history, and also represented a dramatic shift in the magma chemistry and eruption style. The entirety of the erupted products from Santa María had previously been a series of basaltic to basaltic-andesitic magmas. They were produced in a period of 75,000 years between 102-25 k.a., after which the volcano entered repose (Williams and Self, 1983). This production of dacite therefore represents a new phase of activity, one in which the production of evolved magmas through fractional crystallisation and assimilation represents the dominant magmatic process beneath the volcano.

Twenty years after the Plinian eruption occurred, dacite lava began to erupt effusively out of the vent. Over the past ninety plus years, this eruption has continued uninterrupted, with over a cubic kilometre of material being erupted to form a series of domes. The chemical composition of the magmas has changed over time, with the material gradually decreasing in silica content over time from 68% to around 62% in 2002 (Scott et al., 2013).

In a study done at the University of Bristol with additional funding from the Geological Society of London, samples were collected from the eruption deposits of the 1902 eruption and analysed both qualitatively and quantitatively to decipher what processes were ongoing beneath the volcano in the build-up to eruption. Textures of both the whole rock and phenocryst phases suggest that magma mixing was extensive and heterogenous, while analyses of amphibole compositions gave estimates for the storage conditions of the dacite pumice and the enclaves that were found within them.

2 Fieldwork

During the spring of 2017, fieldwork was undertaken as part of a project investigating petrological aspects of the poorly understood 1902 eruption. Previous fieldwork locations that had been studied on on the volcano were primarily located towards the north or west of the volcano. In this study, fieldwork was focused at four locations to the southwest of the volcano, and included one location where an at least partial stratigraphy was preserved from the eruption.

The samples and outcrops showed that there had been a fairly simple sequence to the eruption. The majority of the deposit showed a simple upwards coarsening trend suggesting an increase in the eruption intensity as it went on. The final part of the deposit showed the introduction of basaltic-andesite scoria, which immediately preceded the abrupt termination of the eruption. Above the pumice and scoria deposit lay a number of thin brown ash layers, which are interpreted as deposits from the series of phreato-magmatic events that are known to have occurred after the termination of the Plinian phase. Finally, the deposit was capped by a thick structureless ash unit, which is likely to be from a dome-collapse event that occurred in 1929.

3 Results

3.1 Mineralogy

Surprisingly, the eruption products could be divided into three different categories based on the phenocryst mineral assemblages that were present. The bulk of the eruption deposit was composed of dacite pumice containing amphibole, plagioclase feldspar and rarely orthopyroxene phenocrysts. Physically mixed within the pumice were variably-sized mafic enclaves which held a similar phenocryst population of plagioclase and amphibole. However, no pyroxenes were present at all in these enclaves. Finally, another mafic component was identified within the

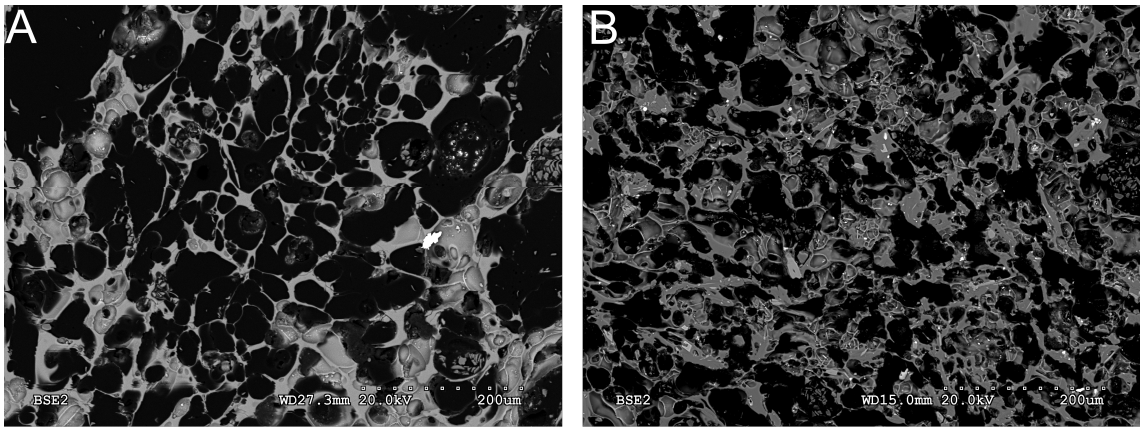

Figure 1: Back-scatter electron images of the groundmass textures of the three different magmas. All images taken at 180× magnification. A) Image of SM-1.2, showing vesicle textures in non-banded pumice. B) Image of SM-3.1, showing vesicle textures within a grey-coloured band.

eruption deposit as the scoria, which is only present in the top 4 cm of the pumice deposit. This was an entirely distinct mafic magma that showed no signs of having been physically mixed with the dacite pumice, and the clasts were only mixed during deposition from the eruption column. This material was very different from the previous two magmas, with a mineral assemblage containing clinopyroxene, olivine and plagioclase feldspar.

These three assemblages show conclusively that there were at least three magmas present during the eruption. Previous investigations of this eruption have shown that the dacite was most likely created by fractional crystallisation of large volumes of un-erupted basaltic-andesite that was left over during the earlier phases of cone construction, with minimal amounts of assimilation. They have also identified the mafic components that were present in the eruption deposits, however no distinction is made between the scoriaceous material and the enclaves found in the pumice. This material has previously been interpreted as a recharge event of the magma chamber, however there has not been an explanation for why there are two mafic magmas.

3.2 Textures

Investigation of the samples revealed a number of micro- and macroscopic textures within the samples and crystals. These textures provided a number of clues to help identify the different processes that were happening pre- and syn-eruption. On the macro scale, the pumices featured a number of banding textures distinguished by colour, as well as hosting abundant mafic magma enclaves. These were also present on the micro scale and as antecrysts.

The pumices retrieved were either white, grey or showed bands of varying thicknesses. The initial interpretation was that these were likely chemical differences resulting from mixing of the dacite and basaltic-andesite magmas, however, examination of these bands using a scanning electron microscope (SEM) showed that the difference was actually entirely physical, with the darker colour being caused by smaller and less well-formed bubbles with thicker bubble walls (Fig. 1). Curiously, these regions within the pumice were also typically associated with small enclaves of mafic magma, which are generally hotter than more silicic magmas (see section below). Therefore the bands could be interpreted as regions where localised heating had occurred and affected the vesiculation of the magma during eruption.

The presence of enclaves within the eruptions products was another very important clue for the interpretation of the magmatic system. Again, the initial interpretation was that the enclaves were the result of mixing of the basaltic-andesite within the dacite. However, a comparison of the mineralogy of the clasts immediately showed that this was unlikely. Whereas the mafic scoria found had the phenocryst assemblage clinopyroxene-olivine-plagioclase, the mafic enclaves had

the simpler assemblage amphibole-plagioclase, which is the same as was present in a large number of the dacite pumices.

3.3 Thermobarometry

Another important finding used the composition of the mineral phases, specifically amphiboles, to provide estimates for the temperature and pressure conditions within the magma chamber before eruption. This information is vital for us to understand the processes that were ongoing below a volcano before it erupted and what conditions lead to the eruption. In this case, we found that the amphiboles recorded a very wide continuous range of temperatures and pressures from 180-635 MPa and 860-1015°C. Cross-referencing these conditions with the sampling location and the position in the stratigraphy, it is possible to see that the first material erupted was from the shallowest parts of the magma chamber, and the last material was the deepest. Previous research into the storage conditions have produced much more varied estimates of storage conditions (Singer et al., 2014; Scott et al., 2013; Andrews, 2014). These new estimates overlap the previously published results and also suggest that the magma was stored over a wider and deeper range.

As the mafic enclaves also contained amphiboles, it was possible to use the same thermobarometric method to estimate its storage conditions. These revealed a large overlap between it and the deepest and hottest of the dacite hosted amphiboles (940-1015°C, 300-550 MPa). These enclaves have a large range of sizes and volumes present suggesting variables amounts of mixing and disaggregation. They are found within nearly every pumice sample analysed, so mixing was likely extensive pre-eruption. The precise nature of the relationship between the three magmas is hard to identify, but due to the similarity of the amphiboles present in the two hosting magmas, they are likely related in their genesis. Fractional crystallisation of amphibole and plagioclase from the remnant basaltic-andesite formed and separated the dacite, and after the introduction of a heat source i.e. the recharge of event of basaltic-andesite, the older mafic material was mixed within the dacite. Research on the ongoing lava dome eruptions has suggested that a large, chemically stratified magma chamber exists beneath Santa María, and mixing of the lower-most regions of the system could explain the presence of the enclaves. Large differences in temperature and viscosity probably then precluded the recharge magma from physically mixing with the dacite.

4 Conclusions

The 1902 eruption of Santa María volcano was a very strange eruption. After 25,000 years of repose, the volcano erupted with a tri-modal composition, containing a large (around 8 km^3) proportion of dacite as well as minor amounts of two mineralogically distinct mafic magmas, one of which was erupted as scoria at the end phase of the eruption but showed no signs of physical mixing with the rest of the erupted magmas, and one which had been physically mixed into the dacite and was erupted as enclaves in the pumice. The dacite and the enclaves overlapped significantly in terms of their estimated storage conditions (180-635 MPa and 860-1015°C for the dacite and 300-550 MPa and 940-1015°C for the enclaves).

5 References

Andrews, B. J. (2014). Magmatic storage conditions, decompression rate, and incipient caldera collapse of the 1902 eruption of Santa Maria Volcano, Guatemala. *Journal of Volcanology and Geothermal Research*, 282:103–114.

Scott, J. A., Pyle, D. M., Mather, T. A., and Rose, W. I. (2013). Geochemistry and evolution of

the Santiaguito volcanic dome complex, Guatemala. *Journal of Volcanology and Geothermal Research*, 252:92–107.

Singer, B., Jicha, B., Fournelle, J., Beard, B., Johnson, C., Smith, K., Greene, S., Kita, N., Valley, J., Spicuzza, M., et al. (2014). Lying in wait: deep and shallow evolution of dacite beneath Volcán de Santa María, guatemala. *Geological Society, London, Special Publications*, 385:SP385–2.

Williams, S. N. and Self, S. (1983). The October 1902 plinian eruption of Santa María volcano, Guatemala. *Journal of Volcanology and Geothermal Research*, 16(1-2):33–56.

Catherine Goddard | Mike Coward Fund – £1000 | Progress Report

What can be inferred about the strength of the lower crust from examining the roots of exhumed fault zones?

Motivation

Major crustal-scale faults have long been recognised as complex systems combining an earthquake prone (seismogenic) upper-crustal portion and an aseismic lower-crustal portion. Measurements from boreholes tell us that the upper crust is strong when it is intact, but the cores of faults in the upper crust can be weak. The strength of the lower crust, both outside and within faults/shear zones, remains a major outstanding research question. Therefore, this project is motivated by the question: **'What can be inferred about the strength of the lower crust from examining the roots of exhumed fault zones?'** One way of quantifying the strength of the lower crustal segments of fault zones is to examine evidence for previous steady-state flow stresses that are preserved in ancient shear zones - an approach termed 'paleopiezometry'. I have developed a new method of measuring historical stresses in multi-mineral rocks, based on the average size of misoriented crystallographic domains within grains, termed 'subgrains'. I have collected samples in order to employ this 'subgrain piezometer' to determine the strength of the lower crustal portion of a major continental-scale fault zone, The Great Slave Lake Shear Zone (GSLSZ), Northwest Territories, Canada. This locality was once an active transform fault, joining two tectonic plates during the Proterozoic.

Fieldwork – August 2018

Stretching 25km in breadth, the GSLSZ is one of the widest shear zones documented to date. Petrological studies of the area provide evidence of granulite facies conditions (temperatures of 650–1100°C and pressures of 3–10 kilobars) making the GSLSZ a type example of the mature deeper sections of brittle faults. Four of us worked in the field for a total of 10 days. In addition to me, this included my two supervisors, Prof. Lars Hansen (Oxford) and Dr David Wallis (Utrecht), and a collaborator, Brendan Dyck (Simon Fraser), who joined the team to advise on metamorphic petrology. Two transects across the shear zone were made, one to the north and one to the south of our basecamp location. The rocks were everything we had hoped for– mylonites as far as the eye could see. Great exposure meant we were able to extract samples at regular intervals across the shear zone. Each day we would conduct our 'hit and run geology', trailing from outcrop to outcrop snatching samples for latter SEM analysis. For one day of the fieldwork we were fortunate enough to have Dr Edith Martel, Northwest Territories Geological Survey, join us with a helicopter. This enabled us to extend our transect to the furthermost extent of the GSLSZ. In addition to incredible rocks, we found ourselves having a number of equally exciting interactions with other residence of the area. There was 'Mikey' the 200+ kilo musk ox who had a Mexican standoff with two of our group, the local beaver, who would swim lazily past each evening, and not forgetting the two bears, Brutus and Heidi. Thankfully, the latter pair never got too close for comfort. What did get much too close, and caused considerable discomfort, were the hordes of mosquitoes.

Laboratory work – 2019

The majority of the work on the project will take place during the coming year. Currently ~50 rock samples from the GSL shear zone have been thin sectioned. At the beginning of December, I travelled to Utrecht University to use their automatic polisher in order to prepare the thin sections for EBSD analysis in the New Year. I shall apply our new piezometer to these samples, exploring the stress distribution across the shear zone, spanning rocks deformed at all depth levels in the mid-lower crust, as well as local stress variations around structures such as hard, mafic enclaves. One such enclave has been mapped already and can be seen in the figures below. **As soon as this analysis is complete I will submit a full report of my fieldwork to The Geological Society**. I will also be presenting this work at the Holsnøy seminar on lower-crustal earthquakes in Norway next June.

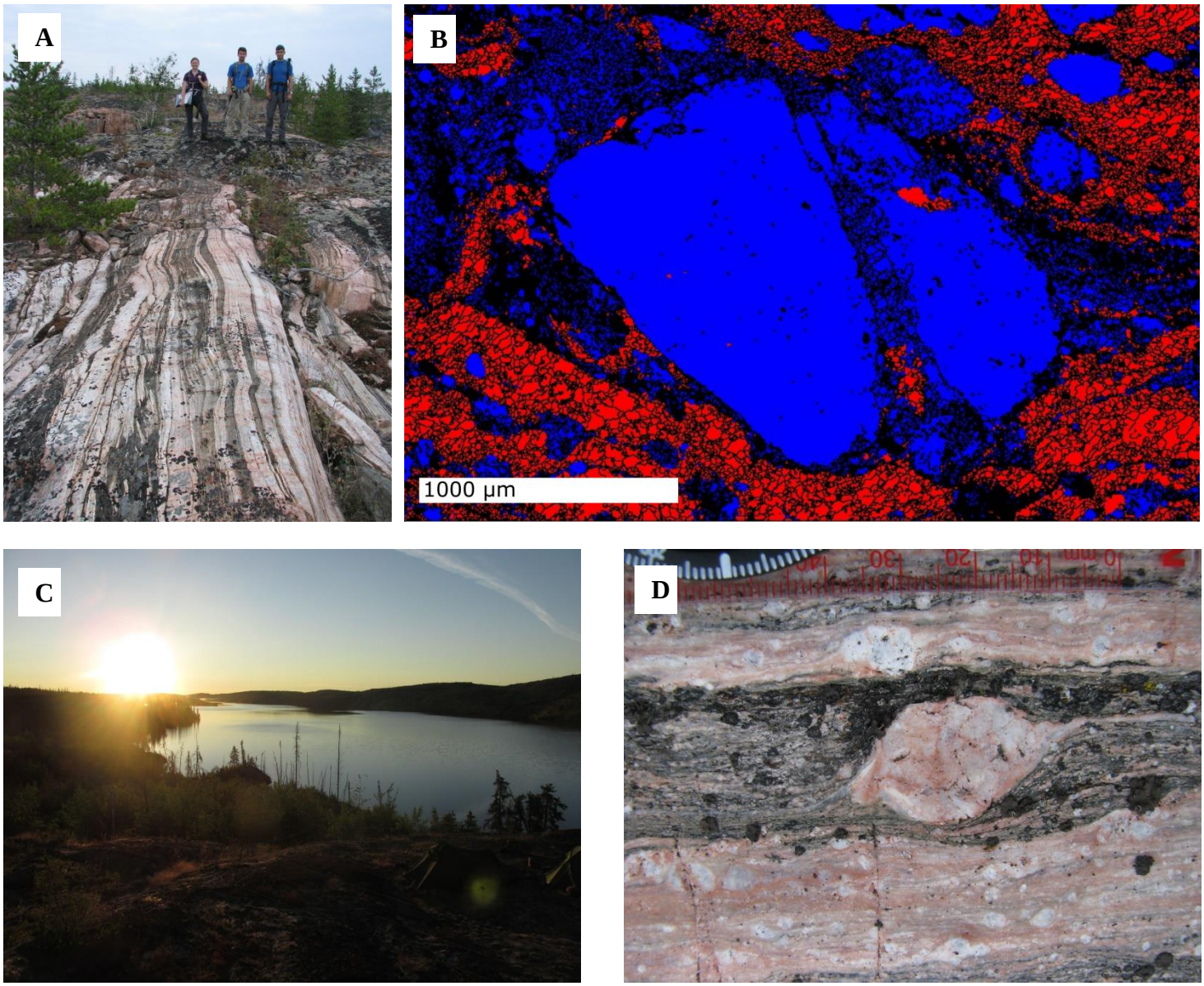

Figure 1: A) Mylonites from the Great Slave Lake shear zone, B) Electron backscatter diffraction map (EBSD) of a porphyroclast of feldspar (blue) surrounded by deformed recrystallised quartz (red). The back lines represent the grain boundaries. C) Photograph of our basecamp lake. D) feldspar porphyroclast.

Name: Joshua Grinham (jg223@st-andrews.ac.uk)

Subject: Out-of-Phase Magnetic Susceptibility

Funding Received: £1,050

Using imaginary magnetic susceptibility for the analysis of rock and mineral samples is an intriguing concept when first encountered, although of course when you realise its name stems from the mathematical concept of imaginary numbers your eyes may begin to glaze and it does lose a little of its exciting spark. The name I prefer is out-of-phase, less exciting but more descriptive. The phenomenon is a quirk of measuring a substance's magnetic susceptibility in an alternating magnetic field - ie. one produced with alternating electric current as opposed to direct current. But first let's begin with basics; what is magnetic susceptibility?

'Real' or in-phase magnetic susceptibility is a measure of the magnetic response to an applied magnetic field, stemming ultimately from the electron distribution in the material in question. When this applied magnetic field is constant, this relationship is defined by the following equation:

$$M = kH$$

Where ***k**, volume susceptibility,* is the ratio of the magnitude of the magnetisation *(per unit volume)*, ***M***, of the material to the strength of the applied field, ***H***.

In a time-varied scenario as involved with an alternating field this becomes a tad more complex. The equation representing the field becomes:

$$H(t) = H_0\cos(\omega t)$$

whilst that representing the magnetisation of the material becomes:

$$M(t) = M_0\cos(\omega t)$$

For many materials the ratio M_0/H_0 does not vary significantly through time, meaning this ratio continues to define the magnetic susceptibility of the material. However, things get interesting when this is not the case. Imagine instead that the susceptibility varies not in perfect harmony with the applied field, but instead a lag exists - ie. that there is a 'phase difference' between the two. If we call this lag between the two Δt the equation for M(t) above becomes:

$$M(t) = M_0\cos(\omega t-\Delta t)$$

Now we have a field which is still varying according to the equation for H(t), but a magnetisation that is varying out of time with it to the tune of Δt. There is a phase difference, δ, between the two. It is here that the out-of-phase in out-of-phase magnetic susceptibility comes in. Mathematically, saying something is out-of-phase is the same as saying there are two components to the magnetisation - one of which varies in time (in-phase) with the field, and the other varying out of time (out-of-phase). This brings us to the next logical step; if there is an in-phase and out-of-phase component of magnetisation there must in turn be an in-phase and out-of-phase definition for *k*, henceforth referred to as ip*K and* op*K* respectively. This is old news - Louis Néel dealt with these concepts in 1949 - but as Mike Jackson put it in his article on the subject in 2003 'imaginary susceptibility remains an obscure and little-discussed concept in rock magnetism, despite being both quite useful in sample characterisation and rather interesting in its own right'. This is a state of affairs that he puts down mostly to the lack of commercial magnetic susceptibility instruments at the time using alternating fields for measurements.

This is beginning to change. With the AGICO KYL5-A Kappabridge in the M^3ORE laboratory at the University of St. Andrews we are able to measure not only bulk out-of-phase susceptibility but also its variation with temperature (from -192°C up to 700°C), field strength and orientation; all of which are measured simultaneously with the traditional in-phase result. Already researchers using the laboratory are getting interesting results which are starting to be presented at conferences by Dr. William McCarthy, Charlotte Gordon, Vincent Twolomey, and Oliver Dixon - among others. But in order to truly exploit the potential of this technique a 'big data' approach is needed to compare the out of phase behaviours of a range

of mineralogical and rock samples and create a reference database that can be used for sample characterisation.

It is this approach that we, thanks in large part to the generosity of Geological Society of London's grant, have been able to start over the course of this last year. A computer program has been written to extract the raw magnetics data from the propriety data file formats used by the M^{3}ORE laboratory equipment to both produce a user friendly EXCEL worksheet of the results as well as begin the process of populating a mySQL database server with the data collected in the lab for future studies. Although functional it is very much still in development, with plans to increase compatibility with older file formats and those used by equipment in other university labs. The end goal is making a program that has the potential to be used in any rock magnetics laboratory to process data and populate a common large reference database.

As suggested earlier, part of the the work undertaken this year was to begin building this reference database using the result of analysis run on 'standard' mineralogical samples. Already over 130 referenced samples have been collected in the lab and processed for out-of-phase bulk and field dependent susceptibility - with many having also been investigated for variation with temperature as well. These results are already influencing the research output of the laboratory, with two posters due to be presented at conferences in January building on results showing that high conductivity materials not traditionally regarded as having useable out-of-phase susceptibilities, such as copper, have significant ones. This new knowledge is already showing positive potential; the most promising is the prospect of being able to provide directional information about the progression of alteration in granite porphyry deposits through the use of out-of-phase Anisotropy of Magnetic Susceptibility. Whereas the in-phase magnetic fabric is dominated by the primary fabric of the granite, predominately multi-domain magnetite, the secondary fabric of alteration is captured by out-of-phase minerals - information that until now has been lost using the traditional methods. Although this work is still ongoing, it also shows the possibility of using out-of-phase susceptibility for identifying the minerals involved in this alteration.

In summary, this is work that has exciting potential. Use of magnetic susceptibility is already well established. Traditionally in-phase magnetic susceptibility and its variation with temperature, field strength, and frequency has been widely applied in mineral classification, grain size determination and magnetic fabric orientation. However it is typically dominated by a single magnetic mineral phase and valuable information that could be derived from the other mineral phases present is lost through saturation of this in-phase signal. Out-of-phase magnetic susceptibility measured simultaneously and as a distinct component of susceptibility offers a solution to this problem. Hopefully, the age of it being just an 'obscure and little-discussed concept' is soon to be replaced by one in which it is common place to use both in-phase and out-of-phase susceptibilities side-by-side.

Figure 1: *Roldan Fan – Early Miocene alluvial fan deposits, northern margin of Ebro Basin*

Geological Society Research Grant Report

Awardee: Daniella Guy
Title: Facies variations at a continental basin margin, Ebro Basin, northern Spain
Award: Elspeth Matthews Fieldwork Grant
Amount: £1165

Summary

Models for the distribution of facies in continental basins typically assume basin-margin alluvial fans, axial river systems and basin-centre lakes (e.g. Gawthorpe & Leeder 2000). Subsurface data from hydrocarbon bearing basins has shown that the facies relationships are more complex and a new understanding of basin-margin depositional patterns is required. Excellent exposures of early Miocene deposits along the northern margin of the Ebro Basin in Northern Spain provide an opportunity to examine the relationships between locally-derived alluvial fan deposits, larger-scale fluvial systems and localised lacustrine facies in detail.

Background

The Ebro Basin is a foreland basin which formed in the late Oligocene to Miocene as a response to flexural loading by the Pyrenean orogenic belt. In the area north of Huesca, previous work (Nichols & Hirst, 1998; Nichols & Thompson, 2005) on Early Miocene exposures has shown that the alluvial Roldan and Nueno Fans occur at the basin margin and lacustrine facies in between around the village of Sabayes. Huesca Fluvial System deposits are coeval with these marginal facies and are well exposed at Lierta nearby. The Ebro Basin was endorheic at this time, with sediments aggrading in the basin centre for many hundreds of metres, extending kilometres across, making it possible to correlate coeval facies.

In 2018, I had the opportunity to visit this area of northern Spain (Figure 2), to investigate the continental facies relationships at the basin margin during fieldwork supported by funds awarded from the Elspeth Matthews Fieldwork Grant. Detailed mapping the facies boundaries provided a case study for continental facies relationships for hydrocarbon reservoirs in the subsurface, where abrupt lateral facies variations may occur and hence reservoirs in wells only a few hundred metres apart may vary significantly in character.

These studies contributed to my Petroleum Geoscience Masters' project whilst studying at Imperial College London and form the basis of a research paper in progress with colleagues Gary Nichols, Phil Hirst and Amanda Owen.

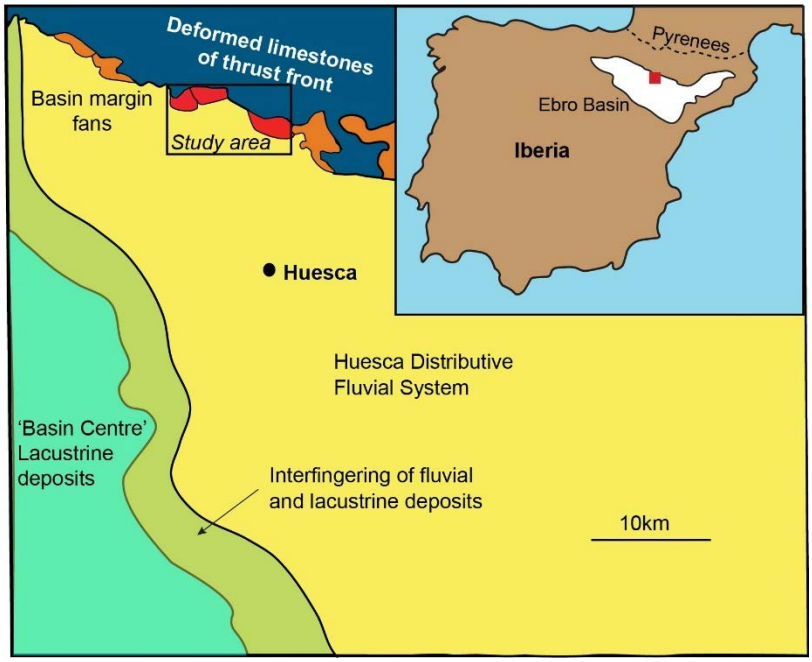

Figure 2: *Location map of the study area of the Ebro Basin, northern Spain*

Fluvial facies

The Huesca System is a Distributive Fluvial System (sensu Weissmann *et al.* 2010) that extends up to 50 km south from the northern boundary of the Ebro basin and forms the majority of the Sariñena Formation. The fluvial deposits can be broadly split into: (1) lenticular to sheet-like sandstone fluvial channel bodies and (2) mudstone and thinly-bedded sandstone floodplain deposits (Nichols & Hirst, 1998).

Fluvial channels range from ribbon forms (Width:Thickness ratio <15:1) less than 1 m-thick and a few metres wide, to more sheet-like sandstone bodies (W:T >15:1) with thicknesses up to 12 m and over 100 m in width (Gibling, 2006; Nichols & Hirst, 1998). Sandstone bodies are dominantly single river channel fills. Amalgamation of larger bodies is common, representing multiple scour and fill events and are often vertically or multi-laterally stacked. Evidence for lateral migration of channels can also be seen in lateral accretion surfaces.

Fluvial channels in the study area are on average 4 m-thick, they are medium-grained sandstones and often exhibit fining up successions. Huesca fluvial sandstones are petrographically distinct due to their presence of biotite-mica, derived from the granodiorite in the axial zone of the eastern Pyrenees (Hirst & Nichols 1986). Overbank deposits consist of interbedded thin sandstones and siltstones and are often weathered pale beige. Paleosol development is common within the overbank deposits, as pale red horizons approximately 20 cm-thick. The fluvial outcrop at Lierta is located 3 km south of the basin margin (Figures 2 & 3). Here, a 'ribbon' channel (W:T 1:10) can be

observed, with a deep scour. Lateral accretion surfaces suggest a WNW palaeoflow indicating that rivers depositing this sandstone body flowed parallel to the basin margin.

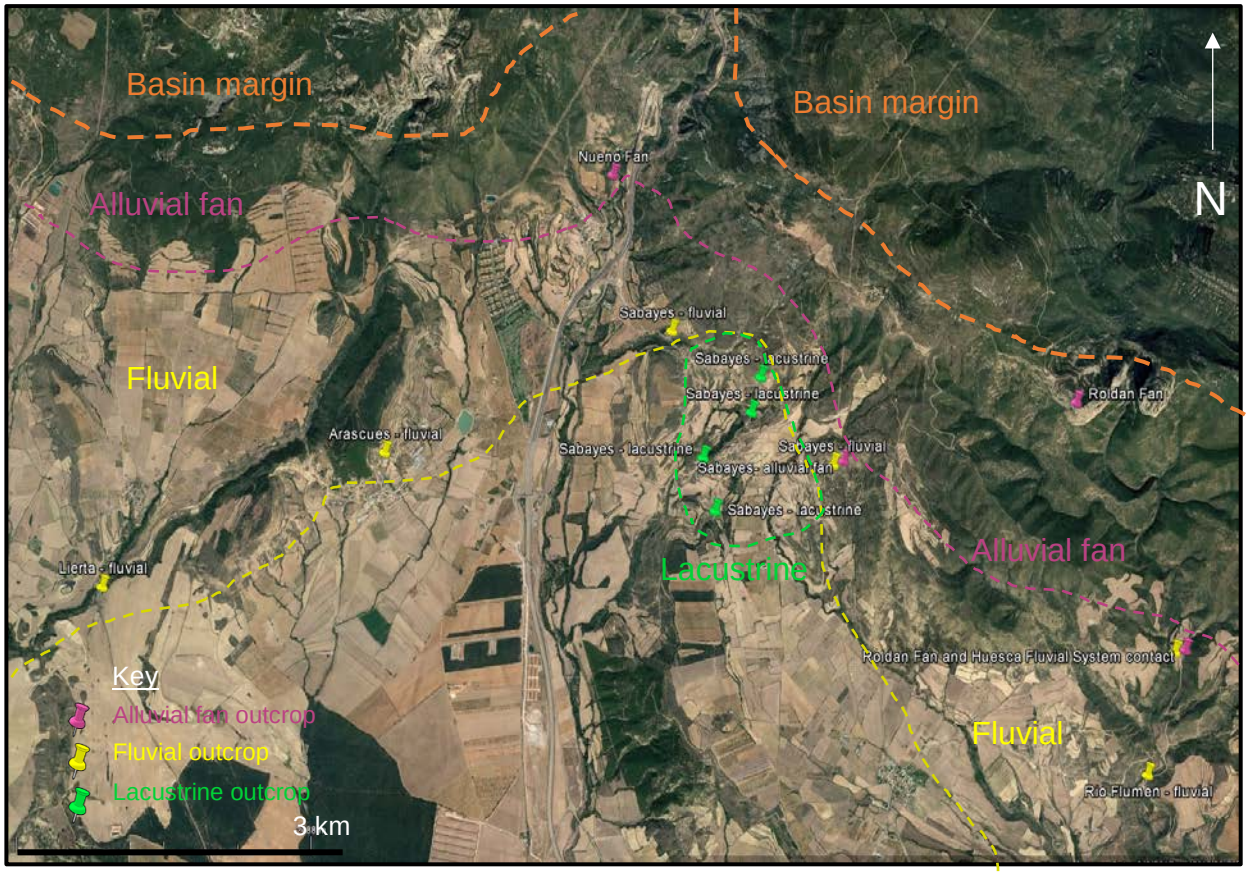

Figure 3: *Location map of fieldwork outcrops (Google Earth, 2018)*

Figure 4*: Fluvial outcrop at Lierta displaying 'ribbon channel', 3 km south of the basin margin*

Lake facies

Lacustrine limestones were recorded by Nichols and Hirst (1989) as interfingering with the distal Roldan fan facies and these occur in the area of Sabayes village (Figure 2).

The lacustrine facies consist of reddish-beige, thinly-bedded fine sandstones to siltstones. Wavy lamination is recorded in some of the fine sandstone beds, indicating a standing body of water. Climbing ripple lamination is seen in the outcrop, suggesting relatively high sedimentation rates. Thin, horizontally-laminated sandstone beds suggest sediment influxes into the lake, while thicker beds of sandstone which have petrographic the characteristics of the Huesca System are inferred to be terminal splays within a background of fine-grained lacustrine sandstones and siltstones.

An outcrop 4 m high and 20 m wide nearby Sabayes village contains lacustrine sediments with common wavy laminations and vertical *Skolithos*-like trace fossil burrows, suggesting the lake was relatively stable at this time (Figure 5). If the total thickness of the mapped lake deposits is taken as 50 m, then based on sedimentation rates, the lake would have existed for over 500,000 years (pers. comm. G. Nichols).

Figure 5: *Lacustrine facies showing wavy laminations and vertical trace fossils at Sabayes*

Walking up through the stratigraphy in the Sabayes village area, a contact is observed between the Huesca fluvial deposits and the lacustrine deposits (Figure 6). This outcrop is younger than the 20 m-thick outcrop that shows wavy laminations and vertical trace fossils. The Huesca Fluvial sandstone is medium-grained, 3 m-thick and is estimated as 65 m wide. The presence of this sandstone body indicates a return to a more fluvial-dominated environment and drying out of the lake.

Figure 6: *Interfingering of thinly-bedded lacustrine sandstones and siltstones and Huesca Fluvial sandstone, near Sabayes village. Notebook for scale resting on the lacustrine facies, with 3 m-thick fluvial sandstone above.*

Lower in the stratigraphy, the presence of nodular gypsum in red-beige mudstones suggests a lake margin setting, as this forms at the sediment-water interface (Figure 7). A contact between the lacustrine and alluvial fan facies is difficult to establish due to lack of outcrop exposure in this area. However, the nodular gypsum in the lacustrine sediments suggests an interaction of the lake and alluvial fan deposits: the calcium sulphate in the water (evidenced by the gypsum) was likely derived from the Nueno fan, which occupies the area northwest of the lake facies (Figure 3).

Figure 7: *Thin, nodular gypsum layers (white) in red-beige mudstones, suggesting a lake margin setting near Sabayes village.*

Alluvial fan facies

Figure 1 displays Early Miocene Roldan Fan deposits. The alluvial fan facies here are comprised of lenticular sheet sandstones, with conglomerates higher in the stratigraphy, which were deposited by sheetfloods.

At Rio Flumen, interfingering of the Roldan alluvial fan and the Huesca System fluvial deposits can be observed in the valley, approximately 5 km south of the basin margin (Figure 8). River channel deposits of medium to coarse-grained, biotite mica-rich sandstone are incised into underlying distal, fine-grained sandstone to siltstone alluvial fan deposits. Palaeoflows in the Huesca System sandstone indicate fluvial channels flowed over the fan surface towards the southwest. Fluvial channels at this locality are sheet-like sandstones, with W:T 1:50 and are predominantly single-storey, isolated channels which are occasionally vertically or offset-stacked. The fluvial channels do not appear to have cut into alluvial fan. Thus, the alluvial fan toe topography must have been low or absent during this time to exhibit the interfingering relationship between the two facies.

Figure 8: *Huesca Fluvial deposits interfingering Roldan alluvial fan deposits, 5 km south of the basin margin.*

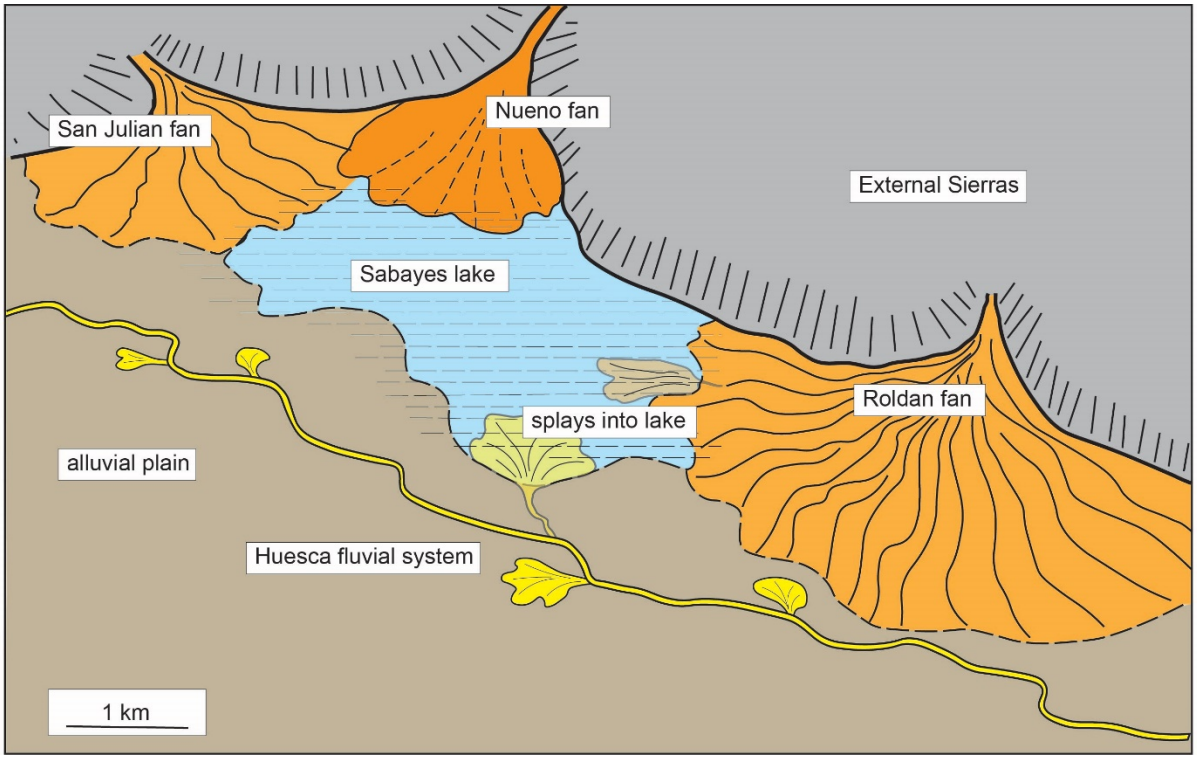

Figure 9: *Palaeogeographic sketch to show the relationships between alluvial fan, lacustrine and fluvial facies at the basin margin*

Conclusion

The funds from the Elspeth Matthews Fieldwork Grant enabled the mapping of the fluvial, alluvial and lacustrine facies boundaries in the Ebro Basin, northern Spain. The fieldwork data collected have provided further insight into the palaeography of the study area and interpretations of the interactions between the river, fan and lake settings adjacent to the basin margin. This study has resulted in a new conceptual model (Figure 9) that is applicable to a range of continental margin settings and allows a case study for subsurface reservoirs which display similar facies relationships.

References

Gawthorpe, R.L. & Leeder, M.R. (2000) Tectono-sedimentary evolution of active extensional basins. Basin Research, 12,195–218.

Gibling, M., R. 2006. Width and Thickness of Fluvial Channel Bodies and Valley Fills in the Geological Record: A Literature Compilation and Classification. Journal of Sedimentary Research, 76 (5), 731-770.

Hirst, J.P.P. & Nichols, G.J. 1986. Thrust tectonic controls on alluvial sedimentation patterns, southern Pyrenees. In: Foreland Basins, (eds P.A. Allen & P. Homewood). International Association of Sedimentologists Special Publication, 8, 153-164.

Nichols, G.J. & Hirst, J.P.P. 1998. Alluvial fans and fluvial distributary systems, Oligo-Miocene, northern Spain: contrasting processes and products. Journal of Sedimentary Research, 68, 879-889.

Nichols, G.J. & Thompson, B. 2005. Bedrock lithology control on contemporaneous alluvial fan facies, Oligo-Miocene, southern Pyrenees, Spain. Sedimentology, 52, 571-585.

Weissmann, G.S., Hartley, A.J., Nichols, G.J., Scuderi, L.A., Olson, M., Buehler, H. & Banteah, R. 2010. Fluvial form in modern continental sedimentary basins: Distributive Fluvial Systems (DFS). Geology, 38, 39–42.

Geological Society Research Grant Report

Awardee: Julie Harrald, The Open University (PhD Supervisor: Angela Coe)
Title: Use of an unmanned aerial vehicle as a tool for mapping complex foreshore deposits.
Award: Annie Greenly Fund
Amount: £1323

Introduction and objectives

The foreshore of NE Scotland, near Helmsdale (ND 030 153) exposes an important succession of Upper Jurassic deposits but presents a challenging environment for recording them to a uniform standard and especially for recording the lateral variation of the beds. The deposits are almost entirely only exposed between the high and low water levels, so field work is only possible around low tide. The tidal range is 3.7 m and the foreshore is 30 – 100 m wide. The beds are faulted and folded but generally young to the north and dip between 5° and 35°. The elevation of the exposure is variable along the foreshore, creating permanently flooded areas, and sheltered areas where seaweed, sand and cobbles accumulate (Figure 1).

Figure 1. The foreshore near Helmsdale.

There are two facies associations in the section: breccias which form reefs, and mudrocks and sandstone which are exposed at a low level (Figure 1). Some of the breccias are stacked to accumulate thicknesses of tens of metres and some occur as isolated beds less than a metre thick. Detailed logging during the PhD project has suggested that the breccias not only vary in thickness but also in lateral extent and geometry. This variability is of significance as it is interpreted to reflect their genesis.

It became evident during fieldwork in 2017 that aerial images of the coastline would provide a more complete overview of the spatial relationship of the deposits than can be obtained by traditional methods. This would also highlight structural features, as well as providing close-up views of beds surrounded by water at low tide. Currently available aerial images for this foreshore are of low resolution, variable quality or taken at high tide.

The grant awarded by the GSL has been used to support a survey using an unmanned aerial vehicle (UAV or drone) to collect high quality images (capturing objects <30 cm in size; Figure 2) along a 5 km section in the brief window of time when the rocks are exposed either side of low tide. The first, highest priority objective of the study was to obtain detailed aerial imagery to provide new perspectives on this sedimentary succession. Whilst the use of drones for structural studies and geohazard monitoring is widespread (e.g. Bemis *et al*., 2014; Vollgger & Cruden, 2016; Mori *et al*., 2016), there are few publications, as yet, of the use of drone imagery to support sedimentological interpretation (e.g. Nieminksi & Graham, 2017). A secondary objective was therefore a short methodology paper on the use of a drone as a tool for the recording of sedimentary deposits in a foreshore setting. The third objective was to resolve disagreement in published maps of the region.

Research undertaken

Preparation

The drone field campaign was carefully planned in advance with the lead and assistant drone pilots, Rick Thomas and Murray Hoggett (University of Birmingham). During the planning we reviewed maps and ground photographs of the foreshore, identified access points, agreed the objectives of the exercise and decided the minimum image resolution that would be required to facilitate subsequent sedimentary analysis. The section was divided into five parts, each of which could be flown within the tide window on one day. These sections were placed in a priority order, in case problems in the field, such as inclement weather, prevented us from completing data collections.

Permission for our proposed work was confirmed with local landowners, including private farmers, a community land holding group and the Duke of Sutherland's Estate. The flight lines were planned and the flight times and battery requirements calculated for each flight section. Arrangements and procedures were also agreed with the Civil Aviation Authority and military bases in NE Scotland, as the area is within restricted airspace (i.e. military low flying between 100 – 250 feet).

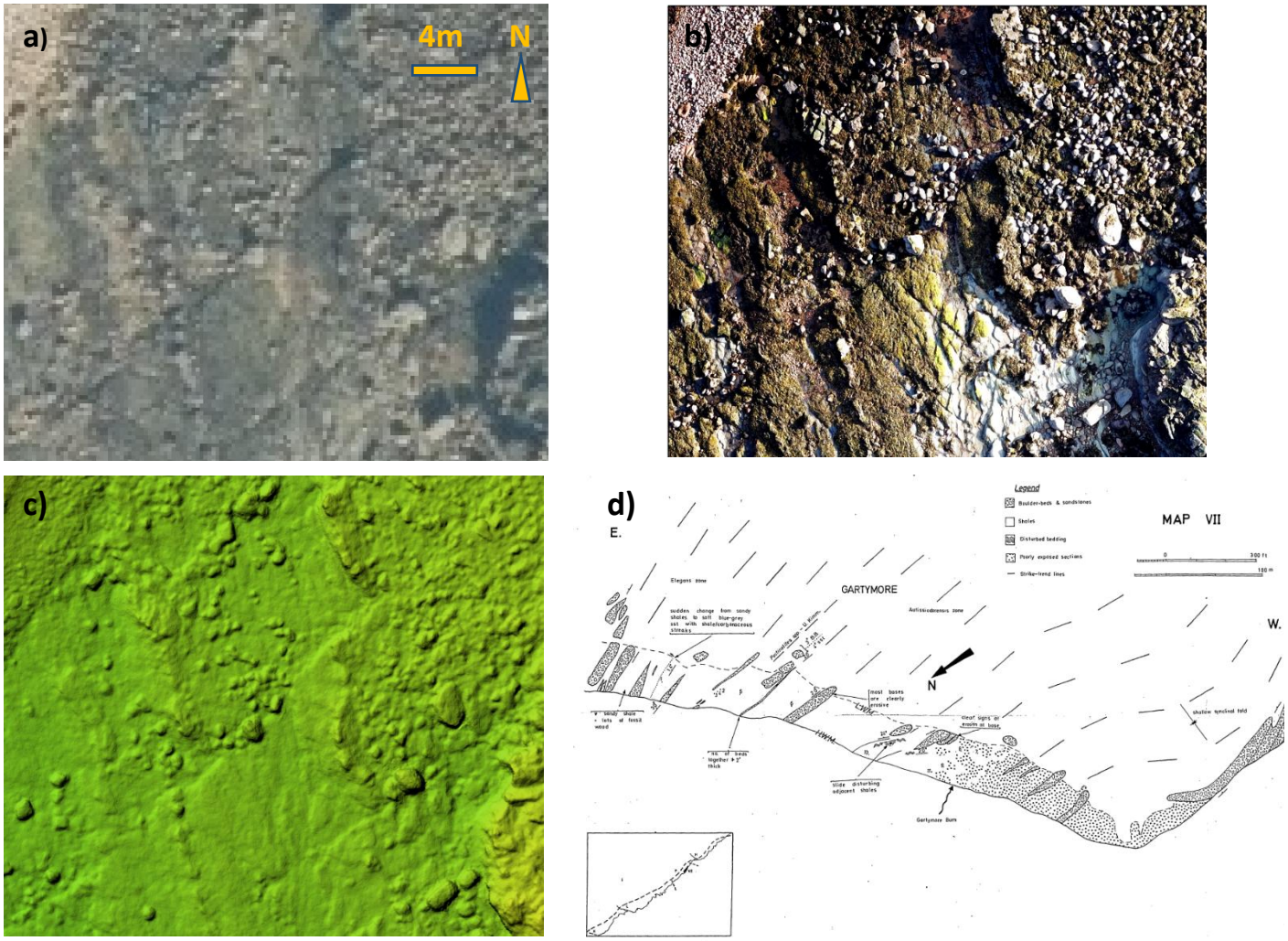

Figure 2. Detail of area shown in orange box in Figure 3. a) OS MasterMap image 2016, 1 pixel = 25cm; b) Drone footage this study, 1 pixel = 1.5 cm; c) DEM from the drone data; d) Linsley's (1972) map of area in Figure 3.

Field campaign

Mid-May 2018 was chosen for the field work. This was when the low tides would be some of the lowest in the entire year, allowing us to capture footage of as wide an exposure of the foreshore reefs as possible. May is also the earliest month in the year when we could reasonably expect to have spells of calm weather, before algae cover accumulates in the summer. Two light-weight drones and one larger drone, each with 4K cameras were used. The larger drone camera also had a polarising filter enabling it to capture images through shallow water in calm conditions. We deployed two drones each day, and carried extra batteries so that we could make continuous use of the time either side of low tide.

Our field campaign was successful in all respects. There were perfectly calm conditions throughout which meant that the smaller drones, as well as the one with the polarising camera filter, were able to take images of rocks beneath the water. Unfortunately however, following the un-stormy winter in 2017-18, the seaweed and recent sediment cover remained extensive, obscuring large areas of the lower-lying beds.

Outputs

For the mapping of the foreshore, several thousand individual images were systematically recorded with overlapping flight lines (65% sidelap and 75% frontlap). These images were processed at the University of Birmingham using structure-from-motion photogrammetry methods. This produced a digital elevation model

(DEM) and a high-resolution, geo-referenced orthomosaic photograph of each of the five sections. A 3D terrain model of each section was produced from the DEM and the high-resolution images. In addition, close-up photographs and videos were taken of the most seaward breccia beds that were inaccessible on foot, to extend / clarify the data gathered by traditional field work.

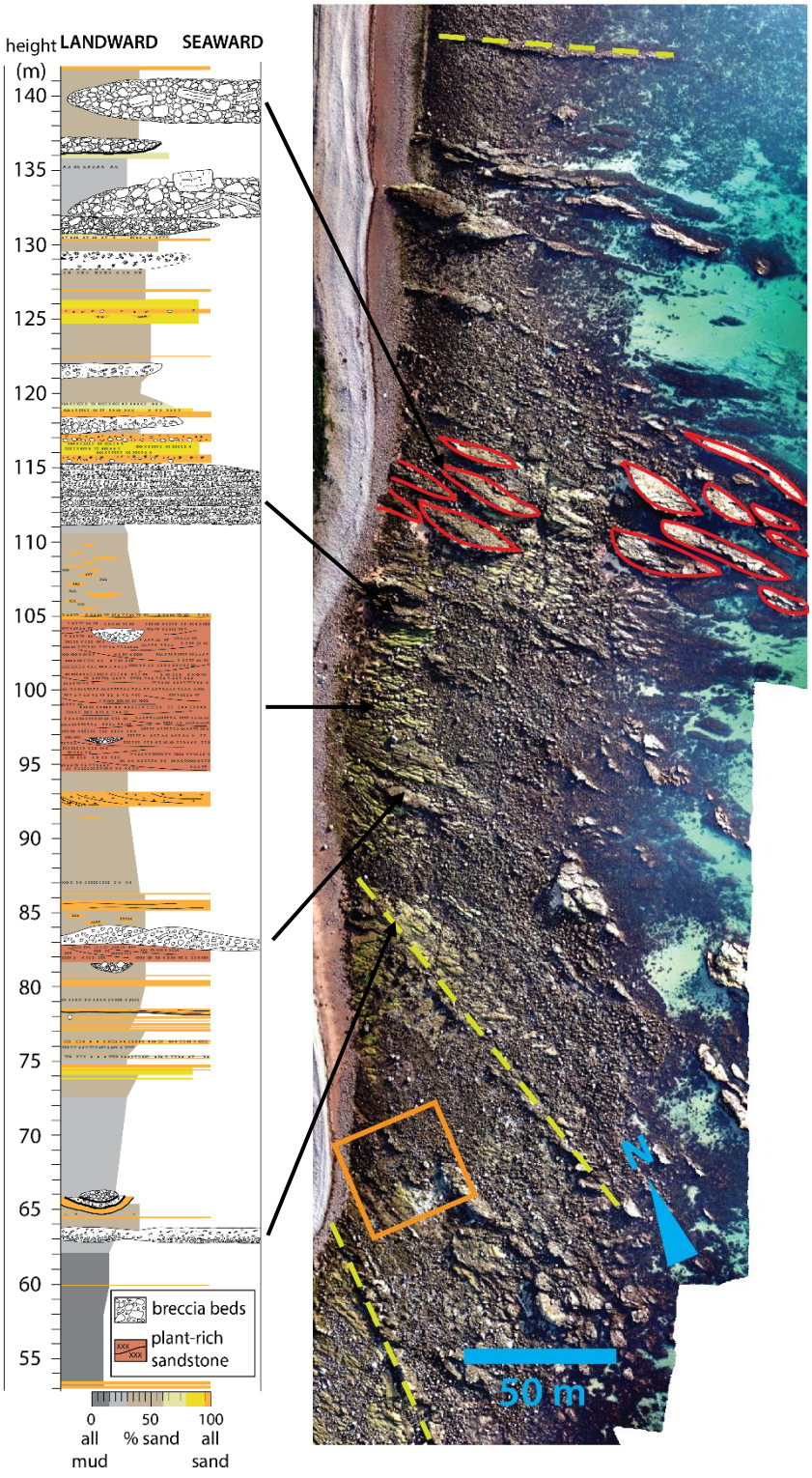

Figure 3. Graphic log and orthomosaic photograph of a 500 m section from this study. The orange box indicates the area covered by Figure 2.

The best aerial imagery available of the foreshore prior to our drone work was that shot by the Ordnance Survey in 2016 (Figure 2a); the contrast in resolution with the drone footage (Figure 2b) is striking (resolution of 1 pixel = 25 cm, compared with 1 pixel = 1.5 cm). Figure 2b and particularly 2c show that there is a small fault from bottom left to top right, and possibly a second fault below this. No faulting is shown on the most detailed of the previous maps of the area (Figure 2d).

Using the new high resolution data we have been able to re-examine the field area, correlating the orthomosaic photographs of each section with the graphic logging produced from shoreline field work. Figure 3 illustrates an interval which shows variation in the lateral extent and geometry of the breccia beds (for instance, those marked in green are continuous, whilst those in red are lensoid); the drone footage reveals that these features extend seaward. Large scale folding is indicated by a change in strike from the bottom to the top of the image, highlighted by the beds marked in green.

Conclusion

The survey has provided invaluable new data, which confirms many (and refutes a few) field observations, reveals new features, provides supporting evidence for the interpretation of the breccia beds based on their shape and continuity, and identifies structure more easily than can be done on the ground. It has also been a useful exercise in the methodology and practical considerations needed to record drone footage in a foreshore location from which a method paper is being prepared. The tasks of matching the drone imagery to the field logs, mapping the foreshore and interpreting the sedimentary processes is ongoing and will form a key part of the PhD thesis and a further manuscript.

References

Bemis, S.P. *et al*, 2014. *Journal of Structural Geology*, **69**, 163-178; **Linsley, P.N., 1972.** Ph.D. Thesis. University of London; **Mori, T. *et al*, 2016.** *Earth, Planets and Space*, **68**:49; **Nieminski, N.M. & Graham, S.A., 2017.** *Journal of Sedimentary Research*, **87**, 126-132; **Vollgger, S.A. & Cruden, A.R., 2016.** *Journal of Structural Geology*, **85**, 168-187.

Chris Holdsworth: '*Understanding the mobility and fate of ecotoxic metals in high pH steel slag drainage waters*' £900 award, March 2018

Introduction

This is the progress report for the research project titled 'Understanding the mobility and fate of ecotoxic metals in high pH steel slag drainage waters' being conducted by Chris Holdsworth. The project was awarded £900 from the Geological Society in March 2018 for Inductively Coupled Plasma Optical Emission Spectrometry (ICP-OES) and Inductively Coupled Plasma Mass Spectrometry (ICP-MS) analysis of water samples taken as part of the research. As of December 2018 the project is in the final data processing stage with final write-up expected to commence in early 2019 for submission in summer 2019.

Background

Steel slag is a by-product of steel-making that is commonly discarded in heaps on-site at steel works. Worldwide production of steel slag is reported as 170-250 million tonnes per year[1] and whilst slag is increasingly reused in road aggregate and other similar materials, countries like the UK with an extensive steel-making history have substantial legacy steel slag heap quantities. When steel slag interacts with water dissolution of the lime (CaO) and metallic constituents (e.g. V and Cr) of the slag occurs. This produces hydroxyl ions that elevate solution pH and produce an alkaline leachate[2+3]. These leachates can contain concentrations of ecotoxic metals (V, Cr, etc.) that breach water quality standards. Similarly, tufa-like calcium carbonate ($CaCO_3$) precipitation in watercourses that leachates drain into can present challenges for benthic organisms[2+3]. In this study the mobility and fate of ecotoxic metals at a case study site in Consett (NE England) are examined (see Fig. 1) by performing a selection of geochemical analyses on leachate water and tufa samples. Potential opportunities for utilisation of steel slag and its associated leachates as a circular economy resource will also be explored[4+5].

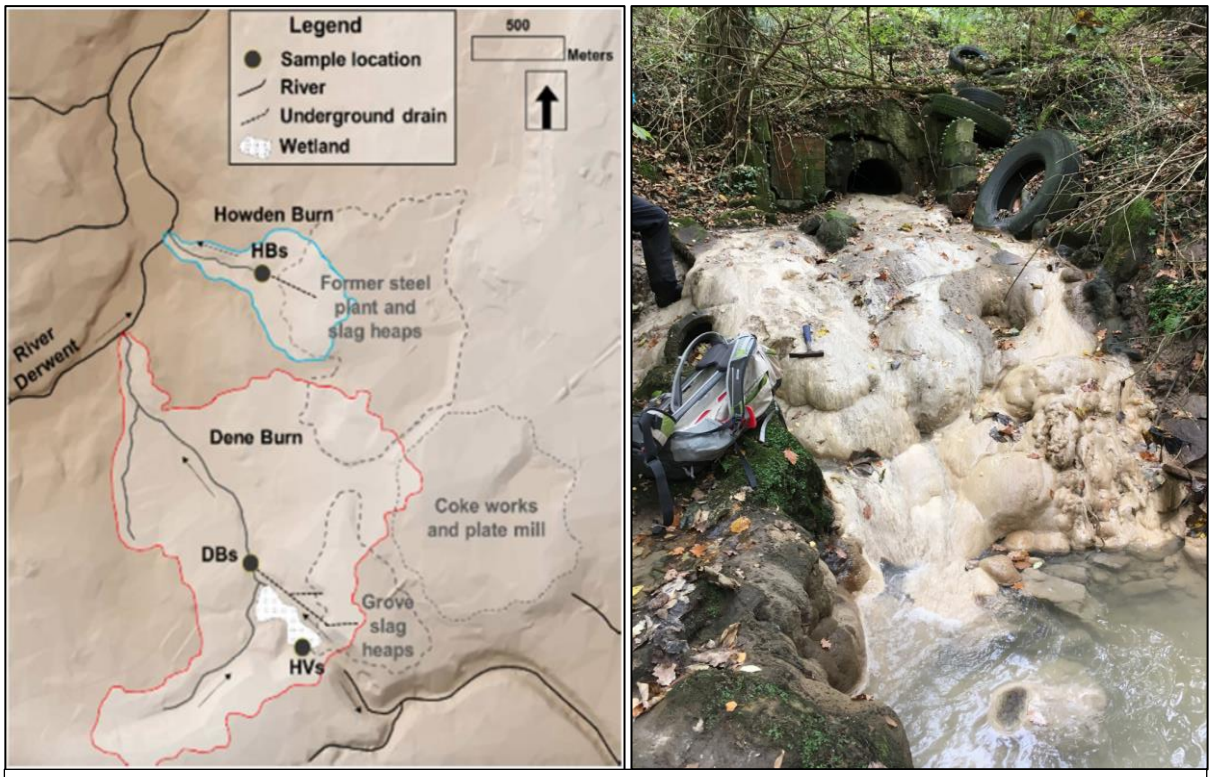

Figure 1: A map adapted from Mayes *et al.* (2018) showing the geography of the Consett steel works case study site (left) and a photograph showing the point of outflow of the Howden Burn from the steel works slag heaps where there is significant calcium carbonate ($CaCO_3$) precipitation.

Project aims and objectives

The original aim of this project as stated in the grant application was to test the hypothesis that alkaline leachates are sequestering ecotoxic metals in the Howden Burn, thus preventing any further dispersion into the wider hydrosphere and biosphere. Three specific objectives were stated:

1. What are the concentrations of ecotoxic metals in the water, tufas and slag?

2. Does ecotoxic metal concentration change downstream in water and tufa samples?
3. What are the optimal ambient conditions for metal storage (temperature, rainfall, etc.)?

Methodology

To answer the above aim and objectives a series of analyses has been conducted on leachate water and tufa samples taken across the profile of the Howden Burn. The analyses performed are as follows:

- ICP-OES and ICP-MS analysis of water samples taken at 5 points across the Howden Burn profile from first emergence from the slag heap ('spring') to the confluence with the River Derwent – water samples were taken in October 2017, February 2018 and July 2018 to account for seasonal variations in temperature and precipitation*** [objectives 1 & 2]**
- ICP-OES and ICP-MS analysis of 3 bulk rock tufa samples taken from top, middle and bottom Howden Burn profile points and bulk rock steel slag heap samples **[objectives 1 & 2]**
- Laser Ablation ICP-MS (LA-ICP-MS) analysis of 3 tufa samples taken from top, middle and bottom Howden Burn profile points and steel slag heap samples **[objectives 1, 2 & 3]**
- Clumped isotope analysis of 2 tufa samples taken from the top and bottom of the Howden Burn profile **[objective 3]**

******funded by £900 granted from The Geological Society in March 2018*

As outlined, the three sets of water samples taken between 2017 and 2018 allow for an assessment of the seasonal controls on ecotoxic metal concentrations in the Howden Burn system (temperature, precipitation, etc.). Similarly, bulk rock and LA-ICP-MS analysis of tufa and steel slag heap samples allows for a comparison between inter and intra-sample metal concentrations. Clumped isotope analysis focuses on the thermal controls on tufa precipitation both at the top and bottom of the Howden Burn system (inter-sample), and through time (intra-sample).

Current progress

As of December 2018 all of the analyses listed above have been carried out at facilities across The University of Glasgow [LA-ICP-MS], Scottish Universities Environmental Research Centre (SUERC) [ICP-OES & ICP-MS] and Imperial College London [clumped isotopes]. The water ICP data and clumped isotope data have now been processed, whilst the LA-ICP-MS data is currently still being processed. Given the £900 awarded by The Geological Society was used for ICP water analysis, the remainder of this report will focus on that dataset.

The three sampling dates for water in the Howden Burn captured a variety of temperature and precipitation scenarios, including relative weather extremes. February 2018 water samples were taking during the week preceding 'Beast from the East' and followed a wet winter. Conversely, July 2018 water samples were taken following weeks of abnormally dry and warm weather. These contrasting hydrological scenarios are reflected in the data gathered on these dates (see Fig. 2) – metal concentrations in Howden Burn flow were on average highest in July's sample set (green line) and lowest in February's sample set (red line). Consequently, precipitation and a subsequent increase in river discharge appears to be diluting ecotoxic metal concentrations in the Howden Burn. This suggests that whilst Howden Burn ecotoxic metal concentrations vary through time, the absolute quantity of material being liberated from the source steel slag does not vary significantly. Moreover absolute ecotoxic metal input is constant, but precipitation and thus discharge varies, producing variation in concentrations in the Howden Burn. This theory is supported by previous work done by Mayes *et al.* (2008) and Riley & Mayes (2015), which documents the inverse relationship between Howden Burn discharge and ecotoxic metal concentrations & pH.

Down-stream evolution (site 1 = upstream; site 5 = downstream) of ecotoxic metal concentrations displays on average a slight decrease on all three sampling dates. This and the above conclusions regarding rainfall are important factors to consider as the project moves forward into the final data interpretation stage. They are particularly significant when assessing the hypothesis that alkaline leachates are sequestering ecotoxic metals in the Howden Burn and providing a natural buffer to the hyperalkaline conditions produced from the interaction of steel slag with water.

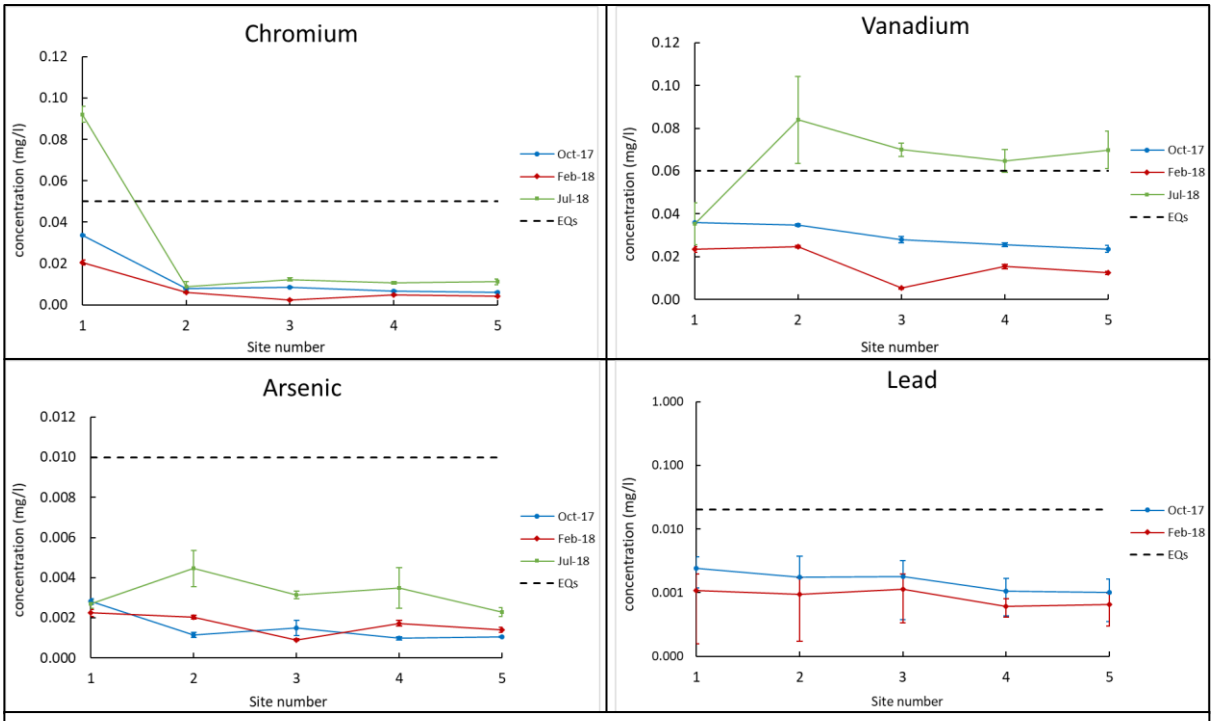

Figure 2: Concentrations of 4 example elements tested for in Howden Burn water samples: Site number 1 – 5 represents sampling points from top-to-bottom of Howden Burn profile; different coloured lines represent different sampling dates; dashed lines represent Environmental Quality Standard concentration for each element in mg/l or ppm.

Next steps

These initial results have already been presented at Goldschmidt's 2018 conference in Boston, USA, during oral session 13m: 'Contaminants in the Environment: Environmental Cycling of Metals, Metalloids and Emerging Inorganic Contaminants'. Updated project findings with bulk rock ICP and clumped isotope data were then presented at Scottish Alliance for Geoscience Environment and Society (SAGES) 2018 Annual Science Meeting and 10th Scottish Symposium on Environmental Analytical Chemistry in November 2018.

Once the LA-ICP-MS data processing is completed that will allow for a cross comparison between water and rock ICP data and clumped isotope data, to assess the system as a whole and fully evaluate the project hypothesis. Thesis submission is scheduled for May 2019 and two publications are planned from this – one regarding the flux of ecotoxic metals in the Howden Burn system and buffering of anthropogenic tufas in hyperalkaline leachate environments; one regarding kinetic effects and CO_2 hydroxylation in hyperalkaline environments and implications for clumped isotopes.

Beyond this it is my intention to share and discuss findings with the local council (Durham), water supplier (Northumbrian Water) and the Environment Agency, who have already provided historic water monitoring data for the project. I am also hoping to contact the Consett community to offer to speak to them about the project and my work, particularly I grew up just 45 minutes away from the town.

Final comments

I would like to say a huge thank you to The Geological Society for the award of this research grant. It has allowed for analysis of water samples taken across 2017 and 2018, with it capturing some significant and rare weather extremes! This increased the scope of the project because it allowed for an assessment of the seasonal controls discussed previously and ultimately provided valuable insight into what controls the toxicity of the Howden Burn. Thank you to all involved.

References

[1]USGS (2018), Mineral Commodity Summaries, Iron and Steel Slag Statistics and Information. [2]Mayes et al. (2008) Water Air and Soil Pollution 195, 35-50. [3]Riley and Mayes (2015) Environ Monit Assess 187: 463. [4]Deutz et al. (2017) Geoforum 85, 336-344. [5]Renforth et al. (2009) Applied Geochemistry 24, 1757-1764.

Investigating the spatial-distributions of coseismic landslides in a glacial environment, Langtang Valley, Nepal

Joshua Jones, University of Plymouth, £1100

The spatial-distributions of cosesimic landslides in Nepal are fundamentally controlled by latent hillslope stability as moderated by parameters relating to topography, seismicity, meteorology, geology and climate. However, despite the fact that many valleys within the Greater Himalayas are glaciated, it is apparent that the vast majority of landslide research in Nepal has focused on non-glacial landscapes, a trend that is continued in the wider literature (Mccoll, 2012). This is a problem, as glacial processes are commonly observed to lead to the development of unstable to metastable features such as glacial debris-cones, alluvial-fans, moraine fields and sediment-mantled slopes, all of which are highly susceptible to failure (Huggel et al., 2012). These observations suggest that the landslide response of glacial and periglacial landscapes may be different to that of non-glacial landscapes. As such, the long-term aim of this case study is to investigate whether the controls on landsliding within a glacial landscape are comparable to those in a non-glacial landscape.

The location selected for this case study was Langtang Valley, which is located 60 km north of Kathmandu near the Nepal-China border (Fig. 1). Langtang Valley is a typical U-shaped valley, now part of the Langtang river catchment, which is 46% glaciated (Immerzeel et al., 2012). The lithology of the valley is currently very poorly constrained, mapped by the Nepal Department of Mines and Geology as simply undifferentiated gneisses, migmatites, quartzites and schists. As such, as well as providing an excellent natural laboratory to investigate the characteristics of landslides in a glacial environment, this is a region in which our geological understanding would benefit from further research. Furthermore, Langtang Valley was severely impacted by the 2015 Gorkha earthquake, which triggered over 250 landslides across the valley. This included the devastating ‘Langtang Avalanche’, a massive debris-fall composed of glacial ice, snow and rock, which completely buried the village of Langtang killing over 350 people. This demonstrates that this region needs robust landslide hazard management and mitigation, which will require an improved understanding of how landslides in the valley are controlled, as well as reliable susceptibility and risk maps.

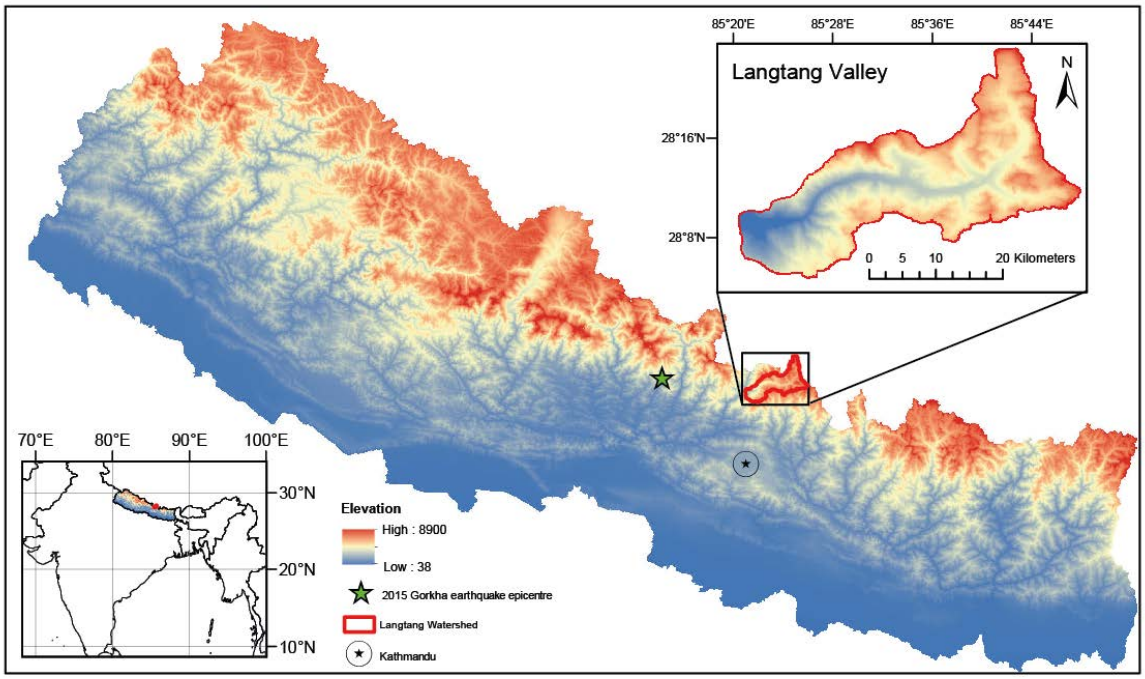

Figure 1. Location map of Langtang Valley

The specific objects of this project were:

1. To better constrain our geological knowledge of Langtang Valley by mapping/measuring outcrops and structural features in the field.
2. To assess the typology, morphology and dominant controls on landslides within this glacial landscape by mapping landslides in the field.
3. To use these data, combined with other remotely sourced data, to develop a statistical landslide susceptibility map for Langtang Valley.
4. To quantify how the landslide response of a glacial to periglacial landscape compares to a non-glacial landscape by comparing the results of 2 and 3 with similar studies in non-glacial landscapes.

To complete the objectives of this project it was necessary to conduct fieldwork with the valley. The focus of the fieldwork was to map the locations, typologies and morphologies of coseismic landslides across the Valley, as well as variations in lithology, geomorphology and structural geology. The fieldwork was undertaken during a 10-day period in October 2018 by myself, recent Plymouth University MGeol graduate, Timothy Webster, and our excellent local guide, Ngmia Crpa. The first three days of the fieldwork were spent trekking from Syraprubesi to the town of Kyanjin Gompa, mapping landslides on the northern side of the valley as we hiked. The next three days were spent mapping the area surrounding Kyanjin Gompa, including the nearby peaks of Kyanjin Ri and Tsergo Ri, which saw us reach elevations of 4987 m. Our final three days were spent trekking back to Syraprubesi, this time mapping the south side of the valley. To fully map a landslide we would record its location using a handheld GPS, measure its size using a TruPulse laser ranger finder, do a geomorphological sketch of the hillslope, record the lithology of the debris/back scar, measure any visible foliations, faults or intrusions, and record any other interesting observations. Whilst doing this we also got multiple opportunities to talk to different people about our work, which was a great opportunity for some impromptu science communication!

Left, Tim and I doing some impromptu science communication next to the debris fan of a large landslide. Right. a view of Langtang Lirung peak (7200 m) with multiple landslides and alluvial fans in the foreground.

As well as being able to collect loads of great quantitative data, the trip allowed us to talk to numerous local people about their experiences of living and working in such a dangerous environment. This led to several quite poignant moments, including am emotional description from our guide of his experiences during the 2015 earthquake. It transpired that he had lost dozens of friends and family members during the event, and was himself left tapped without supplies within Langtang Valley for several days. His account was harrowing, and reminded me that as scientists we cannot allow ourselves to become detached from the human elements of the things we study.

Top left and right, Tim, Ngima and I at the summit of Tsergo Ri.. Bottom left, Ngima showing us his skills with the geological hammer! Bottom right, the back scar and debris fan of the devastating Langtang Avalanche.

Overall, we managed to map 185 landslides, define four main lithological units, and take over 160 measurements of foliations and faults. In terms of improving our geological knowledge, it was found that the lithology of the valley is dominated by garnet gneisses, schists and very pervasive leucogranite dykes and sills, whilst foliations were found to predominantly dip towards the east. In terns if landslide typology, over 80% of the mapped landslides were rockfalls, with the remainder showing flow and creep mechanisms of failure.

Since returning to the UK, the focus has been on analysing these data alongside other remote data sources relating to topography and land use, to quantify the dominant controls on the distributions of landslides across the valley. This has mostly been done using linear regression modelling, which is a statistical method commonly used to understand multi-variate problems. The main results of this ongoing analysis are that elevation, hillslope angle and land use are exerting by far the most dominant controls on landslide occurrence across the valley. This project is very much still in progress, and the next step will be to use the results of the regression modelling to develop a full susceptibility map for Langtang Valley which visually quantifies the locations most likely to experience future failures. Once this has been accomplished, the susceptibility map and regression results will be compared with similar studies from non-glacial regions to assess how the landslide response of these different landscapes compare.

Acknowledgements.

This work was also supported by the Natural Environment Research Council through the EnvEast Doctoral Training Partnership [grant number NE/L002582/1]. It was also supported by my supervisory team: Dr Sarah Boulton, Dr Georgina Bennett, Dr Michael Whitworth and Dr Martin Stokes, as well as my field assistants Timothy Webster and Ngima Crpa.

References

Huggel, C., Clague, J.J., and Korup, O., 2012, Is climate change responsible for changing landslide activity in high mountains? Earth Surface Processes and Landforms, v. 37, p. 77–91, doi: 10.1002/esp.2223.

Immerzeel, W.W., van Beek, L.P.H., Konz, M., Shrestha, A.B., and Bierkens, M.F.P., 2012, Hydrological response to climate change in a glacierized catchment in the Himalayas: Climatic Change, v. 110, p. 721–736, doi: 10.1007/s10584-011-0143-4.

Mccoll, S.T., 2012, Paraglacial rock-slope stability: Geomorphology, v. 153–154, p. 1–16, doi: 10.1016/j.geomorph.2012.02.015.

Early Chinese ankylosaur and sauropod osteological and endocranial descriptions

Logan King
School of Earth Sciences, University of Bristol

Awarded £2700 from the William George Fearnsides Fund
Geological Society Grant Report 2018

Introduction

The usage of the CT scanning has been a prominent methodology for the past few decades that has been heavily used in the past couple of decades (Racicot, 2016). Moreover, much of recent dinosaur palaeoneurological research has been dominated by studies of non-avian theropods or the theropod-to-avian transition (Balanoff et al. 2013; Fiorillo et al., 2009; Witmer & Ridgley, 2009). While plenty of recent research has given descriptions of non-avian, non-theropod endocasts ()

China has a wealth of Jurassic dinosaur fossils that help to illuminate a key point of dinosaur evolution. The Institute of Vertebrate Paleontology and Paleoanthropology (IVPP) has graciously allowed me to use some of their non-avian, non-theropod specimens to

Data Collection

After being awarded the William George Fearnsides Fund, I travelled IVPP in Beijing, China. The point of my trip was to collect CT scans from an undescribed ankylosaur and the sauropod, *Xingxiulong chengi*. The original sauropod discussed in the application, *X. chengi*, was scanned but deemed too incomplete to utilize in future research. However, two other sauropods, *Xinjiangtitan shanshanesis* and another undescribed mamenchiosaurid, were scanned and given to me to make 3D models. These dinosaurs are perfect for expanding previously made datasets and are contain fine enough detail to map how the endocasts evolved from the Middle Jurassic to the K-Pg extinction.

Preliminary Results

The braincase of the ankylosaur (ZLJ0143) is incredibly well-preserved; however, the braincase (Fig. 1) did not produce good enough scans to replicate the endocast. We hypothesize that the imperfect CT data was not due to the preservation of the fossil but due to the amount of time the braincase was scanned. In the future, it will be scanned for a longer amount of time. Rescanning the specimen will be completed when it has been returned to Beijing from the Guangdong province of China. The braincase itself is large and fused together, not uncommon for thyreophorans. There are some elements (e.g. a raised occiput) that help support our hypothesis that this is indeed a Jurassic ankylosaur.

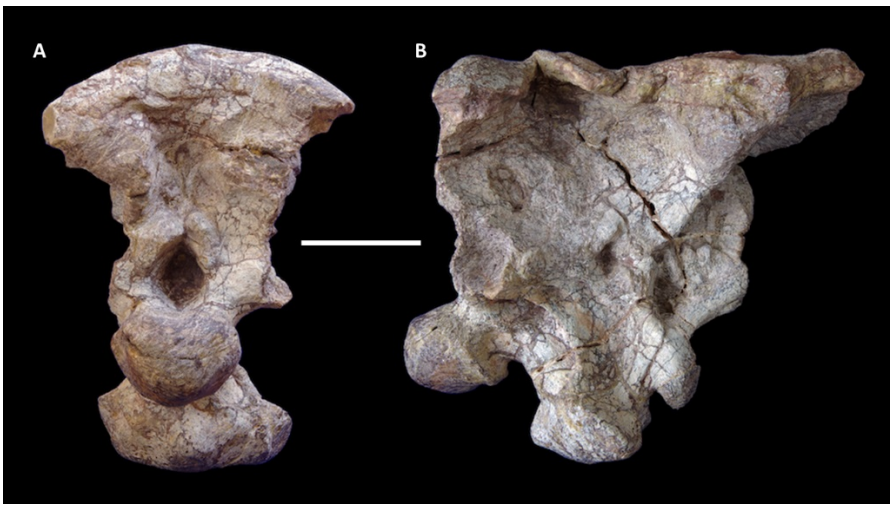

Figure 1. Posterior (A) and right lateral (B) views of the braincase from the unnamed ankylosaur. Scale bar = 5cm.

Aside from the ankylosaur braincase, some elements of the postcranial anatomy were preserved (Fig. 2) and are a part of the ongoing description. A large humerus (ZLJ0145), caudal vertebra (ZLJ0144), and ilio-sacral block (ZLJ0144) was also imaged and sent to me upon my return from Beijing. These fossils will be the focus of further study to help determine the identity of the Lufeng ankylosaur. Currently, the anatomy that has been noted so far suggests that the animal had a suite of basal and derived characteristics. For example, the condyles of the humerus favour more derived ankylosaurs; however, the low number of fused sacral vertebrae in the ilio-sacral block more reminiscent of *Scelidosaurus*, the earliest known thyreophoran to date.

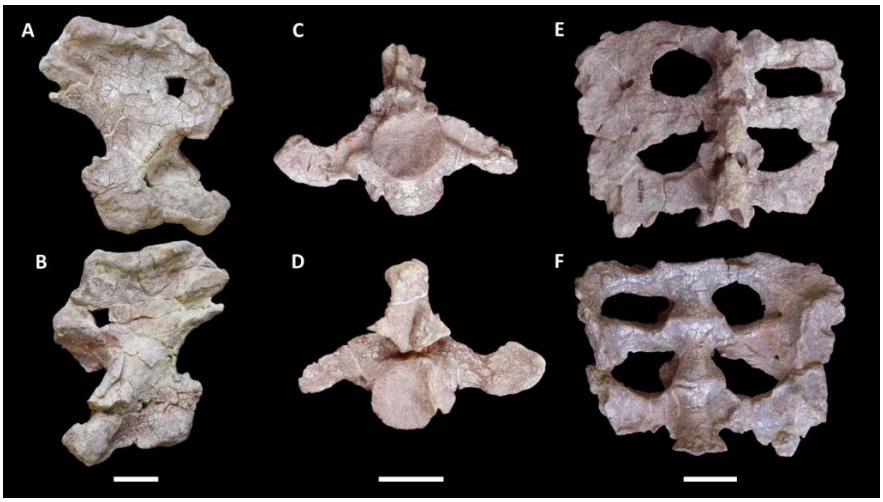

Figure 2. Postcranial remains of the unnamed ankylosaur provided through the IVPP/University of Bristol collaboration. The left humerus in dorsal (A) and ventral (B) view, a single caudal vertebra in proximal (C) and distal (D) views, and the ilio-sacral block in dorsal (E) and ventral (F) orientation. Scale bar = 5cm.

As for the sauropods, only *Xinjiangtitan* has been segmented and returned to IVPP (Fig. 3). The endocast itself is typical for a sauropod in that it is short and stocky with a prominent dural expansion. There is a substantial dural covering that has obscured the surface anatomy along the dorsal surface of the endocast. There is a potential anomaly with the 3D model. If the optic lobe is present as it appears to be, it would be a very rare lobe on a sauropodan endocast (Sereno et al., 2007). The ventral portion of the endocast would normally be much deeper with a pituitary fossa that would create a large bulb where the pituitary gland would have been housed in life. However, the ventral anatomy was partially missing due to the incomplete nature of the braincase. Some of the cranial nerves were preserved and project ventro-laterally along the endocast.

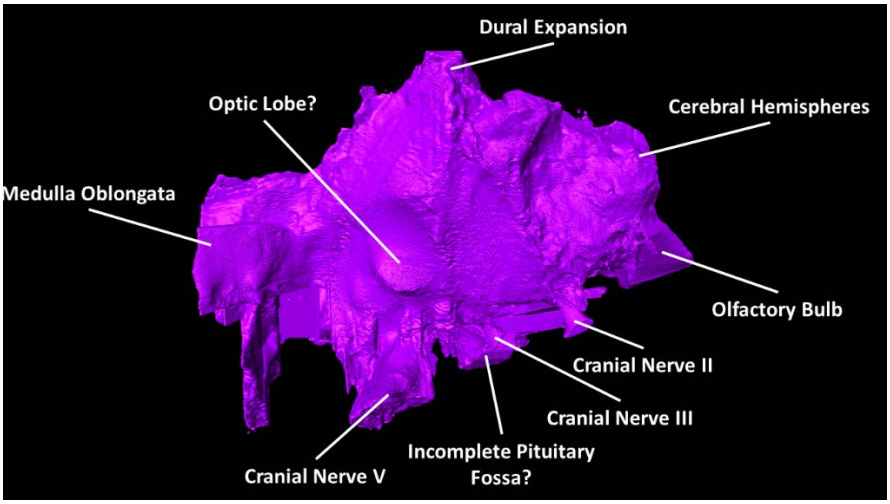

Figure 3. Generalized, labelled right lateral view of the endocast from *Xinjiangtitan shanshanesis*.

The other sauropod I mentioned, an undescribed mamenchiosaurid from Gansu province, is still being reconstructed. This specimen may need to be rescanned in the future due to the poor quality of the CT scans that were made.

Future Work

Once I have gotten a better scan set for the unnamed ankylosaur, I will begin to reconstruct an endocast. The endocast will complete an ongoing description of the braincase and postcranial anatomy. Moreover, the ankylosaur may represent the earliest known ankylosaurid. The imagery available to me right now suggests a wide range of features are present even in the limited remains. Establishing a data matrix and phylogenetic study will help to name the taxa as well as potentially push back our knowledge of thyreophoran evolution.

Xinjiangtitan has been returned to IVPP and is being used to help describe the skull with a team in Gansu province. The unknown sauropod is still being reconstructed but is suffering from the same issues the Lufeng ankylosaur – it may require rescanning for a longer time. Both endocasts will be used to compare how shape changed between sauropods throughout the Mesozoic. This may prove to be a vital part of understanding how neurosensory portions of the brain changed in dinosaurs that experienced gigantism throughout their evolution.

References

Balanoff, A. M., Bever, G. S., Rowe, T. B., & Norell, M. A. (2013). Evolutionary origins of the avian brain. Nature, 501, 93-96.

Fiorillo, A. R., Tykoski, R. S., Currie, P. J., Mccarthy, P. J., & Flaig, P. (2009). Description of two partial *Troodon* braincases from the Prince Creek Formation (Upper Cretaceous), North Slope Alaska. Journal of Vertebrate Paleontology, 29, 178-187.

Holloway, R. L. (2017). On the making of endocasts: the new and old in paleoneurology. In Digital Endocasts: from Skulls to Brains, 1-8.

Racicot, R. (2016). Fossil secrets revealed: x-ray CT scanning applications in paleontology. The Paleontological Society Papers, 22, 21-38.

Sereno, P. C., Wilson, J. A., Witmer, L. M., Whitlock, J. A., Maga, A., Ide, O., & Rowe, T. A. (2007). Structural extremes in a Cretaceous dinosaur. PLoS ONE 2:e1230

Witmer, L. M., & Ridgely, R. C. (2009). New insights into the brain, braincase, and ear region of tyrannosaurs (Dinosauria, Theropoda), with implications for sensory organization and behaviour. The Anatomical Record, 292, 1266-1296.

Brendan T. McCormick Kilbride
University of Manchester

Progress report on volcanological fieldwork in Rabaul, Papua New Guinea

Rabaul is a restless caldera volcano, located on the Gazelle Peninsula of East New Britain province, Papua New Guinea. A vast explosive eruption in 683 AD formed the 7-km crater now flooded by the sea and known as Simpson Harbour. A natural harbour, the Rabaul area today is home to around two hundred thousand people. Rabaul Town itself was formerly the capital of East New Britain province, before being largely destroyed by a sequence of explosive eruptions in 1994, centred on two small volcanic cones, Tavurvur and Vulcan, on either side of the caldera. These vents have been active for well over a century, resulting in hundreds of deaths and damage to local infrastructure. The regional capital is now located in Kokopo, at a greater distance from the direct volcanic hazards, but Rabaul remains an important centre of activity for the local population, who bring crops for market there, as well as a major port and cruise ship stop. A major motivation for volcanological research in Rabaul is keeping the local people safe from future eruptions.

Figure 1. Google Earth image of Rabaul caldera with town margins outlined in red and locations of the active volcanic cones Tavurvur and Vulcan marked by name. Yellow triangle indicates location of Rabaul Volcanological Observatory. Field of view is ~10 km across.

Today, Rabaul is monitored by Rabaul Volcanological Observatory (RVO). The main locus of activity is the cone of Tavurvur which last erupted in 2014. Unrest today comprises low level seismicity and the release of heat and gases through hot springs and fumaroles. In general the temperature of gas emissions at the surface is ~100-120 degC, indicating substantial interaction with subsurface groundwater and perhaps only limited magmatic degassing at depth. However, we don't know much about gas emissions from Rabaul. Over the past 15 years, satellite observations indicate that Tavurvur has been one of the top-10 emitters of volcanic sulfur dioxide (SO2) into the atmosphere, although emissions peaked in the major eruptive sequence of 2006-08 and have been declining ever since. It is not clear whether the low levels of activity at the volcano at the present time indicate a drift back towards quiescence or whether degassing is still occurring and the system is repressurising towards its next eruption. This will not be answered by our work alone but by providing new instruments to RVO and training in their use we are building capacity for monitoring and hazard forecasting that directly complements ongoing seismic and geodetic surveying. Tavurvur is known to erupt with little warning, beyond short-lived seismic swarms detected by the RVO network and a degree of precursory inflation (described to me in conversation with local people as sea-level dropping quickly over the day leading up to the eruption). Since the eruptions of Tavurvur (and Vulcan) have been extremely violent, flinging large ballistics several hundred metres from the vent and burying the surrounding landscape in tephra, establishing means of issuing reliable early warnings is a key goal for RVO's monitoring activities.

Brendan T. McCormick Kilbride
University of Manchester

Supported by funds from Deep Carbon Observatory, the NERC COMET program, and the Geological Society of London, I have been working in Papua New Guinea since 2016. Later this year, I will make my third visit to Rabaul. This progress report describes work done in October 2018 and planned for May 2019. My work mainly focusses on the study of volcanic gas emissions. I am interested in the use of changing gas chemistry and emission rate to understand or forecast changes in unrest as well as using gas chemistry to probe the ultimate origins of volcanic fluids from deep Earth reservoirs. In Rabaul I am focussing on three main sub-projects: (i) installing a MultiGAS instrument for real-time monitoring of gas chemistry on the Tavurvur crater rim, (ii) collecting gas and hot spring fluid samples for chemical analyses in laboratories in the UK and the US, (iii) collecting rock samples from past eruptions in order to study temporal evolution in magma volatile contents (using volatiles trapped in mineral-hosted melt or fluid inclusions).

Figure 2. BTMK with MultiGAS instrument on Tavurvur's eastern crater rim. The instrument is placed in directly in the gas plume and measurements are written directly to an onboard micro-SD card. Note that data could also be radioed directly to the observatory.

Due to inclement weather shortening our available working window at Rabaul, the majority of the 2018 campaign focussed on the deployment of a MultiGAS instrument on Tavurvur's crater rim, and training of my RVO colleagues in data acquisition and interpretation. The MultiGAS must be placed in close proximity to escaping volcanic gases, which are then drawn through the instrument's internal sensors by means of an onboard pump. Due to the threat of sudden eruptions and the steep, unstable terrain of the crater interior, our goal was to find a location on the crater rim where the instrument could be placed in contact with emitted gases, without any need for personnel to descend into the crater (we had explored this during the 2016 campaign and found it too unstable for safe access). We identified an ideal location on the eastern crater rim, with an extensive area of sulfur-encrusted ground and numerous fumarolic outlets for gas escape. Preliminary results indicate rather carbon-rich and sulfur-poor gas compositions, consistent with low (~100 degC) gas temperatures and a likely degree of hydrothermal scrubbing. In May 2019 I plan to sample gas emissions from these fumaroles and use noble gas isotopic analyses to more fully explore the mixing of magmatic, crustal and air components. Meanwhile the MultiGAS has unfortunately not been consistently operational on the crater rim due to malfunctioning hardware. Repairs are not complete and we will redeploy in May.

My gas sampling at Rabaul has so far focussed on crater wall fumarole samples and gases emitted from hot springs in the sea around the caldera. Poor weather conditions in October 2018 limited my ability to gather reliable gas samples on that trip and the main body of the planned

Brendan T. McCormick Kilbride
University of Manchester

Figure 3. View looking ~SW across Rabaul caldera, with active cone Tavurvur to the left of the image and Rababa hot springs in the centre right foreground. Rababa is the hottest site of non-fumarole degassing in the caldera and based on analyses conducted on September 2016 samples, there remains significant magmatic influence on the volatile emissions (from mantle-rich helium compositions). This site will be re-sampled in May 2019.

sampling will happen during May 2019. I am targeting 2-3 fumarole sites on the crater rims, 2-3 bubbling hot spring locations around the caldera and will also sample gas emissions from areas of intense soil degassing (identified using temperature surveys and measurements of CO2 emissions by accumulation chamber).

In September 2016, we collected tephra erupted from Vulcan and Tavurvur in the 1994 and 2006 eruptions, as well as relatively fresh volcanic bombs erupted in the 2014 explosive sequence. I plan to expand this sample collection in May 2019 by collecting rocks from the deposits of large caldera-forming eruptions in the more distant past. The goal is to extract (from crushed rocks) mineral-hosted fluid inclusions that I can chemically analysed to build up a volatile stratigraphy for Rabaul over hundreds/thousands of years. The analyses on fluid inclusions will largely take place at the University of Manchester and will chiefly focus on noble gas isotope chemistry.

Finally, I would like to thank the Geological Society of London (Elspeth Matthews Fund) once more for their generous financial support to my research.

Figure 4. Gathering tephra samples from the 1994 eruption of Vulcan.

Geological setting and palaeobiology of north Africa's first stegosaur: implications for herbivorous dinosaur evolution and biogeography

Susannah Maidment, Department of Earth Sciences, The Natural History Museum, London, UK.

Stegosaurs are a group of dinosaurs characterized by a bizarre array of plates and spines extending from the neck to the end of the tail. Stegosaurs are best known from the Late Jurassic of Laurasian continents, their remains being ubiquitous in terrestrial deposits of this age. However, the remains of Middle Jurassic stegosaurs are very rare, and consequently, much remains unknown about the early evolution of the group.

To date, only two definitive stegosaurs are known from Gondwanan continents: *Kentrosaurus aethiopicus* from the Upper Jurassic Tendaguru Formation of Tanzania, and the enigmatic *Paranthodon africanus*, from the Lower Cretaceous Kirkwood Formation of South Africa. It remains unclear whether the absence of stegosaurs from Gondwana is because they were genuinely rare there, or is a sampling bias resulting from a lack of collecting in Jurassic strata in the southern hemisphere. This question can only be answered with further discoveries, and thus any stegosaurian occurrence from Gondwana represents a significant data point.

In 2016, the Natural History Museum purchased some stegosaurian dinosaur fossils found in the Middle Atlas Mountains of Morocco from a commercial collector (Fig. 1). Many Moroccan fossils are excavated by farmers before being sold on to commercial dealers. The farmers often lack the scientific training to gather contextual data, such as the formation, depositional environment, or taphonomic conditions in which the specimen was found. Such information is extremely important to palaeobiologists because it allows an understanding of the age of the specimen, the environment in which the animal was living, and potentially how and why it is preserved. Information communicated to the Museum upon purchase was that the specimen was from the Jurassic of Boulemane. Boulemane is a small town in the Middle Atlas Mountains; examination of the literature indicated that Jurassic rocks in the area are Pleinsbachian (lowermost Lower Jurassic) to Bathonian (Middle Jurassic), and the Bathonian strata are represented by the El Mers Group, which include terrestrial rocks from which sauropod dinosaur fossils have previously been reported. It therefore seemed extremely likely that the new specimens were from the Bathonian, making them the oldest definitive stegosaur remains known anywhere in the world, and the first from north Africa.

I was invited by the Natural History Museum to work on the specimen in 2017, and continued to work on it after I moved to the Museum on a permanent basis in February 2018. My examination of the specimen indicated that it possessed several characteristics unique within stegosaurs, making it a new genus and species. However, aspects of the preservation, particularly the colour of the bones, suggested that the specimens may have come from different horizons, and thus may be from multiple individuals. My interpretation of the specimens was severely limited by the lack of contextual information, so, funded by the Garwood Fund, I went to Morocco to attempt to track down the location from where the specimens originally came, and gather data about the stratigraphy and taphonomy. I was accompanied on the trip by David and Allison Ward, Scientific Associates at the Natural History Museum who have been carrying out palaeobiological fieldwork in Morocco for over 20 years, and consequently have a network of invaluable contacts across the country. Most important of these is Moha Segaoui, a fossil dealer who also runs guided geological tours, and has been guiding fieldtrips for UK palaeobiologists and geologists for many years. Moha acted as our guide and translator for the trip, and also proved a very reliable source of wisdom and advice.

Our first aim was to meet with Prof Driss Ouarhache, a sedimentologist and stratigrapher at the Université Sidi Mohamed Ben Abdellah in Fes. Driss is an authority on the sediments of the Boulemane area, and guided us through the stratigraphy (Fig. 2). The El Mers Group is divided into three formations: the El Mers 1, 2 and 3. The El Mers 1 comprises shallow marine and intertidal facies overlain by terrestrial red beds, while the El Mers 2 and 3 represent shallow marine deposits. Dinosaur fossils have been noted in the 'couches rouges' of the area since the 1940s, and these correspond with the terrestrial deposits of the El Mers 1 Formation.

Having explored the stratigraphy and depositional environments of the El Mers Group, we headed south to Er Rich, to meet Moha Ouhuiss, the fossil dealer who sold the fossils to the NHM and someone the Wards know well. Moha and his cousin Said were extremely helpful and Said offered to take us to the village where the excavators lived. The next morning we followed Said north from our hotel in Midelt to a small village reached by a dirt road just outside of Boulemane, called Achlouj. Said introduced us to a farmer who offered us tea, and then accompanied Said and I to another farm some distance from the village, where the farmer who had excavated the fossils lived. The land next to the house was badlands cut into red beds, extremely similar to those of the El Mers 1 Formation that Driss had shown us on the other side of Boulemane. As the farmer guided us up and down the valleys, I noted abundant bone washing out (Fig. 3). There were also numerous large pits from where bones had been excavated. The farmer

explained that he collected most of the fragmentary material from drainages, where it washed out, and also excavated larger bones. We returned to Achlouj to a lunch of turmeric goat and very sweet tea.

We subsequently returned to the badlands and were able to study the stratigraphy and depositional environments in more detail, again receiving excellent hospitality in the form of grilled chicken and tea. The sediments exposed are all terrestrial, and appear to have been deposited by rivers and on floodplains consistent with our interpretation that these represent the El Mers 1 Formation. The lower part of the section comprises green silts interbedded with thin calcareous sandstones, which I interpret as overbank deposits, while the upper part consists of red mudstones with rootlets and thicker channel sandstones, which represent floodplain palaeosols and river channels (Fig. 4). Dinosaur fossils are found in a distinct unit at the top of the green silts. This unit is mottled orange, and contains abundant charcoal and jarrosite, and the matrix of the NHM stegosaur specimens match this unit. The El Mers 1 Formation has been reliably dated to the Bathonian based on biostratigraphy, and we collected some sediment samples to attempt to confirm that.

It is difficult to determine whether our specimens represent a single individual. On balance, it seems possible that they were excavated from different locations. But they appear to be from a single unit (albeit one that is several metres thick), and they share a number of features unseen in other stegosaurs. Thus, the NHM stegosaur represents a new genus and species which we will name in a forthcoming publication. Phylogenetic analysis indicates that the species is more closely related to two European Late Jurassic taxa, *Dacentrurus* and *Miragaia*, than it is to any other stegosaur, rather than being closely related to other African stegosaurs. Finally, statistical analysis of diversity patterns among Gondwanan armoured dinosaurs relative to sampling effort indicates that stegosaurs might genuinely have been a rare part of Gondwanan Mesozoic terrestrial faunas, and their absence is not a result of a sampling bias.

The El Mers 1 Formation in the Boulemane area appears to be extremely fossiliferous. I aim to formalize a collaboration with Prof Ouarhache and Université Sidi Mohamed Ben Abdellah, apply for further funding, and return to the area to carry out further excavations with the help of the local diggers in the future.

Figure 1. A stegosaurian humerus, one of the specimens acquired by the Natural History Museum from the Middle Atlas Mountains of Morocco. **A**, lateral, **B**, posterior, **C**, medial, **D**, anterior, **E**, dorsal, **F**, ventral view. **dpc**, deltopectoral crest; **dr**, descending ridge; **hd**, head; **ld**, scar of the *m. latissimus dorsi*; **mt**, medial tuberosity; **tt**, *m. triceps* tubercle. Scale bar equal to 20 cm.

Figure 2. From left to right: David Ward, Moha Segaoui, Allison Ward and Driss Ouarhache.

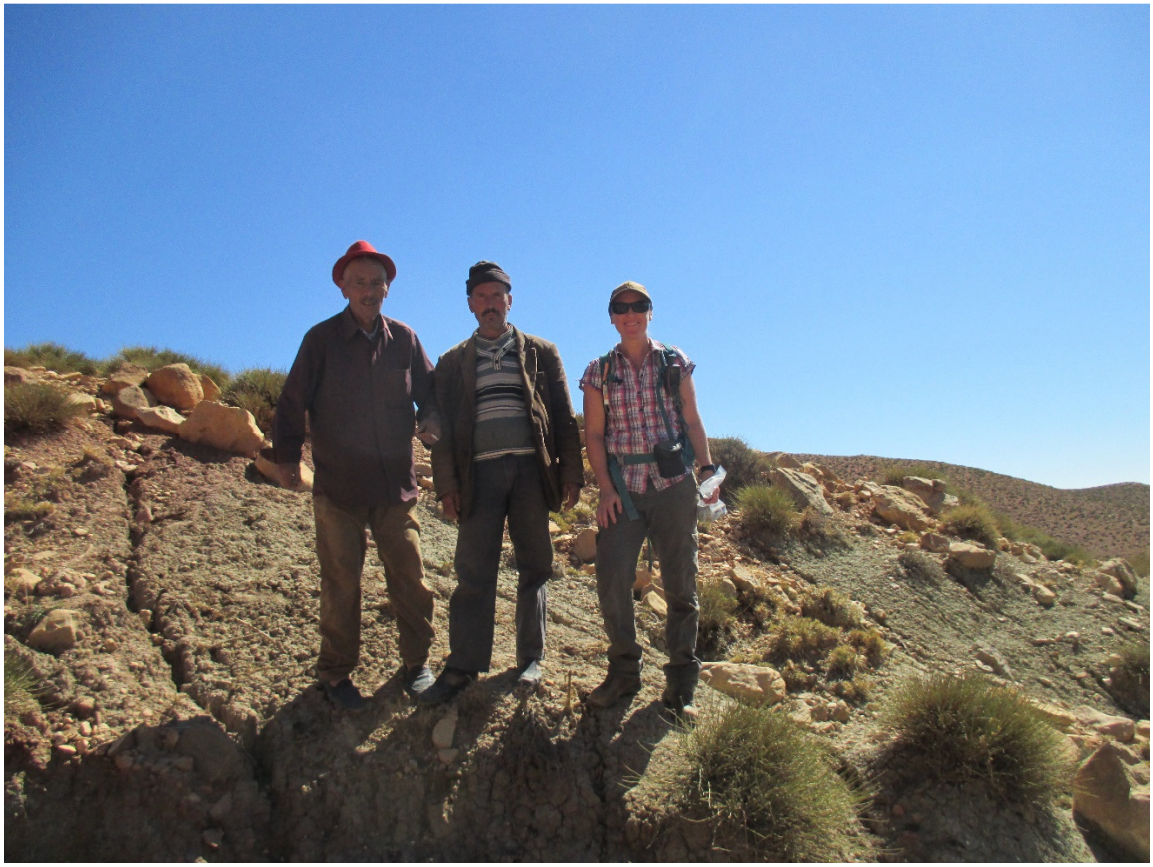

Figure 3: The author with local farmers who excavate fossils in the area

Figure 4: Terrestrial deposits of the El Mers 1 Formation cropping out at Boulafa. The fossiliferous unit is the grey unit immediately below the first bright red horizon.

Citation: Maidment, S. C. R., Raven, T. J., Barrett, P. M. & Ouarhache, D. In prep. North Africa's first stegosaur: implications for Gondwanan thyreophoran dinosaur diversity. *Gondwana Research* [To be submitted].

The Geology of Bell Island

Burrowing animals and the Decline of Precambrian Matgrounds

Catherine Mascord

£997.64 award from the Elspeth Matthews Fund.

Introduction

One of the most significant periods in the history of life on Earth is the Cambrian (541-485 Million Years Ago), which saw a rapid increase in animal complexity and diversity in an evolutionary event known as the Cambrian Explosion.

One of the most notable, but often ignored, elements of the Cambrian Explosion was an increase in oxygen levels and the mixing of sediment on and within the seafloor, brought about by the evolution of complex burrowing animals (infauna). These animals rework and mix the sediment as they burrow, allowing oxygen from the water column to penetrate to a greater depth, as a result they played a major role in oxygenating the Early Cambrian Sea and continue to do so on the seafloor today (Figure 1) (McIlroy and Logan, 1999). In the absence of complex burrowing organisms the Precambrian seafloor was characterised by widespread anoxia (McIlroy and Logan, 1999). The few Precambrian burrowing animals were limited to simple near-surface ecological niches, rarely penetrating to depth of more than a few millimetres into the sediment (Figure 1) (Gehling, 1999, Droser et al., 2002, Pecoits et al., 2012).

Without infauna to break it up the Precambrian seafloor was blanketed in a layered microbial community known as a microbial matground. Matgrounds are formed when microbes glue themselves and the host sediment together through the secretion of Extracellular Polymeric Substances (EPS) (Parsons et al., 2016), increasing the sediment and the matgrounds resistance to erosion. In shallow marine conditions the primary producers in these communities is usually photosynthetic, with the uppermost layers of the matground made up of diatoms or cyanobacteria (Stal, 2002, Bolhuis and Stal, 2011). Matground communities are all but extinct today, and are limited to anoxic, nutrient deficient or polluted areas of the sea and lacustrine bed; with most of the modern seafloor characterised by complex infauna displaying a range of burrowing behaviours.

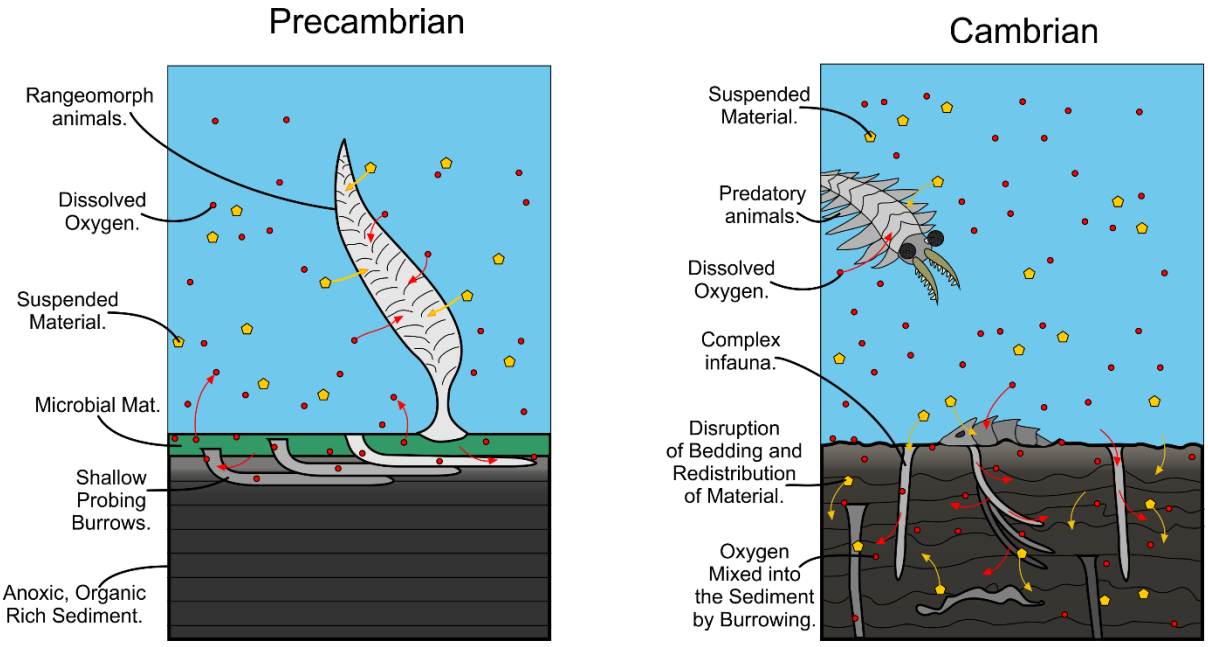

Figure 1: *A broad diagram illustrating the changes in the sedimentary conditions within the sediment showing the introduction of oxygen into the sediment by infauna and the redistribution of material.*

In the fossil record the shift from matground to infauna-dominated seafloor is preserved as a decline in the abundance of microbial sedimentary textures, including wrinkle structures and elephant skin fabrics, and an increase in diversity and ichnodensity of trace fossils (Fedonkin, 1978, Crimes and Droser, 1992, Jensen, 2003).

By the late Palaeozoic the preservation of microbial textures in the fossil record had declined significantly, only seeing major resurgences after mass extinctions (Gerbersdorf et al., 2009, Mata and Bottjer, 2012). Examining how trace fossils interact with these microbial textures, either directly, or by examining their relative distribution in the rock record, could provide an important insight into the mechanisms behind the decline of matgrounds and the role infauna played in it.

Unfortunately, successions preserving both Precambrian-like matgrounds and complex infauna are rare within the fossil record. However, in recent work by Harazim et al. (2013) in the lower-Ordovician aged rocks of Bell Island, Newfoundland, found the island preserved bedding planes containing coexisting matgrounds (Wrinkle Structures and Elephant Skin Textures) and trace fossils.

With the funding provided by the Geological Society of London, fieldwork to the island was performed between the 11th and 22nd of June, 2018, allowing the matgrounds and trace fossils to be properly documented and examined. Geological specimens were also collected for later thin section analysis and CT scanning.

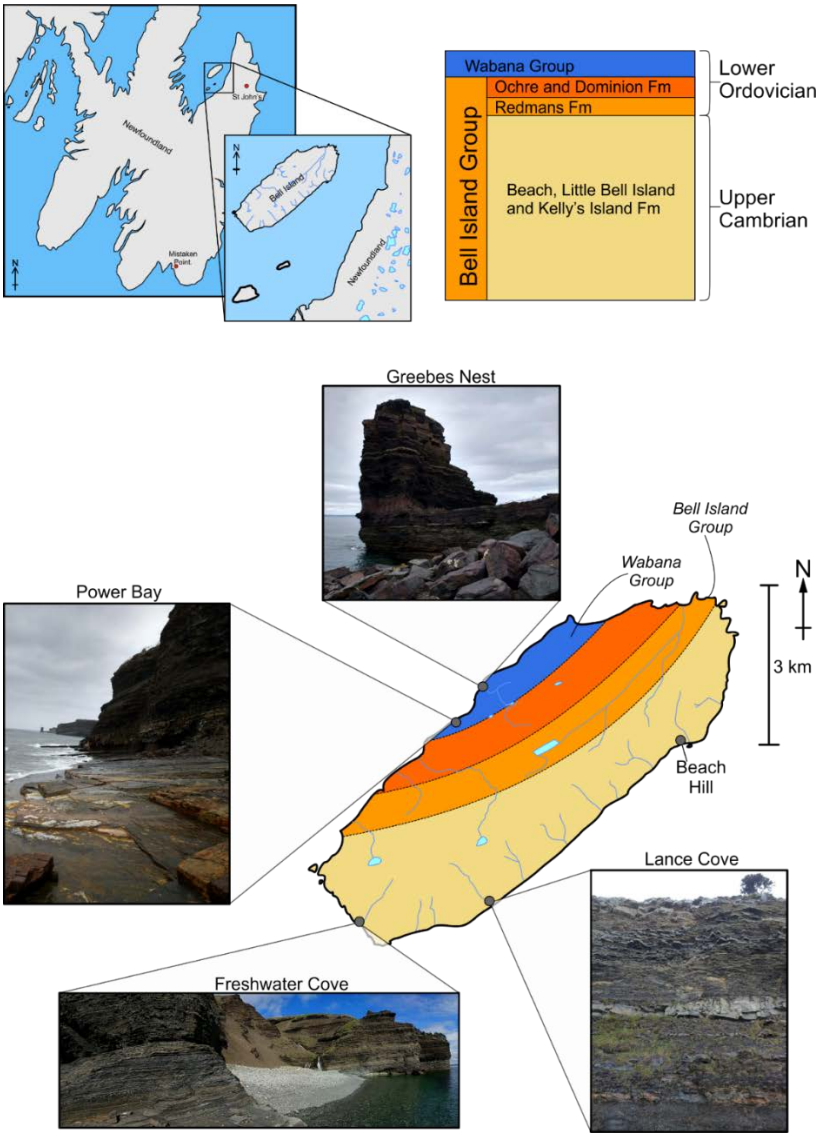

Figure 2: *A rough Geological map and Stratigraphic column of Bell Island, highlighting the main sites visited, the rough map of the geological unit's is based on King (1988).*

The Geology of Bell Island

Found just off the western coast of Newfoundland (Figure 2) near St Johns, Bell Island is relatively low-lying with few hills or other geographical features. Outcrops inland are uncommon, however there is a near continuous exposure around the island's coastline. Five main field sites were accessible without a boat and were visited as part of the fieldwork (illustrated in Figure 2).

The island is part of the Bell Island and Wabana groups dating from the Upper Cambrian to the Lower Ordovician (Figure 2) (Ranger et al., 1984, King, 1988, Harazim et al., 2013). The geology shows little variation over the island itself, with all the outcrops visited characterised by interbedded calcitic sands, ironstones and siltstones/mudstones. Sedimentary features preserved within the rocks are typically limited to symmetrical ripples and shallow crossbedding within the sandstone beds, the siltstones and mudstones lack sedimentary features, save simple layering.

The interbedded sandstones and mudstones, with the crossbedding and symmetrical ripples preserved in the sandstone indicative of wave action, consistent with deposition in a shallow marine environment. As such, the lithology is interpreted to be the result of deposition in a shallow marine environment above the storm wave base, likely within the photic zone. This is consistent with previously published paleoenvironmental interpretations of the island by Brenchley et al. (1993) and Harazim and McIlroy (2015).

Trace Fossil Associations of Bell Island

While the geology remains relatively consistent, and body fossils are comparatively rare throughout the Bell Island and Wabana groups, the ichnoassemblage (trace fossils) can vary significantly from outcrop to outcrop. Trace fossils were observed at all five field sites and can be divided into three broad assemblage types a matground assemblage, a 'simple' predominantly shallow tier (near surface) trace fossil assemblage and a more 'diverse' trace fossil assemblage containing vertically oriented and deep tier burrows.

Fossil Matgrounds

The Matgrounds are preserved either as wrinkle structures or as elephant skin fabrics (Figure 3), both of which are preferentially preserved on the boundary between the sandstones and the mudstones/siltstones. The two textures can be seen on the same bedding plane and can blend laterally into one another, indicating they form part of the same matground assemblage. The presence of a matground also appears to have an impact on the sedimentary micro-fabrics and composition observed in thin section. Specimens taken from matground dominated sandstones will typically contain micro-laminations/fibres of muscovite micas between the rounded quartz grains (Figure 4). The abundance of mica in the matground textures is visible even in the hand specimens, which typically have a shiny appearance. The orientation of these mica layers can change in response to burrowing behaviour within the mat and can be observed folding around burrow infills in thin section (Figure 4).

The matgrounds may be associated with simple horizontal, non-branching, trace fossils which cross cut through both the wrinkle structures and elephant's skin textures (Figure 5). These trace fossils remain near the surface, rarely penetrating deeper than a few mm.

Figure 3: *Left- an example of the typical wrinkle structures seen on Bell Island, this example was preserved on the bedding planes at Lance Cove. Right- the Elephant's skin textures preserved at Grebes Nest.*

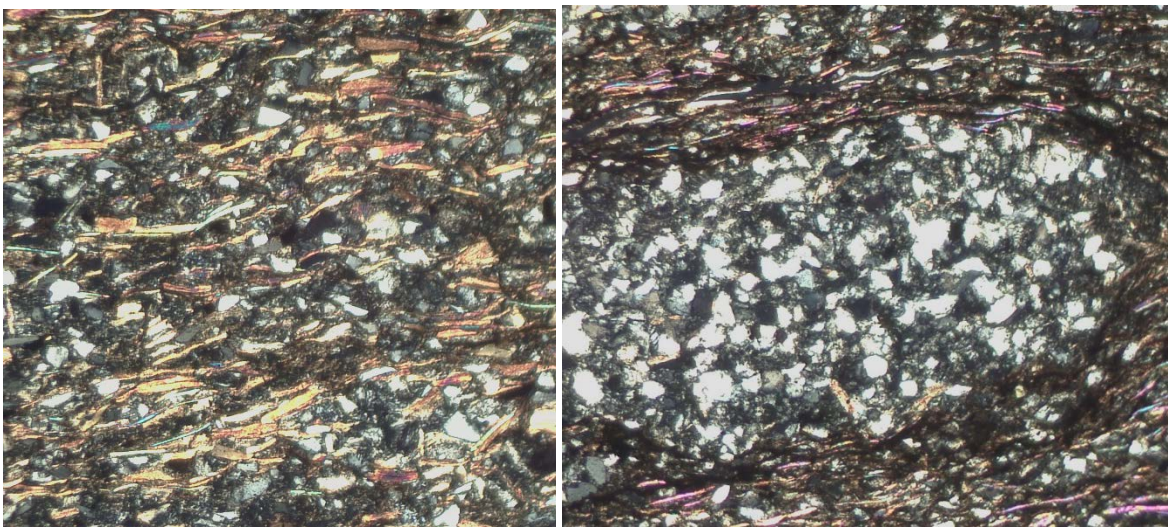

Figure 4: Left *- a thin section through a microbial texture, showing the abundance of mica layers.* ***Right*** *- The folding of the mica layers around a burrow. The burrow infill is predominately made up of clean quartz grains.*

Figure 5: *Simple trace fossils cross cutting through the matground. Photographs taken at Lance Cove (left) and Grebes Nest (right).*

Simple, shallow-tier, Communities

The simple, shallow-tier infauna are predominately made up of small 3 to 15mm in diameter non-branching burrows (Figure 6). These burrows possess a horizontal to inclined orientation, with the burrow depth limited to the top few mm to the uppermost 10 mm of the bed. More complex burrows are also present in these assemblages, albeit much rarer, these include U-shaped *Diplocraterion* burrows, and shallow-tier *Thalassinoides*-like branching burrow networks (Figure 7).

The trace fossils within these assemblages usually form a layer of intense bioturbation directly beneath a matground (within 5mm to 15 mm of sediment stratigraphically), as shown in Figure 6. The smaller burrows and *Diplocraterion* burrows can also or form zones of intense bioturbation around the edges of the matground or within regions of mat tearing and fragmentation - areas where a continuous bed of wrinkle structures/elephant skin textures is broken up into distinct fragments (Figure 8). Within these fragmentation zones larger individual burrows (10-12 mm in diameter) can be seen cutting through, or around the edge of, the matground fragments into the sediment below.

Figure 6: *The small burrows which can be found directly beneath a matground surface, which can be seen in the photograph, and in the surrounding sediment.*

Figure 7: *The large horizontal burrow networks associated with the beds directly above and below the microbial mats. Photographs taken at Freshwater Cove (left) and Grebes Nest (right).*

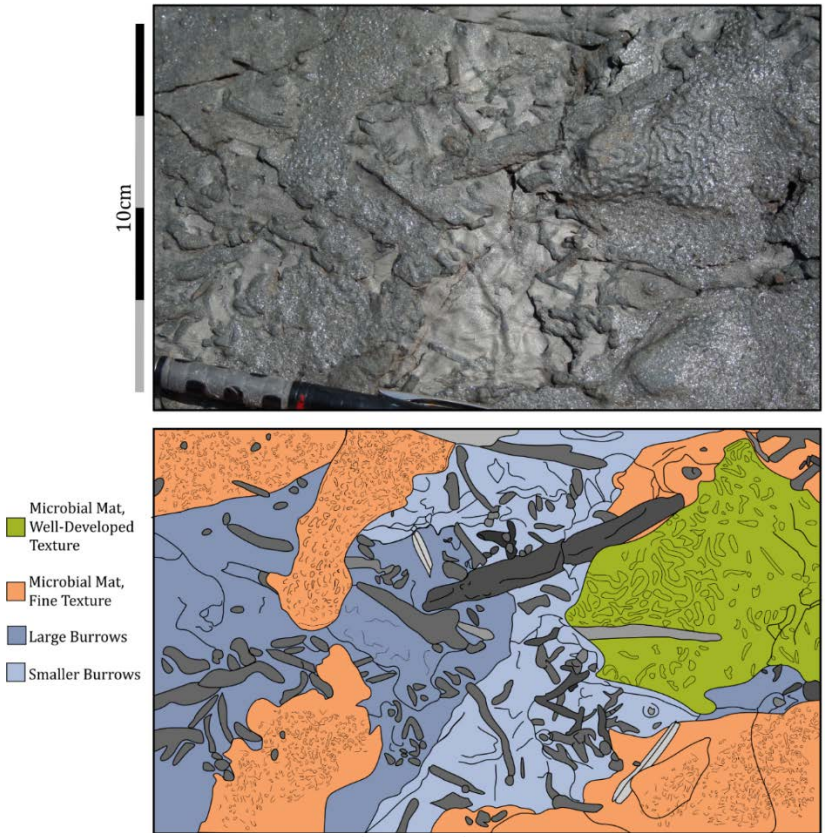

Figure 8: *A zone of Matground breakup showing the distinct fragments of microbial texture and the simple linear burrows associated with it.*

Diverse, deep-tier communities.

More diverse communities of trace fossils with more complex burrowing behaviours are not directly associated with the matgrounds and are usually found in beds above matground textures (100mm to 300mm). These communities contain the simple horizontal burrows seen in the shallow-tier assemblage, however they also contain

vertical deep-tier burrows (Figure 9). These vertical burrows include simple non-branching forms, more complex branching burrows and fan shaped feeding structures produced by methodical sediment mining. Some of these vertical burrowers, while originating well above the matgrounds in the stratigraphy, appear to be exploiting the buried and long dead matground units, as the vertical burrow stems terminate in matground layers. These vertical stems usually terminate in a horizontally oriented radiating fan like-structure. These are most visible at Grebes nest, which contains both cross sections through the stems (Figure 10) and the terminal fan shaped structures which exploit buried matgrounds and cut through the trails and horizontal burrows that formed concurrently with the matground (Figure 11).

Figure 9: *Simple non-branching vertical to sub-vertical burrows seen in the more complex communities. Cross sections through the horizontal burrows can also be seen in the image to the right. Photographs taken at Freshwater Cove and Beach hill.*

Figure 10: *The stems of burrows seen at Grebes nest, which terminate at a buried matground layer.*

Figure 11: *The terminal fan shaped structures from the burrows above observed on the matground containing bedding planes.*

Interpretations and Conclusions

While simpler burrows were found in both infauna-dominated and microbial dominated beds/outcrops, more complex burrows were not found to coexist with the matgrounds. This would indicate communities of simpler shallow-tier infauna with horizontal to inclined burrow orientations are better able to exploit active matground environments and anoxic sediments than deeper tier infauna. These simpler organisms also appear to play a role in matground decline and break up and/or they are able to actively exploit zones of mat break up and mat tearing.

The initial hypothesis than may explain this distribution of infauna is that the smaller shallow-tier burrowers are exploiting an oxygenic microenvironment produced by a photosynthesising microbial mat in the shallow marine environment (Meyer et al., 2014). If the mats present on Bell Island were photosynthesising (which is likely in a shallow marine depositional environment) they would produce an oxygenated ring around the matground and shallow-tier surface sediment, allowing infauna to establish themselves in the otherwise anoxic conditions. Smaller simpler infauna, which have less complex behaviour and lower metabolic demands (Löhr and Kennedy, 2015, Baliński et al., 2013, Parry et al., 2017, Josefson and Widbom, 1988, Levin and Wishner, 1991), may have been more successful at exploiting this microenvironment than larger and/or more complex animals, allowing them to act as pioneers in the colonisation of sediment by infauna.

Once the pioneering infauna were established in the shallow sediment and began to feed on the microbial mat, their burrowing behaviour increased the physical mixing of sediment. This increase in bioturbation drew down additional oxygen from the water column, and redistributed the oxygen produced by the mat itself leading to increased oxygenation of the sediment. The increased presence of infauna may have also assisted matground breakup due to direct feeding and mat tearing by animals moving through the matground, reducing the production of EPS and thus the abundance of sticky sediment. This allowed the sediment to be more readily eroded/mixed through wave and current action, which further encourages the introduction of oxygen into the sediment.

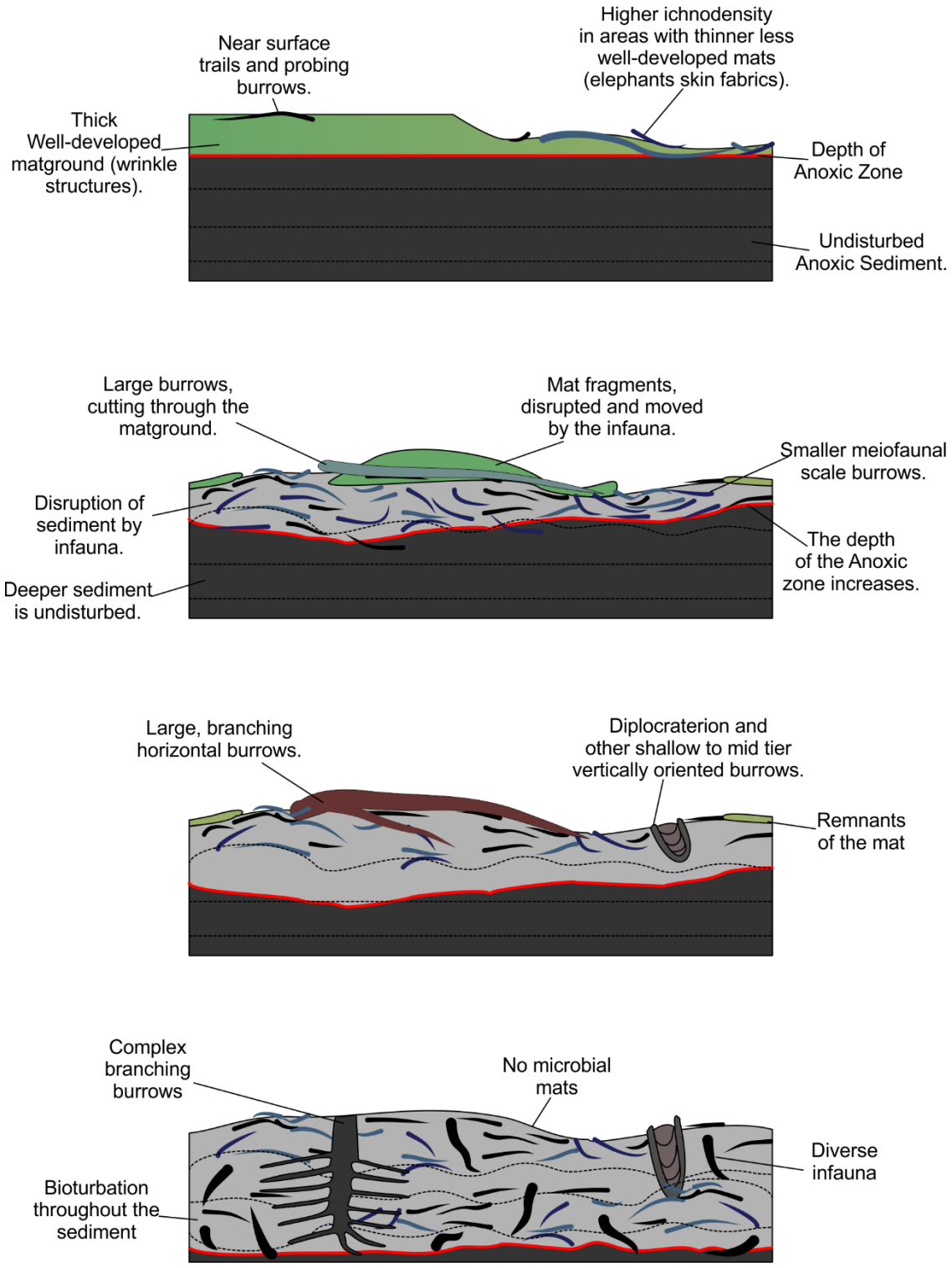

Figure 12: *The decline of the microbial mats and their relationship to the trace fossils.*

The gradual increase in oxygen content and decline of the microbial mat would open up new ecological niches for other infauna allowing further colonisation of sediment, leading to a positive feedback loop, whereby the presence of infauna leads to matground decline and generates new opportunities for additional infauna. Eventually the decline in matground integrity will decrease sufficiently to allow larger more complex infauna to get a foothold allowing diverse communities to develop which would ultimately kill-off the matgrounds (Figure 12).

Work on samples collected from Bell Island, including micro CT scanning to examine any meiofaunal scale burrows preserved within the sediment and its relationship to the microbial mats, is still ongoing and may result in changes to the hypothesis and interpretations in time. However, the initial observations made on Bell Island are

very promising and have provided a number of key insights into the interactions between early infauna and Precambrian matgrounds, allowing the biological mechanisms behind the Cambrian Explosion to be examined.

Acknowledgements

The Author wishes to thank the Geological Society of London for their generous Funding to support the Fieldwork to Bell Island.

References

BALIŃSKI, A., SUN, Y. & DZIK, J. 2013. Traces of Marine Nematodes from 470 Million Years Old Early Ordovician Rocks in China. *Nematology,* 15**,** 567-574.

BOLHUIS, A. & STAL, L. 2011. Analysis of Bacterial and Archaeal Diversity in Coastal Microbial Mats Using Massive Parallel 16S rRNA Gene Tag Sequencing. *The ISME Journal,* 5**,** 1701-1712.

BRENCHLEY, P., PICKERILL, R. & STROMBERG, S. 1993. The Role of Wave Reworking on the Architecture of Storm Sandstone Facies, Bell Island Group (Lower Ordovician), Eastern Newfoundland. *Sedimentology,* 40**,** 359-382.

CRIMES, T. & DROSER, M. 1992. Trace Fossils and Bioturbation: the Other Fossil Record. *The Annual Review of Ecology, Evolution, and Systematics,* 23**,** 339-360.

DROSER, M., JENSEN, S. & GEHLING, J. 2002. Trace Fossils and Substrates of the Terminal Proterozoic-Cambrian Transition: Implications for the Roecord of Early Bilaterians and Sediment Mixing. *PNAS,* 99**,** 12572-12576.

FEDONKIN, M. 1978. Ancient Trace Fossils and the Ways of Behavioral Evolution of Mud Eaters. *Paleontological Journal,* 12**,** 106-112.

GEHLING, J. 1999. Microbial Mats in Terminal Proterozoic Silicilastics: Ediacaran Death Masks. *PALAIOS,* 14**,** 40-57.

GERBERSDORF, S., BITTNER, R., LUBARSKY, H., MANZ, W. & PATERSON, D. 2009. Microbial Assemblages as Ecosystem Engineers. *Journal of Soils and Sediments,* 9**,** 640-652.

HARAZIM, D., CALLOW, R. & MCILROY, D. 2013. Microbial Mats Implicated in the Generation of Intrastratal Shrinkage ('Synaeresis') Cracks. *Sedimentology,* 60**,** 1621-1638.

HARAZIM, D. & MCILROY, D. 2015. Mud-Rich Density-Driven Flows Along and Early Ordovician Storm-Dominated Shoreline: Implications for Shallow-Marine Facies Models. *Journal of Sedimentary Research,* 85**,** 509-528.

JENSEN, S. 2003. The Proterozoic and Earliest Cambrian Trace Fossil Record; Patterns, Problems and Perspectives. *Integrative and Comparative Biology,* 43**,** 219-228.

JOSEFSON, A. & WIDBOM, B. 1988. Differential response of benthic macrofauna and meiofauna to hypoxia in the Gullmar Fjord basin. *Marine Biology,* 100**,** 31-40.

KING, A. F. 1988. *Geology of the Avalon Peninsula, Newfoundland (parts of 1K, 1L, 1M, 1N and 2C)*. St Johns, Newfoundland: Newfoundland Department of Mines and Energy, Map 88 – 01.

LEVIN, L. H., CL & WISHNER, K. 1991. Control of deep-sea benthic community structure by oxygen and organic-matter gradients in the eastern Pacific Ocean. *Journal of Marine Research,* 49**,** 763-800.

LÖHR, S. & KENNEDY, M. 2015. Micro-trace fossils reveal pervasive reworking of Pliocene sapropels by low-oxygen-adapted benthic meiofauna. *Nature Communications,* 6**,** Article number: 6589 (2015).

MATA, S. & BOTTJER, D. 2012. MIcrobes and Mass Extinctions: Paleoenvironmental Distribution of Microbialites During Times of Biotic Crisis. *Geobiology. Special Issue: Microbes and Paleoenvironments,* 10**,** 3-24.

MCILROY, D. & LOGAN, G. 1999. The Impact of Bioturbation on Infaunal Ecology and Evolution During the Proterozoic-Cambrian Transition. *PALAIOS,* 14**,** 58-72.

MEYER, M., XIAO, S., GILL, B., SCHIFFBAUER, J., CHEN, Z., ZHOU, C. & YUAN, X. 2014. Interactions Between Edicaran Animals and Microbial Mats Insights from *Lamonte trevallis*, a New Trace

Fossil from the Dengying formation of South China. *Paleogeography, Paleocilmatology, Paleoecology,* 396**,** 62-74.

PARRY, L., BOGGIANI, P., CONDON, D., GARWOOD, R., LEME, J., MCILROY, D., BRASIER, M., TRINDALE, R., CAMPANHA, G., PACHECO, M., DINIZ, C. & LIU, A. 2017. Ichnological Evidence for Meiofaunal Bilaterians from the Teriminal Ediacaran and Earliest Cambrian of Brazil. *Nature Ecology and Evolution,* 1**,** 1455-1464.

PARSONS, D., SCHINDLER, R., HOPE, J., MALARKEY, J., BAAS, J., PEAKALL, J., MANNING, A., YE, L., SIMMONS, S., PATERSON, D., ASPDEN, R., BASS, S., DAVIES, A., LICHTMAN, I. & THORNE, P. 2016. The role of biophysical cohesion on subaqueous bed form size. *Geophysical Research Letters,* 43**,** 1566-1573.

PECOITS, E., KONHAUSER, K., AUBET, N., HEAMAN, L., VEROSLAVSKY, G. & STERN, R. 2012. Bilateran Burrows and Grazing Behaviour at >585 Million Years Ago. *Science,* 336**,** 1693-1696.

RANGER, M., PICKERILL, R. & FILLION 1984. Lithostratigraphy of the Cambrian? - Lowe Ordovician Bell Island and Wabana Groups of Bell, Little Bell, and Kellys islands, Conception Bay, eastern Newfoundland. *Canadian Journal of Earth Sciences,* 21**,** 1245-1261.

STAL, L. 2002. Cyanobacterial Mats and Stromatolites. *In:* WHITTON, B. (ed.) *Ecology of Cyanobacteria II.* Dordrecht: Springer.

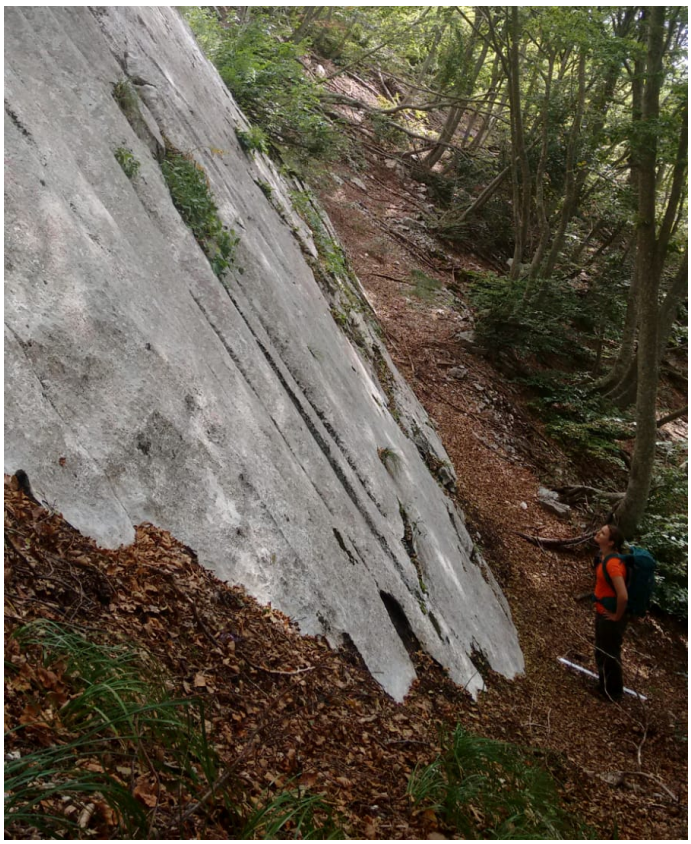

Measuring Holocene throw of normal faults to improve models of Coulomb stress transfer in the central Italian Apennines for assessing seismic hazard

Dr Zoe Mildon
School of Geography, Earth and Environmental Sciences, University of Plymouth

Total value of award £1220, the Jeremy Willson Charitable Trust provided £1000 and the rest was provided through the Mike Coward fund.

Introduction

Understanding whether earthquakes are triggered by static stress changes (so-called Coulomb stress) associated with prior earthquakes depends on how well the pre-existing stress on faults is determined. This analysis is hindered by a lack of knowledge of interseismic loading rates, even where excellent historical records of earthquakes are available. A Coulomb stress model for the central Apennines exists, which includes a 669 year stress history of interseismic loading, plus coseismic stress transferred by 34 M_w=5.6-7.0 earthquakes onto ~80 receiver faults (*Mildon et al.* [2017] and Mildon PhD thesis). However, some faults require additional long-term slip-rate data to improve the spatial coverage of interseismic loading rates. This proposal will make field measurements of long-term slip-rates that will be used to improve the stress history model and study the potential for future seismicity

Fieldwork and future work

The funding from the Geological Society and the Jeremy Willson Charitable Trust allowed me and a field assistant to undertake one week of fieldwork in the central Apennines in September 2018. Dr Lucy Campbell, a post-doc in my department, who

studies lower crustal pseudotachylites and shear zones was my field assistant, and during the week we both learnt from each other.
We visited six different faults (Figure 1), four in the northern part of the central Apennines (Umbria and Marche regions) and two in the Abruzzo region. Four of the faults, Gubbio, Mt San Vicino, Norcia and Scanno, had very little or no data collected on them in the literature prior to this field trip.

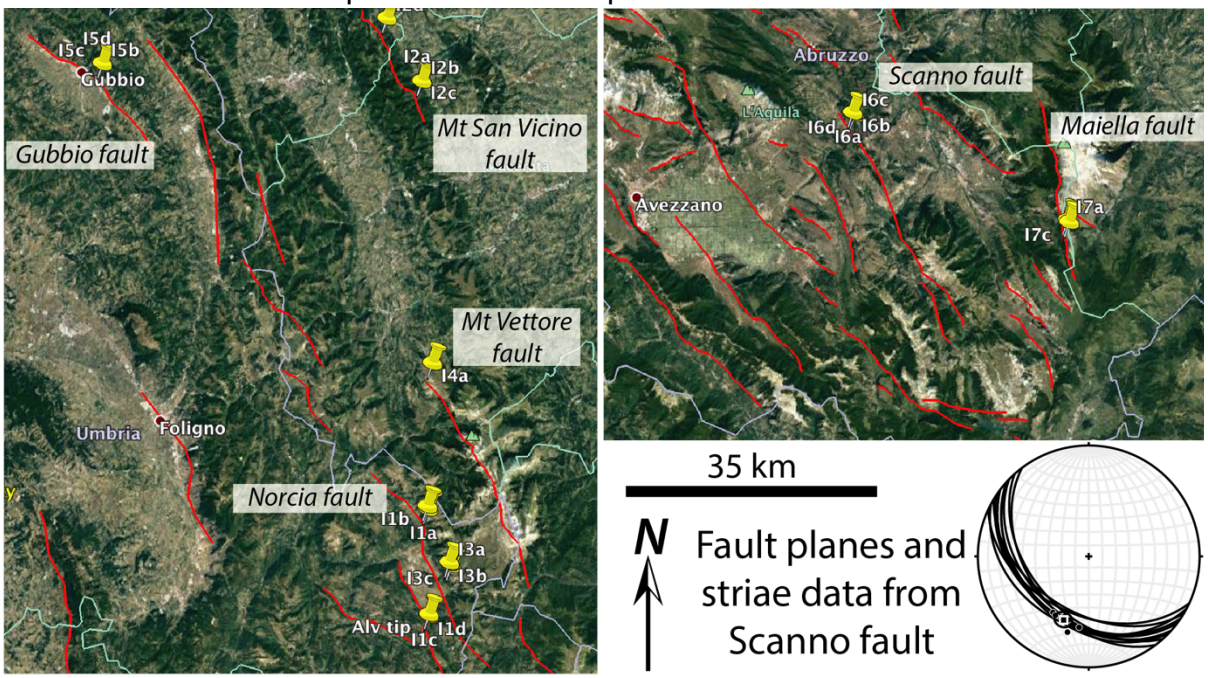

Figure 1 – Summary of all the locations and fault with data collected on this fieldtrip. Red lines indicate the surface traces of active normal faults (most dip to the south-west)

Figure 2- Field photographs. a. close up of a fault plane with frictional wear striae (shown by arrows), b. making a topographic profile in challenging conditions!

Two main types of field data were collected along the faults visited. Firstly, structural data, consisting of measuring the strike and dip of the limestone bedrock fault planes and, where possible, measuring the trend and plunge of frictional wear striae (Figure 2a) which indicate the fault kinematics. Secondly, where possible, topographic throw profiles were constructed across the fault scarp using chain-surveying techniques with a metre ruler and compass (Figure 2b). These profiles could only be collected where the geomorphology was favourable and I could be confident that there had been little or no erosion or deposition to expose or cover-up the fault scarp. Once these profiles were collected, they can be used to interpret the throw (vertical offset) at the location and knowing that the slopes formed at the end of the Last Glacial Maximum (15 ± 3 kya), I can calculate a throw rate. In total four topographic profiles were collected, 2 along the Norcia fault, one on Scanno and one on the Mt Vettore fault. Unfortunately no suitable sites were found on the other faults. However, the Norcia fault is of particular interest because it has had several damaging earthquakes occur in the last 660 years [*Blumetti*, 1995; *Galli et al.*, 2005]. These throw rates collected will be utilized in my Coulomb stress modelling to calculate the interseismic loading rate from an underlying ductile shear zone (as in *Mildon et al.* [2017]). This will likely form the basis for a high-impact paper on the seismic history of this part of the Apennines, and possibly also involving aspects of post-seismic

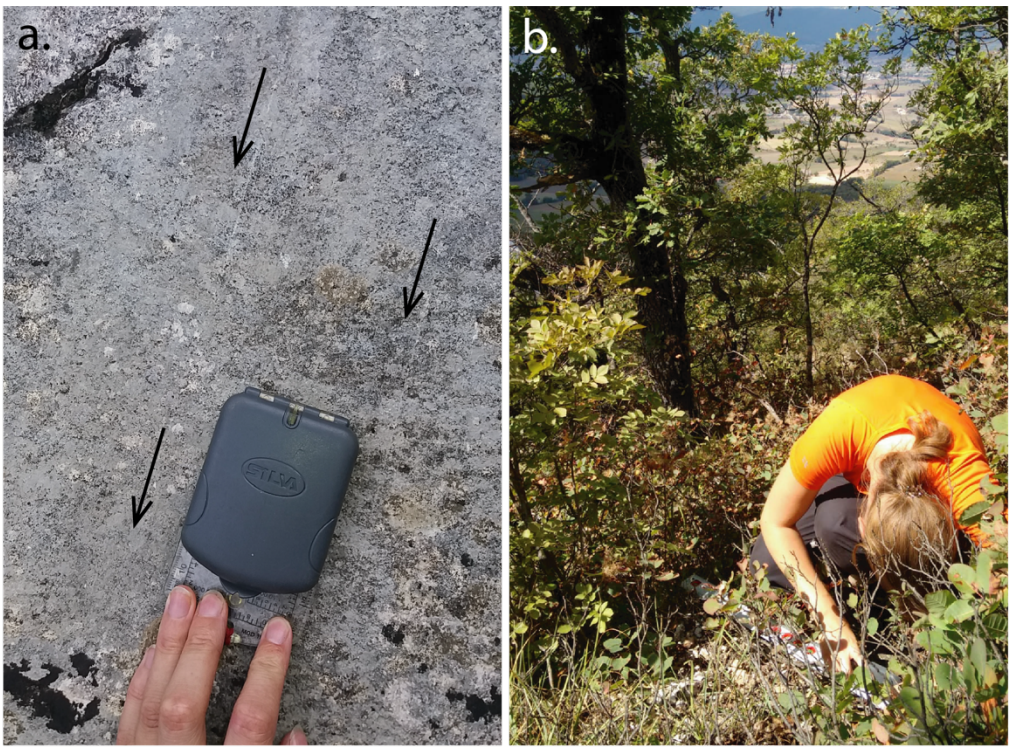

stress relaxation as well as static stress interaction. The data gathered in this study will be published as a new data set, also combining data gathered during my PhD, but as yet unpublished.

An unexpected benefit of the trip was the opportunity to take Dr Campbell as a field assistant, as originally I had planned to take someone else with me but they were unavailable. Dr Campbell studies earthquakes from a very different perspective to me, and I felt that I learnt from her in the field as she had different observations and hypotheses at the faults we visited. We are now working together to utilize my Coulomb stress modelling approach to investigate interaction between ductile shear zones and brittle failure in the lower crust – which we anticipate will form the basis for one or more papers in the future.

References

Blumetti, A. M. (1995), Neotectonic investigation of evidence of paleoseismicity in the epicentral area of the January-February 1703, central Italy, earthquakes, *Perspect. Paleoseismology*, *6*, 83–100.

Galli, P., F. Galadini, and F. Calzoni (2005), Surface faulting in Norcia (central Italy): A “paleoseismological perspective,” *Tectonophysics*, *403*(1–4), 117–130, doi:10.1016/j.tecto.2005.04.003.

Mildon, Z. K. (2017), The link between earthquakes and structural geology; the role of elapsed time, 3D geometry and stress transfer in the central Apennines, Italy, University College London.

Mildon, Z. K., G. P. Roberts, J. P. Faure Walker, and F. Iezzi (2017), Coulomb stress transfer and fault interaction over millennia on non-planar active normal faults: the Mw 6.5-5.0 seismic sequence of 2016-2017, central Italy, *Geophys. J. Int.*, *210*(2), doi:10.1093/gji/ggx213.

A petrological investigation into the triggers of the June 2018 eruption of Volcán de Fuego, Guatemala

Hannah Moore

School of Earth Sciences, University of Bristol

Awarded £363 from the William George Fearnsides Fund

Geological Society Grant Final Report 2018.

Introduction and Background

Volcán de Fuego in Guatemala is one of the most active volcanoes in Central America. The volcano experienced a major explosive eruption on 3rd June 2018, following an increase in above-background activity since 2015. Historically, activity at Fuego varies from effusive lava flows to discrete high-energy events, referred to in this paper as "paroxysms" (Martin and Rose 1981). Paroxysmal activity since 1999 is displayed in Fig. 1. Interspersed with the phases of activity are periods of repose which last up to several decades (Martin and Rose 1981). An example of one of these repose periods is that following the large sub-Plinian eruption in 1974, which lasted over 20 years. The most recent activity of Fuego coupled with an increase in population around the volcano makes research into its nature and behaviour of high importance. Samples from eruptions in 2017 and 2018 have been collected and analysed to interpret the recent processes occurring in the magmatic 'plumbing system'. This study focuses on the textures and compositions of glomerocrysts, which prove to be effective tools for understanding the dynamics of melt and gases and their interactions with the crystal mush zone. The crystal mush zone is a highly crystalline partially molten rock that is at or above the solidus and forms a continuous framework through which melt is distributed (Cashman et al. 2017). Glomerocrysts are distinct clusters of crystals found within melt which represent the crystal mush and record a variety of mineral and glass compositions. Their presence in a melt indicates that the system has incorporated a wide range of materials, from near-solid to largely liquid. Data from the 2017 and 2018 samples are compared to previous studies of the 1974 sub-Plinian eruption and 1999–2003 low-level paroxysmal activity to monitor the evolution of the subvolcanic system over time.

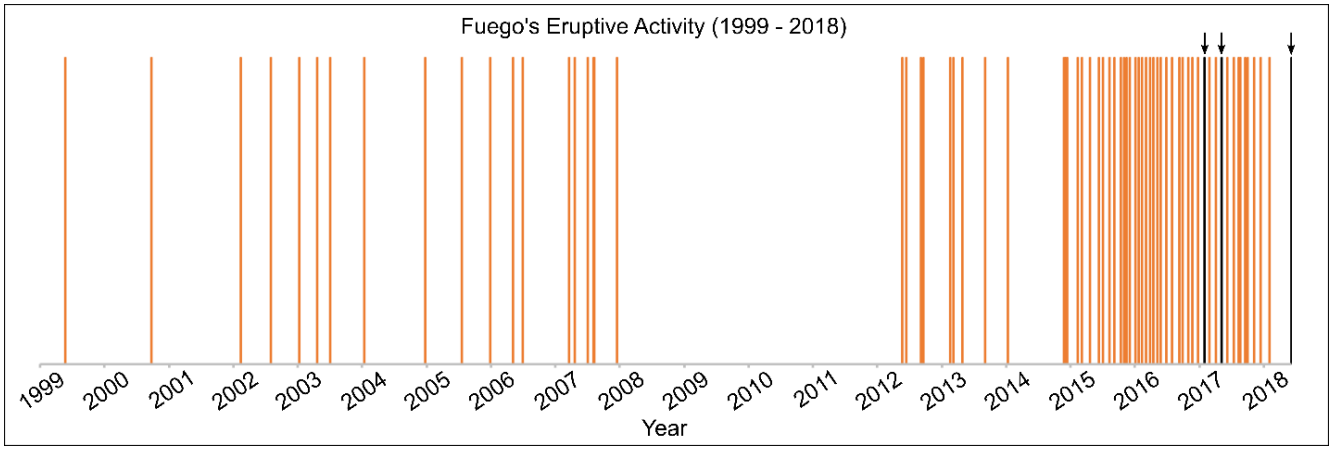

Fig. 1 Schematic diagram of Volcán de Fuego's eruptive activity since 1999. Orange lines represent distinct eruptions (paroxysms) which are considerably larger than minor background activity. Studied paroxysms are highlighted in black. Figure modified from Escobar-Wolf (2013).

Fieldwork and Analytical Methods

The 2017 samples for this study were collected from pyroclastic density current (PDC) deposits of January and May 2017 eruptive episodes, during a field visit to Volcán de Fuego in February and March 2018. They were collected from the Santa Teresa and Ceniza barrancas (drainage ravines) (Fig. 2). These PDC deposits are from relatively large paroxysmal events. Samples of PDC deposits from the more recent June 2018 explosive eruption were also collected as part of a later field visit. The 2018 samples were collected from locations within Barranca Las Lajas (Fig. 2). Lava bombs between 50–100 mm were selected from each sample group for analysis. 13 polished thin sections of these lava bombs were produced at Durham University's Department of Earth Sciences.

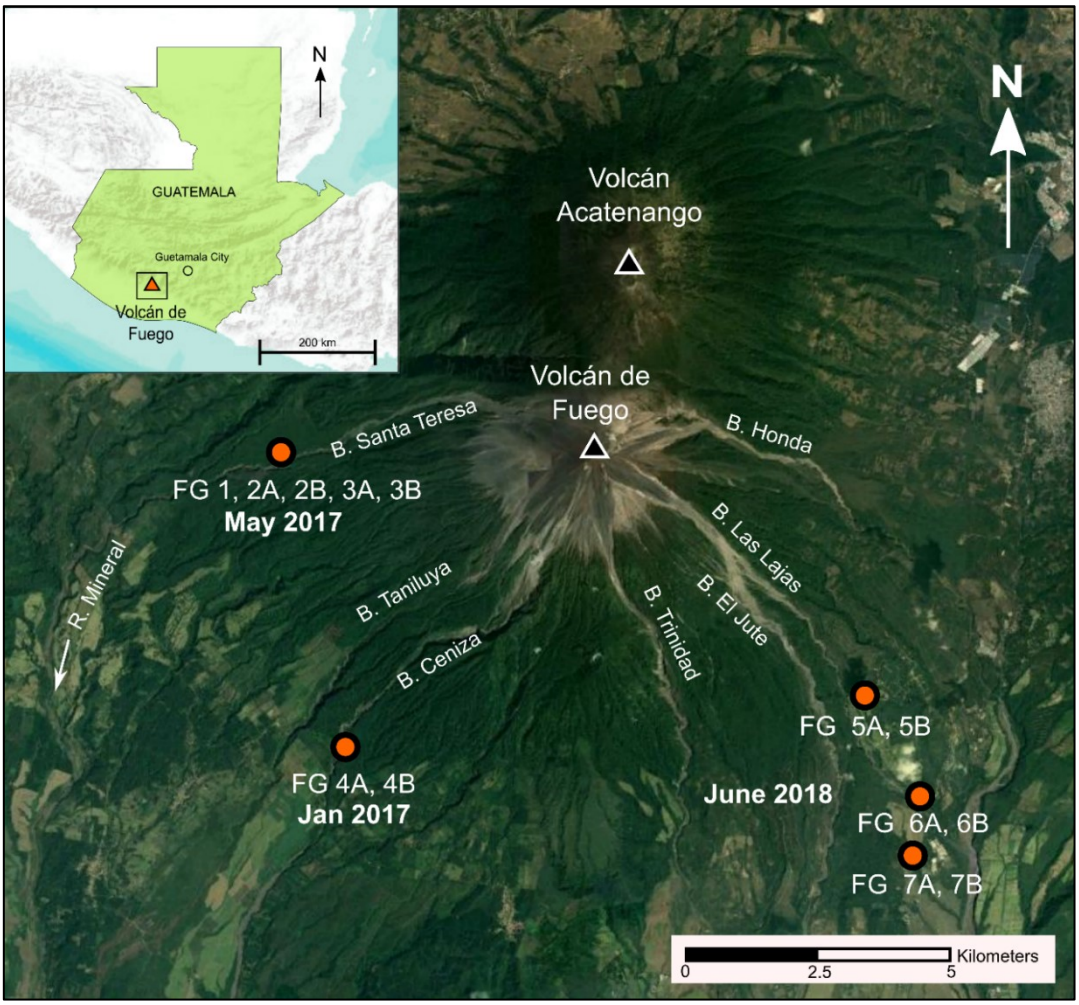

Fig. 2 Aerial view of study area showing sample locations with (inset) location of Volcán de Fuego within Guatemala. Also shown are Fuego's seven *barrancas* (drainage ravines), which control movement of lava flows, pyroclastic flows, and lahars.

Three microscopy techniques were used to perform analysis: optical microscopy, scanning electron microscopy (SEM), and electron probe microanalysis (EPMA). Optical microscopy was performed to obtain detailed descriptions of the samples, focussing on characterizing mineralogy, textures, and groundmass features. Photomicrographs were captured using a reflected light microscope connected to a computer operating NIS-elements software. The software was used to photo-stitch photomicrographs of entire thin sections, phenocrysts, glomerocrysts and interesting groundmass features. Point counting was carried out using an electronic point counting station on the optical microscope to obtain the abundances of crystalline phases, groundmass and glomerocrysts.

Results and Discussion

Textural and compositional analysis, with a focus on glomerocrysts, indicates that the 2017 samples were from the same source as the 1999–2003 magma, i.e. from a shallow system in the upper crust. The 3rd June 2018 samples show distinct differences in textures and compositions, including much lower glomerocryst melt fractions. The lack of melt-rich and smeared out glomerocrysts makes the 2018 samples look overall much more homogenous. The 2018 samples also display thicker plagioclase rims, which suggests longer residence periods than previous paroxysmal phases. This evidence indicates that the June 2018 magma ascended rapidly from depth, having disturbed and entrained deeper, glass-poor parts of the crystal mush.

The new model proposed (Fig. 3), contradicts the models put forward of the 1974 eruption (Roggensack 2001; Berlo et al. 2012) and the 1999–2003 paroxysms (Berlo et al. 2012). The older models describe mixing of two distinct magmas from a vertically extensive system. The “mingling” textures they describe have been reanalysed in this study. They appear to be a product of melt-rich mush material being deformed and smeared into the groundmass of an original, more homogenous magma. It is proposed that, instead of mixing of different magmas from a vertically extensive system, the magma was sourced from predominantly shallow depths. The magma disturbed and assimilated hot mush material, which was then erupted as smeared out glomerocrysts.

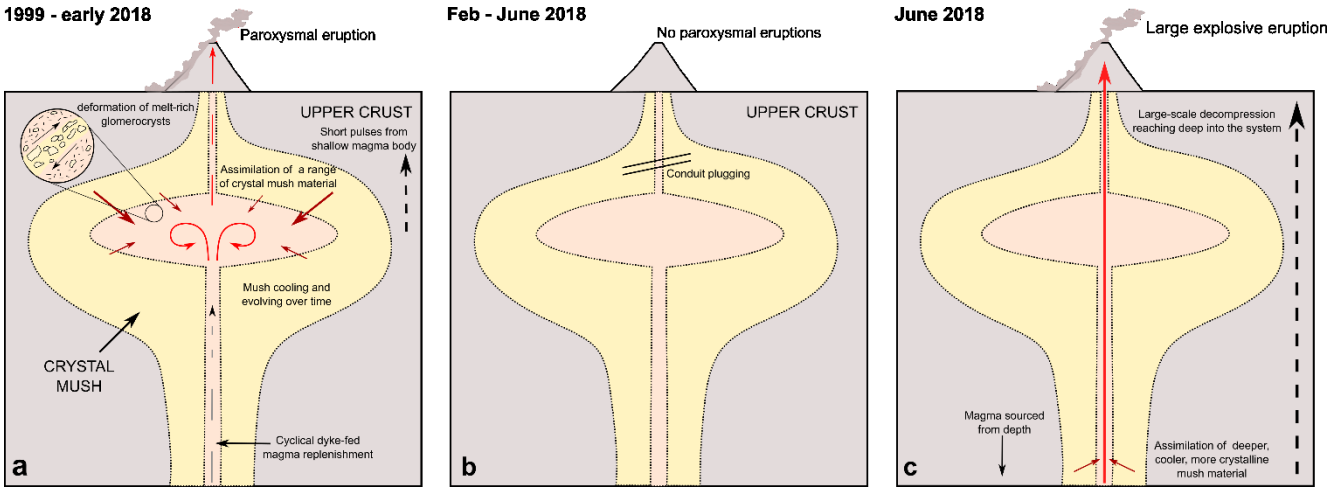

Fig. 3 Conceptual model of the magma storage system since 1999. **a** Small pulses of material from shallow magma reservoir trigger paroxysms. A range of crystal mush material is disturbed and entrained, from near-solid to largely liquid. Glomerocrysts with high melt fraction are deformed and smeared out. **b** Plugging of the system, allowing trapped volatiles to build up pressure. **c** Unclogging and large-scale decompression of the system, sourcing magma from depth which assimilates only cool, highly crystalline glomerocrysts as it ascends.

Future Work

Further investigation should include analysis of late-2017 and early-2018 PDC material, which may hold vital petrological information to help elucidate the evolution of the magmatic ‘plumbing system’. Future work should also include secondary ion mass spectrometry and Fourier transform infrared spectroscopy to yield information about gases and trace elements. Information on volatiles will allow thermobarometry to determine depths from which magma has been sourced. Further analysis and data collection from additional Volcán de Fuego samples will help to reinforce interpretations of the evolution of the magmatic ‘plumbing system’.

References

Berlo K, Stix J, Roggensack K, Ghaleb B (2012) A tale of two magmas, Fuego, Guatemala. Bull Volcanol 74:377–390.

Cashman KV, Sparks RSJ, Blundy JD (2017) Vertically extensive and unstable magmatic systems: A unified view of igneous processes. Science 355:eaag3055.

Escobar-Wolf RP (2013) Volcanic processes and human exposure as elements to build a risk model for Volcán de Fuego, Guatemala. Michigan Technological University PhD dissertation.

Martin DP, Rose WI (1981) Behavioral patterns of Fuego volcano, Guatemala. J Volcanol Geotherm Res 10:67–81.

Roggensack K (2001) Unraveling the 1974 eruption of Fuego volcano (Guatemala) with small crystals and their young melt inclusions. Geology 29:911.

Progress Report

Awardee: Aodhán Ó Gogáin

Award: £400 from the William George Fearnsides Fund.

Title:

CT Scanning Huxley's (1867) small tetrapods from Jarrow, south-eastern Ireland.

During the mid-1800's while mining for coal in north Kilkenny, SE Ireland, a great wealth of fossil material, including plant and fish fossils, was discovered in the Jarrow Coal Seam. Of all the fossils that were found, the most striking were the numerous vertebrates with small leg appendages, the tetrapods. Dated as Langsettian (Pennsylvanian), these fossils, when first described, were some of the earliest vertebrates which showed adaptions towards a terrestrial lifestyle. The honour of describing these tetrapod specimens fell to the famous comparative anatomist T.H. Huxley who named seven species new to science. Despite the scientific and historic importance of the Jarrow specimens they have been relatively understudied with respect to other similar specimens from slightly younger Pennsylvanian coal swamp deposits. This is likely due to the poor appearance of the specimens which are coated in a thin layer of matrix making fine anatomical details difficult to identify with the naked idea. Anatomical features are even harder to identify under a binocular microscope as the specimens "rather lose than gain in clearness by close inspection" as Huxley put it. Additionally, many of the Jarrow specimens suffer from pyrite disease, making them fragile.. Several specimens have been manually prepared or acid etched to form peels, however these methods are time consuming and can and do damage the specimens respectively.

The application of micro computed tomography (µCT) on fossil specimens has become commonplace method in palaeontology given that it is relatively cheap, quick and most importantly it is non-destructive. µCT works by penetrating a specimen with X-rays from a source on one side which are collected by a detector on the adjacent side. This produces a 2D stack of images showing both the external and internal morphology of the specimen. These 2D stacks can then be imported into 3D rendering software which produces 3D models of the specimen. Using such software, the surrounding matrix can be digitally removed, and internal 3D structures can be imaged.

Using the money from the William George Fearnsides Fund, the awardee scanned specimens of two of Huxley's original Jarrow species, NMI.14716 *Urocordylus wandesfordi* and the type specimen of *Ichthyerpeton bradleyae* TCD.T87. Scans were done with the µCT scanner model XTH 225 ST Nikon at the University of Bristol in November 2018. Resulting CT slices were imported into the free 3D rendering software Spiers in order to produce 3D models of the specimens.

Urocordylus wandesfordi, along with two other Jarrow species (*Keraterpeton galvani* and *Lepterpeton dobbsi*) mark the earliest geological occurrence of the order Nectridea, a clade of newt-like tetrapods with elongated tails up to 2/3rds the length of the body. Despite the Jarrow species marking the first occurrence, the nectrideans had already reached a high level of diversity with each Jarrow species being assigned to the three separate families within the Nectrideans, the Scincosauridae (*L. dobbsi*), the Diplocaulidae (*K. galvani*) and the Urocordylidae (*U. wandesfordi*). This means that to get an understanding of the basal characteristics and validity of each family, a better understanding of the anatomical features of each Jarrow nectridean must be provided. CT data and 3D models of NMI.14716 *Urocordylus wandesfordi* has allowed for the description of previously unidentified anatomical features including the position and contacts of posterior midline cranial bones, the medial bone elements on the jaws, part of the palate and the scapula in the shoulder girdle. These models and data will be compiled with previously acquired µCT data from *K. galvani* and *L. dobbsi*. All three nectrideans have now been described by the awardee and he will incorporate them into a cladogram to test the viability of the three nectridean families and the evolutionary relationship between the nectrideans and other early tetrapods. Results will be published in a paper on the Jarrow nectrideans in a yet undecided journal.

Ichthyerpeton bradleyae is the least studied of the original Huxley species having no papers working on the type specimen since Huxley last described it. This may be due to the fact the specimen only preserves the trunk part of the vertebrae, some back-limb elements and part of the tail along with a wide covering of scales over the entire preserved body. A skull was initially described as belonging to *I. bradleyae,* but this has since been reassigned leaving the anatomy and evolutionary relationship of *I. bradleyae* poorly understood. Information from CT-slices of the type specimen of *I. bradleyae* was harder to identify than those in *Urocordylus wandesfordi* due to the covering of dermal scales and the overall preservation of the specimen. This means that 3D modelling is not as effective as above. However, it is not all doom and gloom as the individual slices have provided new descriptive information of the hindlimb elements, including the identification of a femur, fibulae and tibia. More interestingly the morphology of the vertebra can be described and the presence on a small intercentra between each vertebra has been discovered. This allows for the taxonomic placement of *I. bradleyae* within the suborder Tuditanomorpha with a possible placement in the family Gymnarthridae. This would make *I. bradleyae* a “microsaur” a group of early tetrapods with elongated bodies and reduced limbs. “Microsaurs” are now considered polyphyletic, with some groups such as the Gymnarthridae being identified as early amniotes (a group consisting of reptiles and mammals). This goes to highlight the high diversity that is preserved within the

Jarrow assemblage. A paper is currently being compiled on a redescription of *I. bradleyae* to be submitted to the *Journal of Paleontology*.

All results funded by the William George Fearnsides Fund will form part of the awardee's PhD thesis and will be made available to researchers upon publication of the material.

Detailed mapping of damage zones around intersecting faults on Gozo, Maltese Islands

Awardee: David Peacock
Award: Annie Greenly Fund
Amount: £900

1. Background

UAVs ("drones") have become available at reasonable prices over the last few years, and are being increasingly used for detailed geological mapping (e.g., Bemis et al., 2014; Vollgger and Cruden, 2016). UAVs enable the rapid and easy creation of high-quality, low-cost orthomosaics and 3D models, thereby greatly improve the efficiency of fieldwork. Features that are invisible on the ground often show up well when observed from the altitude (e.g., Figure 1). It is wonderful to look down at exposures, through the camera on a UAV, from heights of up to 120 m (the legal UAV height limit in the UK), getting a broad overview of an exposure and seeing structures that are hard to visualise from the ground. Whilst satellite images and traditional aerial photographs are useful, details are lost. UAVs can be flown much lower, enabling much smaller features to be observed, including fractures that are cm long.

The Maltese Islands (Figure 2) show excellent coastal exposures of normal (e.g., Michie, 2015) and strike-slip (e.g., Kim et al., 2003) faults in Cenozoic carbonate rocks. The strike-slip faults near Marsalforn have been particularly useful in developing concepts related to fault damage zones, with Kim et al. (2004) showing damage zones developed at fault tips, along the walls of faults and where stepping and sub-parallel faults interact. Peacock et al. (2017a) introduce the concept of interaction damage zones, created as non-parallel faults approach each other, meet or cross-cut. Preliminary fieldwork suggested that such intersection damage zones are well-exposed near Marsalforn, with conjugate strike-slip faults with displacements of < 1 m interacting and mutually cross-cutting (Figure 3a). Intersecting faults are of interest because they can control fluid flow in rock, with Hermanrud et al. (2014) showing that fault intersections control hydrocarbon column heights in the Barents Sea.

2. Aims of the fieldwork

The aim of the fieldwork was to use UAV data to make detailed maps of interacting conjugate faults and related damage zone near Marsalforn, Gozo. Data were collected to answer the following questions:

- What are the geometries and kinematics of interacting strike-slip faults?
- What damage is associated with these faults?
- How do interacting faults evolve?
- What implications do fault interactions have for the migration of fluids?

3. Using a UAV

There is a tendency for people to fly UAVs manually, especially when collecting images of cliffs. Doing this, however, is challenging and can lead to gaps in the data. The exposure on the beach near Marsalforn has gentle topography and cliffs only ~ 5 m high, so the flight was plotted using the DroneDeploy software (Figure 4). This is an efficient and relatively safe way to collect UAV data, with the flight area and height being plotted beforehand and the software being used to fly the UAV such that overlapping photographs are taken to enable 3D models to be generated. The beach near Marsalform was flown at height of approximately 20 m, producing resolution better than 1 cm per pixel. Additional photographs of specific areas where taken flying the UAV manually at lower heights. The photographs were processed using AgiSoft Photoscan software to create 3D models and orthomosaics that were imported into ArcGIS to generate maps. The orthomosaics were printed and these paper copies were used for field mapping.

4. An unexpected result

Initial interpretation of the faults near Marsalform, based on observations from the ground made during a visit several years ago, was that the sinistral and dextral faults show mutually-cutting conjugate relationships (Figure 3a; e.g., Ferrill et al., 2009). Detail field mapping using orthomosaics showed, however, that dextral faults appear to have initiated at contractional steps along sinistral fault zones (Figure 3b). It is likely that the antithetic dextral faults initiate in areas of relatively high strain, where displacement is transferred between the sinistral fault segments across the contractional step (Figure 3b). In contrast, pull-aparts develop at extensional steps along the sinistral fault zones (Figure 5).

5. Conclusions

UAV technology has great potential to improve geological mapping, enabling the rapid creation of very high-quality and inexpensive 3D models and orthomosaics for detailed mapping. The ability to hover, virtually, up to 120 m above the ground, gives one a better oversight into the geology, sometimes with unexpected results. What you think you see at eye-level can be misleading. Whilst the strike-slip faults near Marsalforn were initially interpreted as consisting on mutually cross-cutting conjugate sets (Figure 3a), detailed mapping using orthomosaics from UAV images showed that dextral faults were generated at contractional steps along sinistral faults (Figure 3b).

6. Expected publications

This short report can be modified to form an article for *Geoscientist* if requested. The mapping will be used as a basis for a paper describing fault development on Gozo, probably to be submitted to the Journal of Structural Geology. It will also be part of a review paper on antithetic relationships to be submitted to Earth-Science Reviews. It is expected that the UAV photomontages will be made available on the SAFARI virtual outcrop database (https://safaridb.com/home). They can also be provided to the Geological Society of London.

Acknowledgement

Funding from the Annie Greenly Fund is greatly appreciated.

References

Bemis, S.P., Micklethwaite, S., Turner, D., James, M.R., Akciz, S., Thiele, S.T., Bangash, H.A., 2014. Ground-based and UAV-Based photogrammetry: a multi-scale, high-resolution mapping tool for structural geology and paleoseismology. Journal of Structural Geology 69, 163-178.

Ferrill, D.A., Morris, A.P., McGinnis, R.N., 2009. Crossing conjugate normal faults in field exposures and seismic data. American Association of Petroleum Geologists Bulletin 93, 1471-1488.

Hermanrud, C., Halkjelsvik, M.E., Kristiansen, K., Bernal, A., Strömbäck, A.C., 2014. Petroleum column-height controls in the western Hammerfest Basin, Barents Sea. Petroleum Geoscience 20, 227-240.

Kim, Y.S., Peacock, D.C.P., Sanderson, D.J., 2003. Strike-slip faults and damage zones at Marsalforn, Gozo Island, Malta. Journal of Structural Geology 25, 793-812.

Kim, Y.S., Peacock, D.C.P., Sanderson, D.J., 2004. Fault damage zones. Journal of Structural Geology 26, 503-517.

Michie, E.A.H., 2015. Influence of host lithofacies on fault rock variation in carbonate fault zones: a case study from the Island of Malta. Journal of Structural Geology 76, 61-79.

Peacock, D.C.P., Dimmen, V., Rotevatn, A., Sanderson, D.J., 2017a. A broader classification of damage zones. Journal of Structural Geology 102, 179-192.

Peacock, D.C.P., Nixon, C.W., Rotevatn, A., Sanderson, D.J., Zuluaga, L.F., 2017b. Interacting faults. Journal of Structural Geology 97, 1-22.

Vollgger, S.A., Cruden, A.R., 2016. Mapping folds and fractures in basement and cover rocks using UAV photogrammetry, Cape Liptrap and Cape Paterson, Victoria, Australia. Journal of Structural Geology 85, 168-187.

Figure captions

Figure 1. Features are often far easier to identify when observed from altitude. (a) Image from the ground in the Nazca Desert, Peru (image from: https://www.pinterest.com/pin/420664421429421399). (b) Aerial photograph showing an image from the Nazca Lines (image from: https://www.airpano.com/360photo/Nazca-Lines-Peru/).

Figure 2. Map of Malta showing the location of the field area, on the coast near Marsalforn, Gozo.

Figure 3. Different types of antithetic relationships. Sinistral faults are shown in red, dextral faults are shown in blue. (a) Oblique view of two conjugate strike-slip fault zones in Liassic limestones and shales at East Quantoxhead, Somerset, UK, which mutually crosscut each other. This is indicated by the intricate pattern of fault segments and areas of relative uplift and subsidence in the interaction zone (Peacock et al., 2017b). (b) Antithetic dextral faults developed at a contractional step along a sinistral fault zone (thicker red lines), near Marsalforn, Gozo.

Figure 4. Data collection and processing using a UAV. (a) Plan of a UAV flight near Marsalforn using DroneDeploy software. (b) Map showing the resultant photomontage, processed using the AgiSoft Photoscan software.

Figure 5. Map of a pull-apart developed at an extensional step along a sinistral fault zone, near Marsalforn, Gozo.

(a)

(b)

Peacock
Figure 1

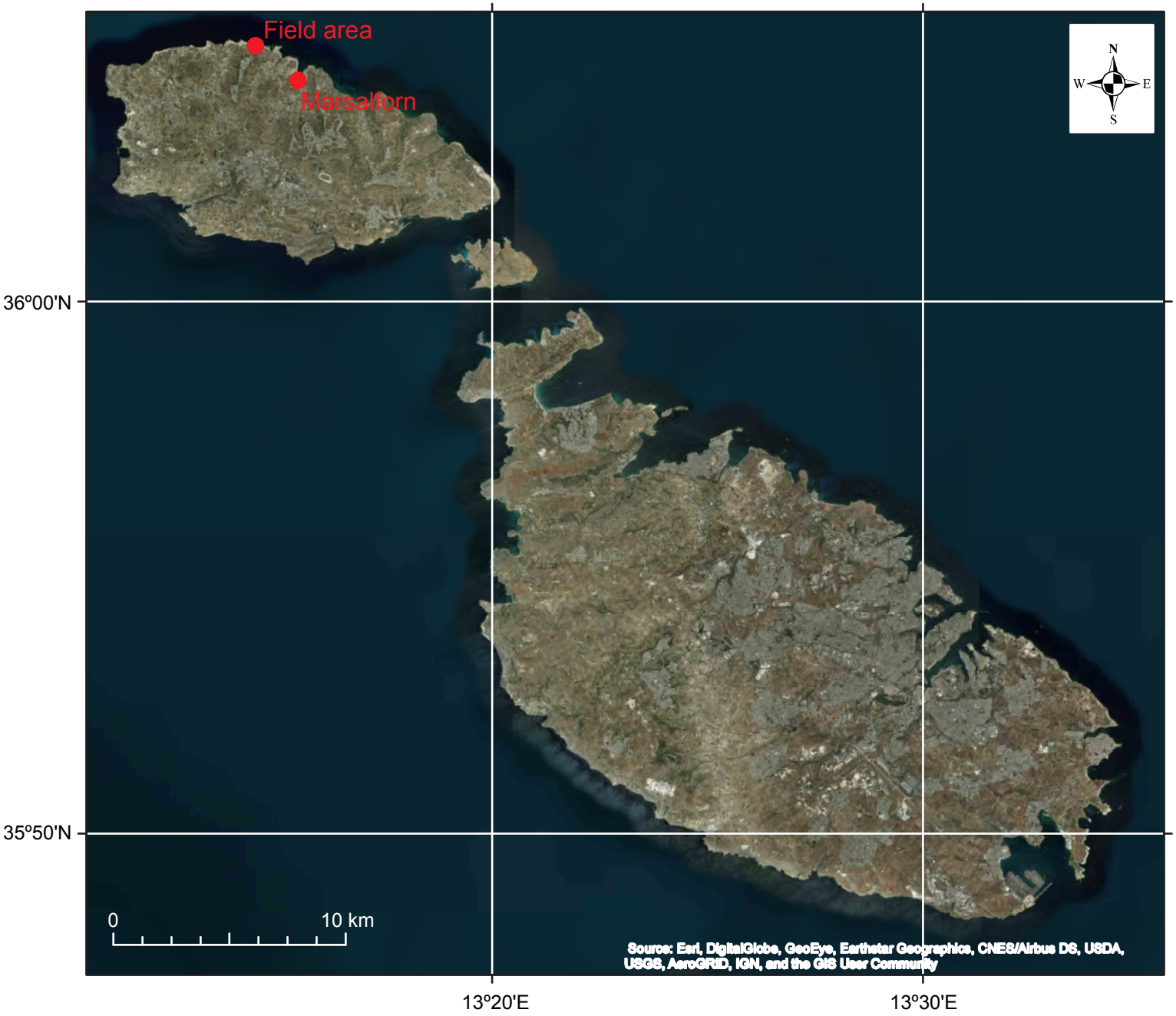

Peacock
Figure 2

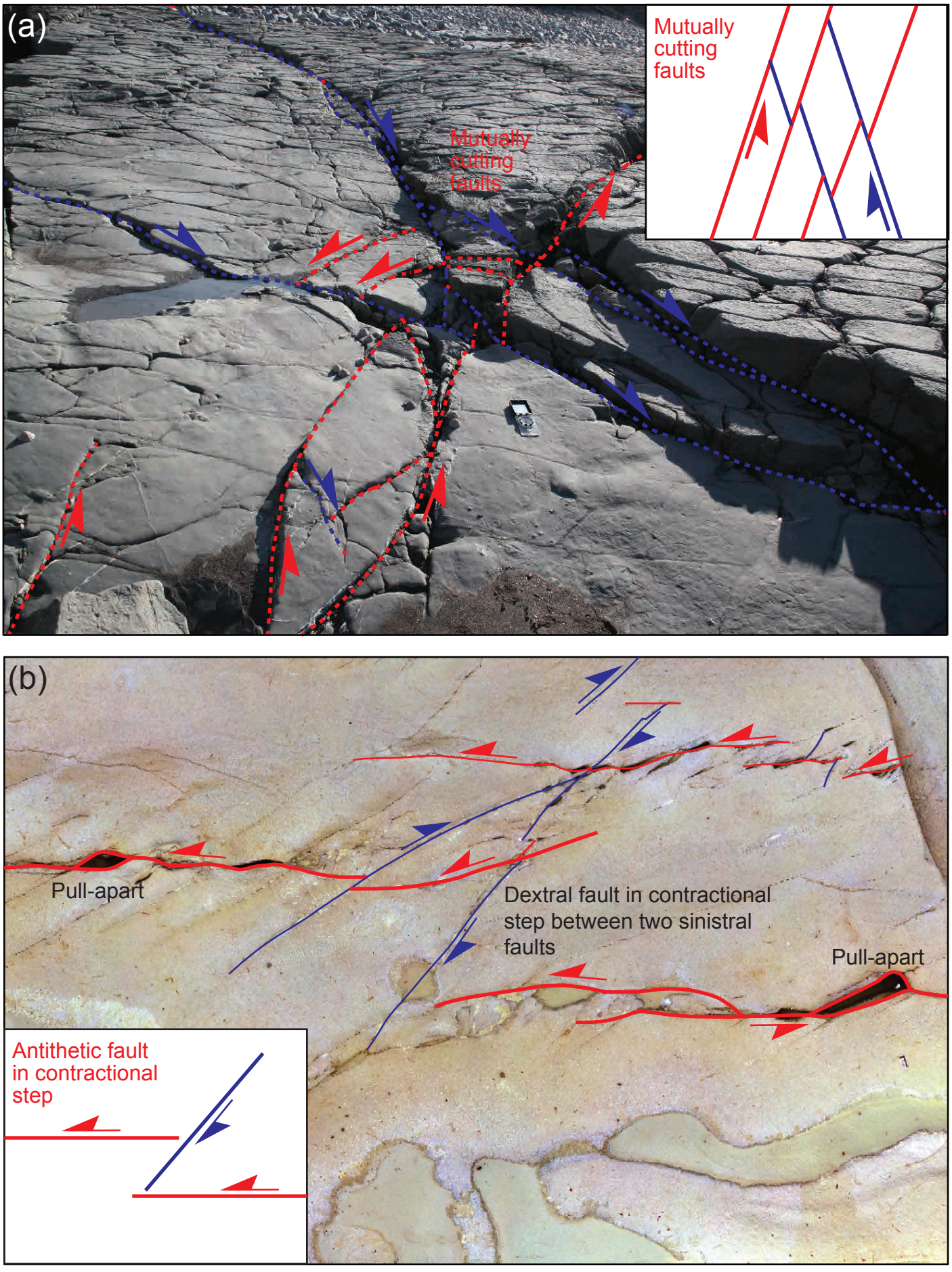

Peacock
Figure 3

(a)

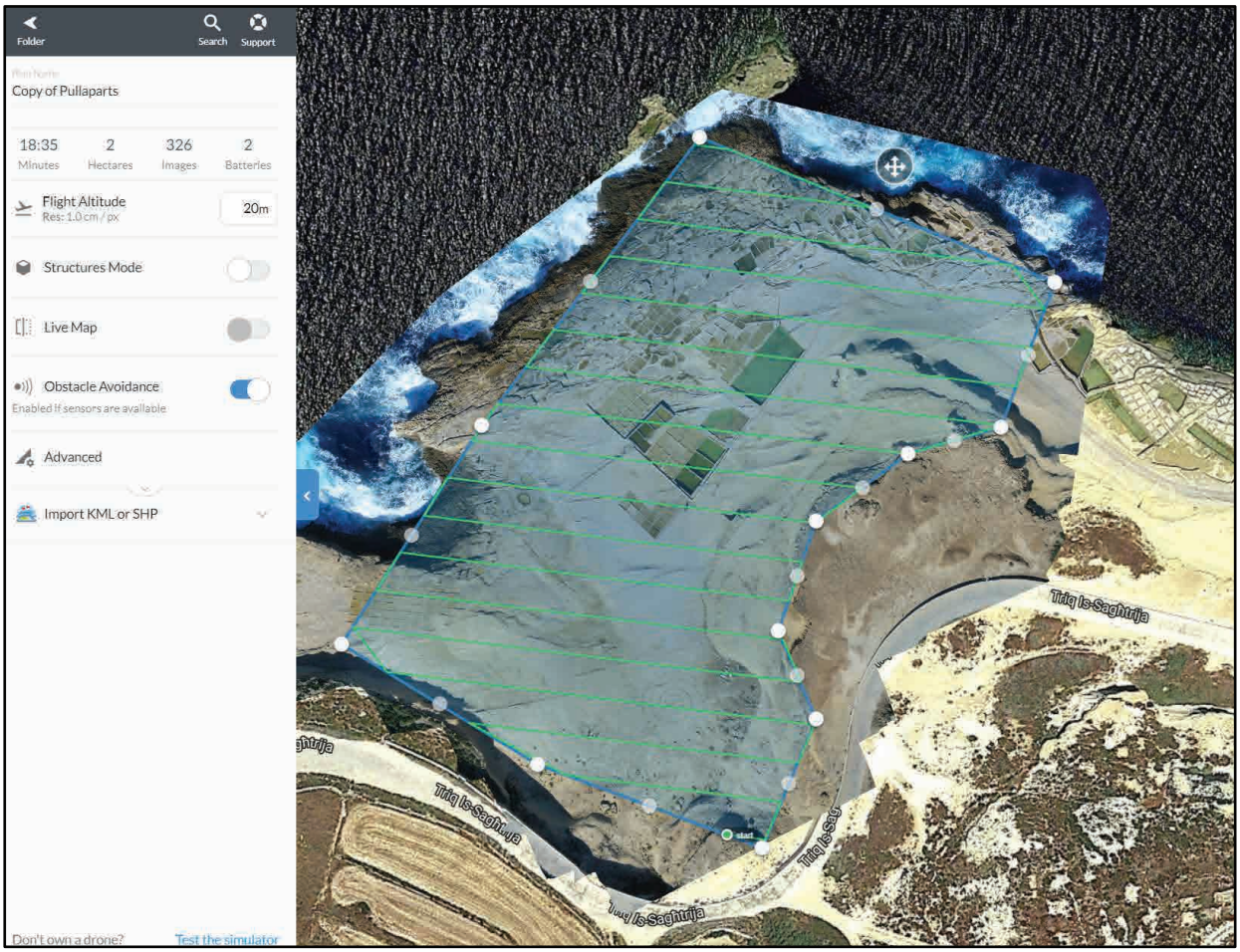

(b)

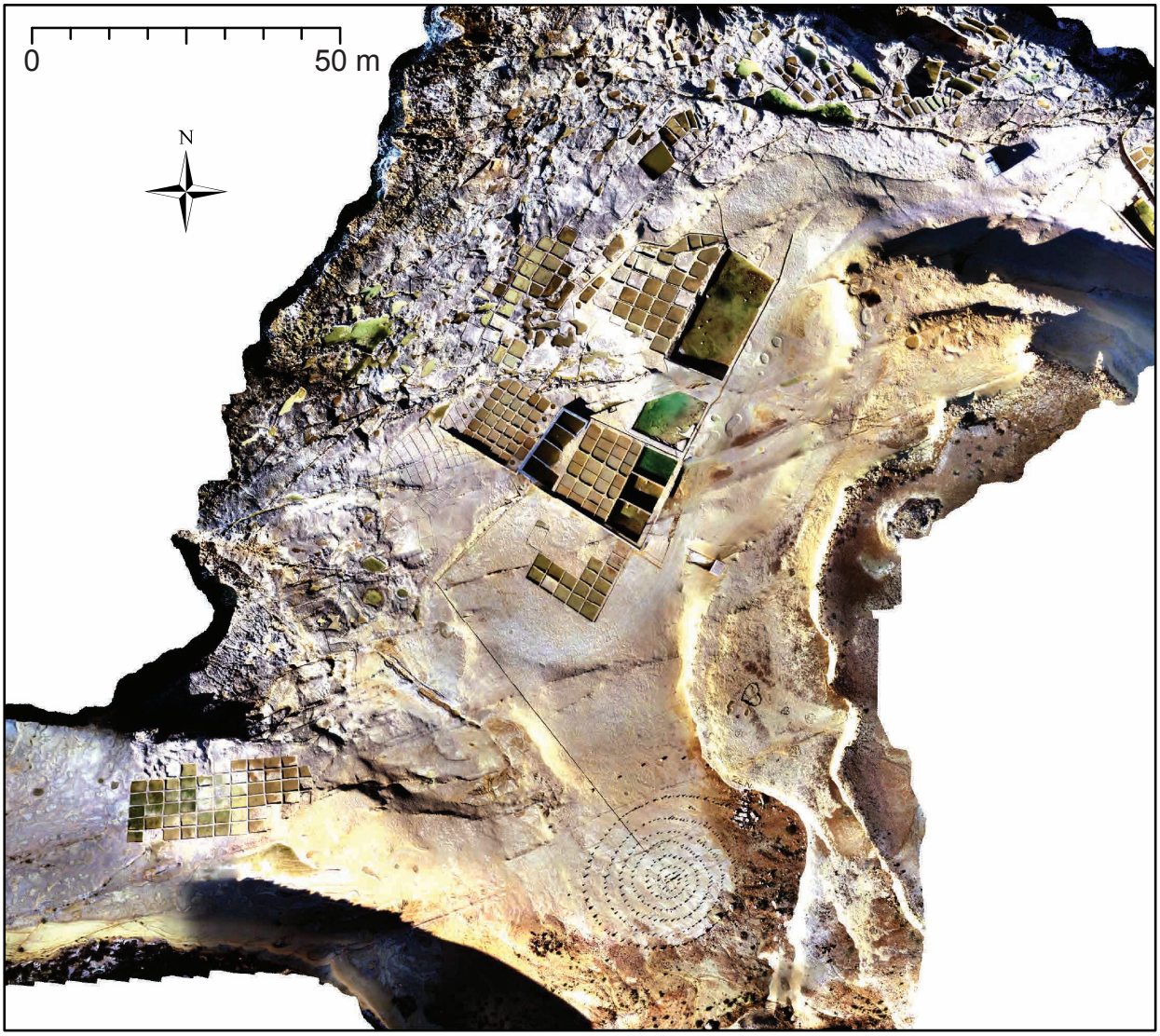

Peacock
Figure 4

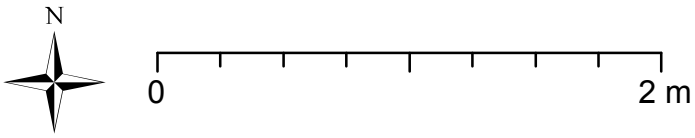

Peacock
Figure 5

Geological Society Research Grant 2018 Progress Report

Field constraints on lithological controls on landscape response times to active faulting in Calabria, Italy

Carla Pont, Imperial College London

Amount received: £1498 from the Elspeth Matthews fund

Motivation

Constraining landscape response times in regions of active tectonics provides crucial insights for using topography to infer active fault slip rate histories and for determining histories of landscape evolution. Rivers play a central role in transmitting tectonic signals to landscapes via incision of substrate. It is generally agreed that the speed at which fluvial knickpoints retreat upstream fundamentally controls timescales over which landscapes record a tectonic perturbation. However, to-date constraints and controls on these rates remain sparse.

Published data on knickpoint retreat rates upstream of active faults for bedrock catchments in Turkey, Italy and Greece suggest landscape response times differ markedly across regions: knickpoint retreat rates varies by more than an order of magnitude, for example retreat rates in Hatay Graben are up to 0.3 mm/yr, while rates in the Gediz Graben are 27.6 mm/yr (*Kent et al., 2017; Whittaker and Boulton, 2012; Roda-Boluda and Whittaker, 2016; Whittaker and Walker, 2015*). So why do we see this range in knickpoint speeds? Bigger catchment areas are expected to drive a faster erosional signal through the fluvial system. However, even when accounting for differences in catchment size, knickpoint speeds still varied by a factor > 6 and the residual signal appears to show weak correlation with the magnitude of fault throw rates. Consequently, landscape response times to tectonics varies significantly between regions even when faults are slipping at the same rate.

Could the remaining differences in knickpoint retreat rates be explained by differences in rock strength? The aim of this fieldwork was to obtain empirical field data on bedrock strength from rivers crossing active normal faults in Calabria to quantify the influence of lithology on landscape response times.

Field Campaign

We measured proxies for rock strength and channel morphology along three river channels in Calabria, Italy crossing the Armo, Scilla and Cittanova active normal fault systems during a 17-day field season in June 2018 (Figure 1). We successfully:

1) Measured in situ compressive strength using a Schmidt hammer of granite, gneiss and calcarenites bedrock channels at 47 different localities upstream of channels crossing active faults
2) At each locality, sampled bedrock exposure at different locations along the channel margin from the base-flow water mark to above the bankfull level to assess any water weakening effects on bedrock strength;
3) Characterised bedrock lithology, weathering, fracture orientation and weathering in order to use establish the best parameters to quantify bedrock erodability; and
4) Measured bankful width, depth and slope at 46 different localities in the field using a Haglof Laser Geo laser range finder as a means to assess channel narrowing effects and to reconstruct stream power and flow velocities relative to the fault

Figure 1 Victoria Fernandes holding the record schmidt hammer reading of 72.

Figure 2 Examples of knickpoints of the Favazzina river in Calabria, Italy upstream of the Armo fault clearly showing the river incising into bedrock. Digger at top centre of bottom photo for scale.

Preliminary Results

Our initial working hypothesis was that rivers would incise quickly through rock units with lower bedrock strength, while knickzones would form where the river steepens as it encounters lithological layers with higher values of compressive strength.

Preliminary observations show no significant difference in intact strength measured using a Schmidt hammer and hence erodabilities between the granite and gneiss rocks along the Calabrian river channels, despite multiple knickpoints. High variability in rebound values for both granites and metamorphic rocks reflected variable weathering states of the rocks along the river channels rather than intrinsic compressive bedrock strength and water weakening effects could not explain this scatter in data. Knickpoints characterised as significant convexities along the river long profile do not correlate with increasing R-value measurements, suggesting that lithology does not play a significant role in governing the shape of the river long profile in this area (Figure 2). R-values also showed no correlation with width of the river channel indicating that any channel narrowing effects may be tectonic rather than lithologically controlled. These results contradict our initial hypothesis and suggest that knickpoint development in Calabria is not lithologically controlled. Preliminary results shown here have already been presented at the British Society of Geomorphology 2018 AGM and the Geological Society support has been acknowledged.

Current and Future Research

As rock strength does not control knickpoint formation in these Calabrian river examples, we think knickzones may reflect temporal and spatial patterns of tectonic uplift, driven by the mapped active normal faults in the region, regardless of rock type. However, further analysis of data collected on fracture orientation and spacing may improve our understanding of whether alternative measures of rock strength are more important for bedrock erosion processes controlling landscape response times. If rock type is not a control on knickpoint development, we will test the extent to which knickpoint location and propagation is determined by varying regional and fault uplift rates over time.

References

Kent, E., Boulton, S.J., Whittaker, A.C., Stewart, I.S. and Cihat Alçiçek, M., 2017. Normal fault growth and linkage in the Gediz (Alaşehir) Graben, Western Turkey, revealed by transient river long-profiles and slope-break knickpoints. *Earth Surface Processes and Landforms*, *42*(5), pp.836-852.

Roda-Boluda, D.C. and Whittaker, A.C., 2016. Normal fault evolution and coupled landscape response: examples from the Southern Apennines, Italy. *Basin Research*.

Roda-Boluda, D.C. and Whittaker, A.C., 2017. Structural and geomorphological constraints on active normal faulting and landscape evolution in Calabria, Italy. *Journal of the Geological Society*, *174*(4), pp.701-720.

Whittaker, A.C. and Boulton, S.J., 2012. Tectonic and climatic controls on knickpoint retreat rates and landscape response times. *Journal of Geophysical Research: Earth Surface*, *117*(F2).

Whittaker, A.C. and Walker, A.S., 2015. Geomorphic constraints on fault throw rates and linkage times: Examples from the Northern Gulf of Evia, Greece. *Journal of Geophysical Research: Earth Surface*, *120*(1), pp.137-158.

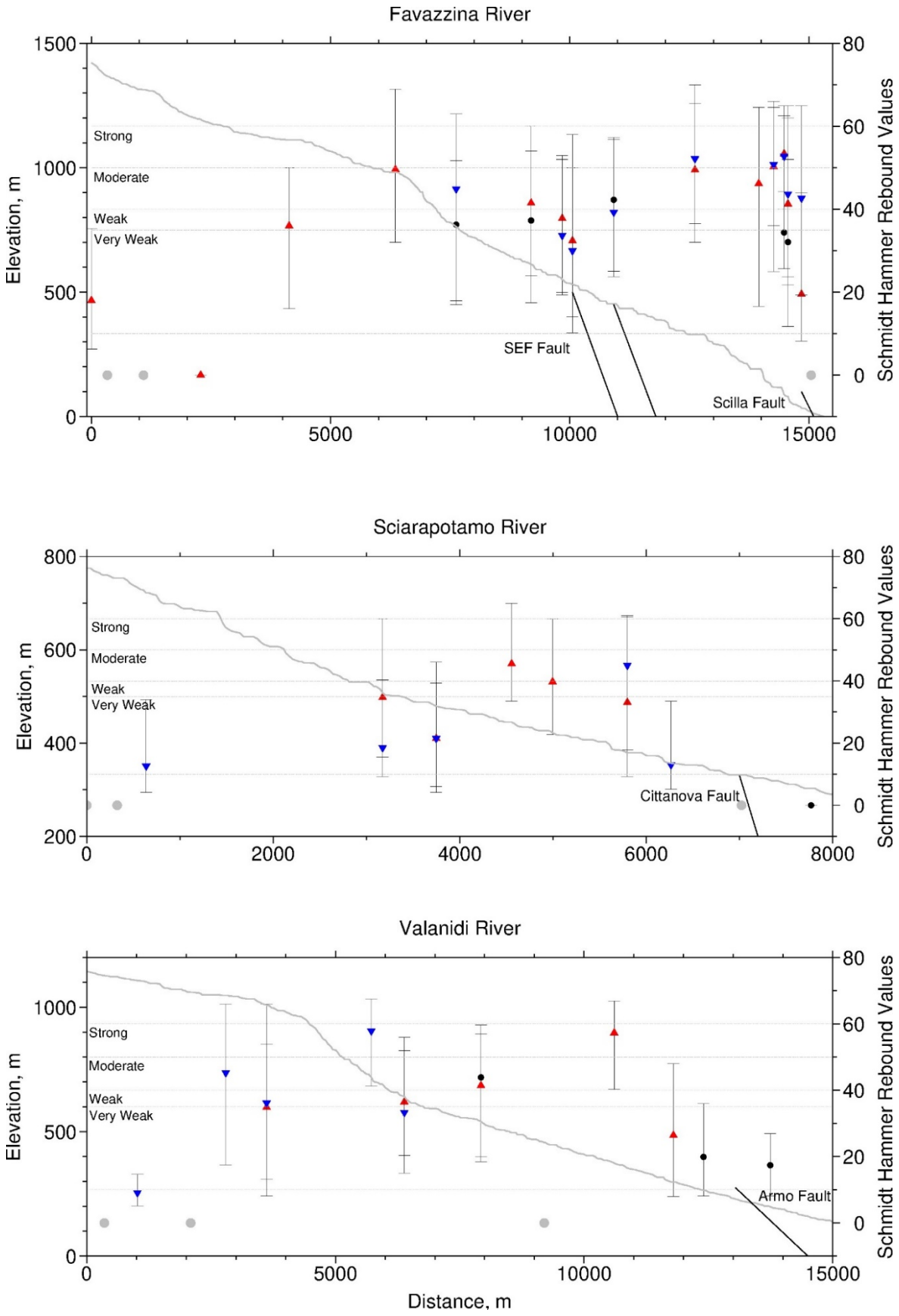

Figure 3 Rock strength measurements plotted against river profiles for the Valinidi, Favazzina and Sciarapotamo river. Blue triangles = sites below waterline; red triangles = sites at or above waterline; black circles = sites above weathering line.

Geological Society Research Grant 2018 Progress Report

Pamela Rattigan, University of Glasgow

£1,560 William George Fearnsides Research Grant

The stratigraphy and emplacement of lava-like and welded ignimbrites on the southern flank of the Las Cañadas Caldera, Tenerife, Canary Islands

1. Introduction

Lava-like ignimbrites are the highest-grade deposits of pyroclastic density currents (PDCs) and form as a result of rapid sedimentation from explosive, low column, ground-hugging eruptions. Due to their ability to maintain higher temperatures (>900°C), they undergo intense welding and ductile deformation, both syn- and post-emplacement, which can extend to the upper surfaces of deposits, creating a 'lava-like' lithofacies with a texture indistinguishable from that of a lava (Ekren *et al*, 1984; Branney & Kokelaar, 1992; 2002). The extra-caldera deposits of the Uncanca Formation (1.59 – 1.07 Ma) are the oldest of a series of three phonolitic caldera-forming eruptions of the Las Cañadas Caldera Complex (Uncanca, Guajara and Diego Hernandez Fms) and is the least documented and understood of the three. The units radially extend ~8 km across the centre of Tenerife (Figure 1) and include a series of lavas, fall deposits and ignimbrites exhibiting a broad range of welding profiles from non-welded to lava-like lithofacies.

Previous work has referred to the latter as lavas (Ridley 1969) and they are briefly described as vent-proximal welded fall deposits (Soriano *et al*, 2002; 2006) but with limited evidence of the emplacement model. Variations in welding have been attributed to transitions from sub-Plinian to spatter-fed, low-fountaining eruptions sourced from conduits at the caldera margin, with subsequent slumping and plug-flow of the hot deposits (Soriano *et al*, 2002; 2006). However, there is field evidence to suggest these units are the result of high grade, topographically controlled PDCs, exhibiting sedimentological structures, both syn- and post-emplacement deformation and a wide range of welding degrees and textures. My application was to obtain funding for the final season of fieldwork to complete sampling, stratigraphical logging and geological mapping to unravel the complex stratigraphy of the area.

Figure 1. Units of the Uncanca and Guajara Formations on the southern Las Cañadas Caldera wall.

2. Fieldwork

The Research Grant went towards the final field campaign of the project that took place for three weeks in June 2018. Through systematic, detailed field analysis, the stratigraphy of the southern flank of the southern Las Cañadas caldera wall has been picked apart, mapped and

correlated across the area. Five members have been identified (Figure 2), representing individual eruptive sequences, and this field season focussed on collecting additional structural data, isopach mapping and detailed centimetre-scaled stratigraphic logging through these units. Variations in grain sizes, juvenile and lithic clast content and distribution, textural and compositional variation, welding textures and variation, were all recorded, noting how these change laterally throughout the deposit. Variations in lithofacies both stratigraphically and laterally within individual members indicate that these are diachronous, oscillating significantly throughout the units.

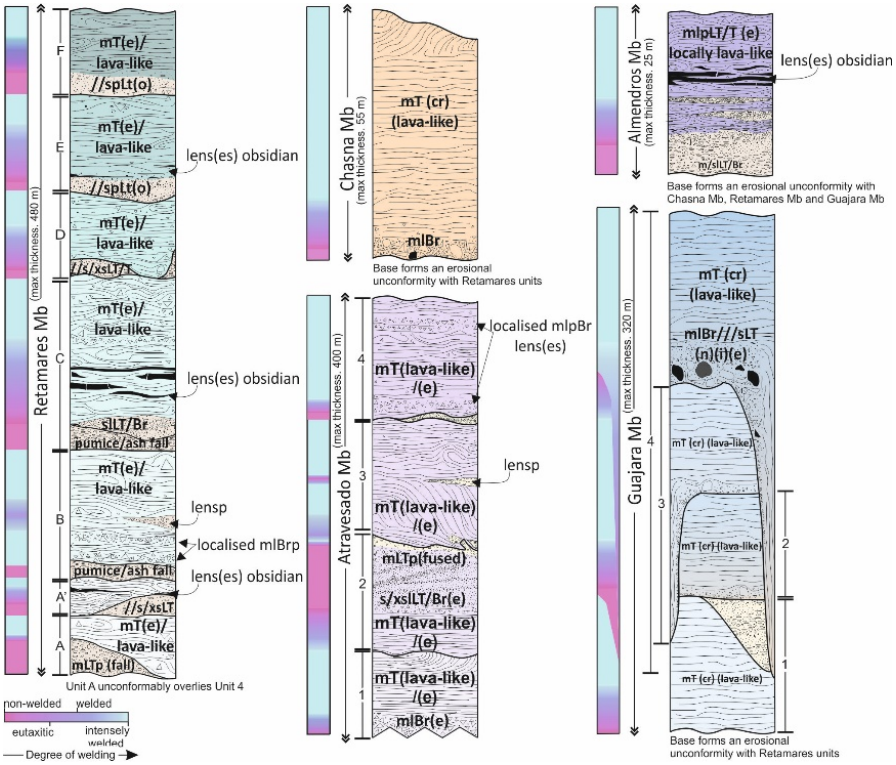

Figure 2. Schematic overview, lithofacies distribution and averaged welding profile of the central southern Las Cañadas caldera wall stratigraphy. Units are simplified and complex relationships between units is not represented, but noted at the base of each member.

My fieldwork uncovered a variety of new and exciting welding textures and profiles, which will contribute to better understanding these types of deposits. Samples were collected from various facies and stratigraphic positions throughout each unit for detailed textural and geochemical analysis. Structural data collected from fabrics, folds, and kinematic indicators (i.e. rotated lithic clasts) indicated two-stages of deformation (syn- and post-depositional), providing an insight into the flow directions for both depositional and post-emplacement slumping processes. With thanks to the William George Fearnsides Research Grant, field data from this field campaign was presented at the 7th IAVCEI International Workshop on Collapse Calderas held within Toba Caldera, North Sumatra, Indonesia in September 2018.

3. Future Work

A petrographical investigation (optical microscopy and SEM) in to the welding textures (both syn- and post-emplacement) and the interaction of pyroclastics at different degrees of welding in each of the lithofacies/ units is underway.

Samples are also being processed for ongoing geochemical analysis (XRF) of each unit to provide insight into the eruptive conditions. These analyses, combined with field data will build a multi-faceted eruption model of the Uncanca Formation, detailing the emplacement conditions, and cooling histories of these deposits, providing an insight into the initial caldera-forming eruptive phase.

The wider aims of my project address the nature and behaviour of these deposits, their place in the stratigraphy of Tenerife, and provide a stronger framework for the understanding of high-grade pyroclastic eruptions and the emplacement of welded and lava-like ignimbrites.

4. References

Ekren, E. B., McIntyre, D. H. & Bennett, E. H. 1984. High-temperature, large-volume, lavalike ash-flow tuffs without calderas in southwestern Idaho. US Geological Survey Professional Paper. 1272

Branney, M. J. & Kokelaar, P. 1992. A Reappraisal of Ignimbrite Emplacement - Progressive Aggradation and Changes from Particulate to Non-particulate Flow during Emplacement of High-Grade Ignimbrite. Bulletin of Volcanology. 54, 504-520

Branney, M. J. & Kokelaar, B. P. 2002. Pyroclastic density currents and the sedimentation of ignimbrites. Memoir / Geological Society of London. 27, 143

Ridley, W. I. 1970. The petrology of Las Cañadas volcanoes, Tenerife, Canary Islands. Contributions to Mineralogy and Petrology. 26: 124-160

Soriano, C. et al, 2006, Conduit-vent structures and related proximal deposits in the Las Cañadas Caldera, Tenerife, Canary Islands. Bulletin of Volcanology. 69: 217-231

Soriano, C. et al, 2002, Welding and rheomorphism of phonolitic fallout deposits of the Las Cañadas caldera, Tenerife, Canary Islands. GSA Bulletin, 114-7:883-895

Geological Society Daniel Pidgeon Fund Progress Report

Thyreophora, the armoured dinosaurs, are a group of bird-hipped ornithischian dinosaurs. They are characterised by their elaborate use of osteoderms, or body armour, on the head and body, and comprise the lineages Ankylosauria and Stegosauria, of which the most famous and recognisable members are *Ankylosaurus* and *Stegosaurus*, respectively. They are a diverse group, with up to 100 species known, and survived from the earliest Jurassic to the latest Cretaceous and lived on every continent. However, despite their familiarity with the general public, and an excellent fossil record, they are relatively understudied, especially in terms of their phylogenetic and evolutionary patterns, with most studies focusing on the form and function of their bizarre ornamentation. This has meant that there has been no previous attempt to build a species-level phylogenetic tree of the thyreophoran dinosaurs, hindering attempts to study their macroevolutionary patterns.

Support from the Geological Society's Daniel Pidgeon allowed me to visit Arizona, Colorado, New Mexico and Utah in the United States in October and November 2018 to visit the New Mexico Museum of Natural History in Albuquerque, the Museum of Northern Arizona in Flagstaff, the Natural History Museum of Utah in Salt Lake City, the Utah State University Eastern Prehistoric Museum in Price and the Denver Museum of Nature and Science to study world-class examples of thyreophoran dinosaurs. The US has one of the highest diversity of thyreophoran dinosaurs from anywhere in the world; the Upper Jurassic Morrison Formation has at least five species, including the iconic *Stegosaurus*, and there are numerous Cretaceous ankylosaurs found from across the continent. This trip allowed me to make first-hand observations of 16 taxa for inclusion into a phylogenetic super-matrix of the thyreophoran dinosaurs as well as systematic observations on enigmatic taxa such as *Denversaurus*.

The nodosaur *Animantarx* from the Utah State University Eastern Prehistoric Museum (left) and the iconic *Stegosaurus* mount in the Denver Museum of Nature and Science (Image source: Tom Raven)

This new, comprehensive phylogeny is still being constructed, with a visit to the eastern US and Canada to come in May 2019, but it will be completed by the end of my second year of my PhD in September 2019 after having seen over 60 taxa first-hand. It will then be used as a backbone for studies of macroevolutionary processes within the Thyreophora, such as on the diversity and disparity across time, as well as character, speciation and extinction rate analyses, providing new insights into the mode and tempo of evolution of these enigmatic Mesozoic dinosaurs.

Tom Raven, PhD student at the Natural History Museum and the University of Brighton

Mass-transport complexes (MTCs) as seals: a case study from the Magnus Field, Northern North Sea

Grant
Daniel Pidgeon Fund: Awarded £1000

Project Team
Imperial College London
Mr. Michael Steventon, michael.steventon13@imperial.ac.uk
Professor Christopher A-L Jackson, c.jackson@imperial.ac.uk
Professor Howard Johnson, h.d.johnson@imperial.ac.uk

University of Leeds
Professor David Hodgson, d.hodgson@leeds.ac.uk

University of Liverpool
Dr. Christopher Stevenson

EnQuest PLC, Aberdeen
Dr. Sean Kelly, sean.kelly@enquest.com

RockType Ltd
Dr. Jenny Omma, jenny.omma@rocktype.com

Overview
Project Aims

1. Assess how the petrophysical and petrographic properties of MTCs basal shear surfaces vary spatially
2. Determine the relationship between basal shear surface seal potential and substrate lithological and compositional heterogeneity
3. Develop a predictive model for MTC seal risk

Key milestones
Since receiving the funds from the Geological Society of London, we have undertaken several activities to reach our original project aims including:

1. **December 2017**: initial Core Store visit to Aberdeen for scoping out relevant intervals of interest for more detail logging in the future
2. **August 2018:** week long Core Store visit to log select target intervals and collect samples for quantitative electron microscope scanning (QEMSCAN) (undertaken by RockType Ltd).
3. **November 2018:** results from QEMSCAN analysis received from RockType.
4. **Present-July:** analysing results and integrating core logging, petrophysical well logs, 3D seismic-reflection data, and QEMSCAN analysis.
5. **July 2019:** final manuscript for journal submission

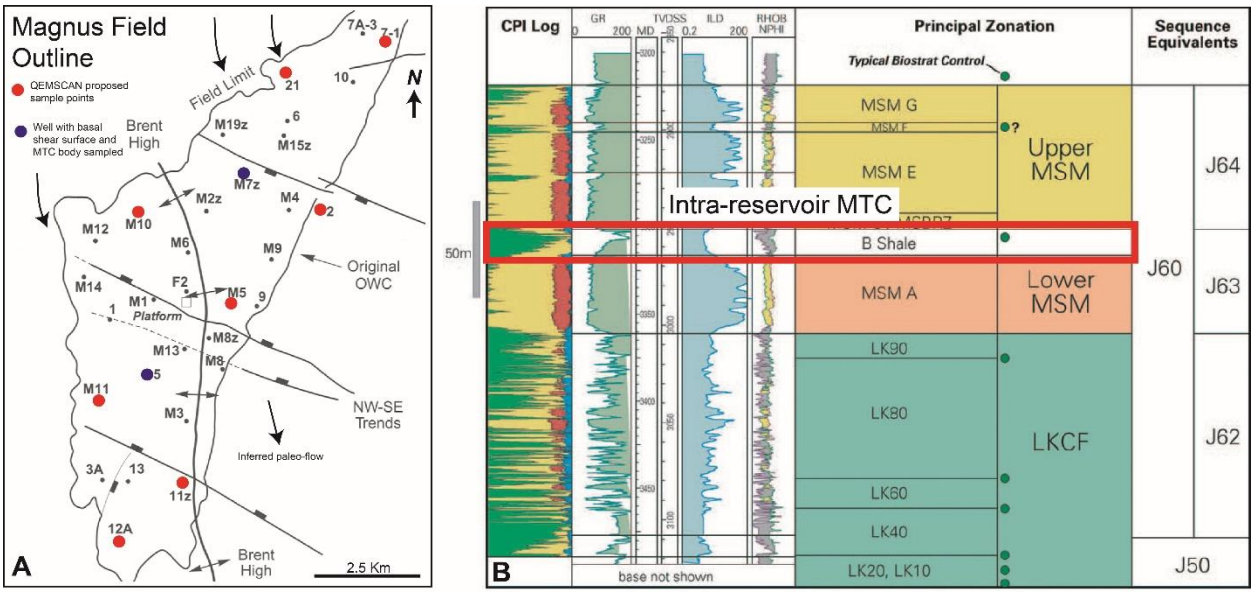

Figure 1: (A) Location map modified from (Morris et al. 1999) note the proposed sample locations which capture proximal and distal areas of the MTC, (B) biostratigraphy of the Magnus Field, note intra-reservoir MTC, modified from (MacGregor et al. 2005).

Summary of work to date:

Core logging

Systematic core logging (69 m) and collection of 15 samples for further analysis was undertaken on 5 wells within the Magnus B-Shale interval and surrounding Magnus Sandstone member (Figs. 1 & 2). The following features have been documented: grain size variations, lithology, volume of shale content, sedimentary structures, deformational fabrics, and an interpretation of depositional processes and sedimentary environments (Fig. 3).

Quantitative Evaluation of Minerals by Scanning electron microscopy (QEMSCAN)

15 samples were taken from well 211/12A-M16 for QEMSCAN analysis to discern mineralogical heterogeneities, depositional textures, quantify depositional processes and understand porosity-permeability distributions (Fig. 4). This includes samples from the MSA sandstone member, B-Shale, and MSC sandstone member.

Current & future work

Currently I am in the process of analysing the data from the QEMSCAN and integrating these with core and petrophysical logs.

The following analyses are in progress:

- Image analysis and segmentation of texture, mineralogy, structure and porosity distributions within the QEMSCAN images
- Plotting of raw data to quantify grain-size trends and quantifying the link between grain size and sedimentary structures on bedform stability diagrams
- Understanding potential genetic relationships in mineralogy between the B-Shale and MSA/C units
- Integrating QEMSCAN results with previous work undertaken on core and petrophysical logs

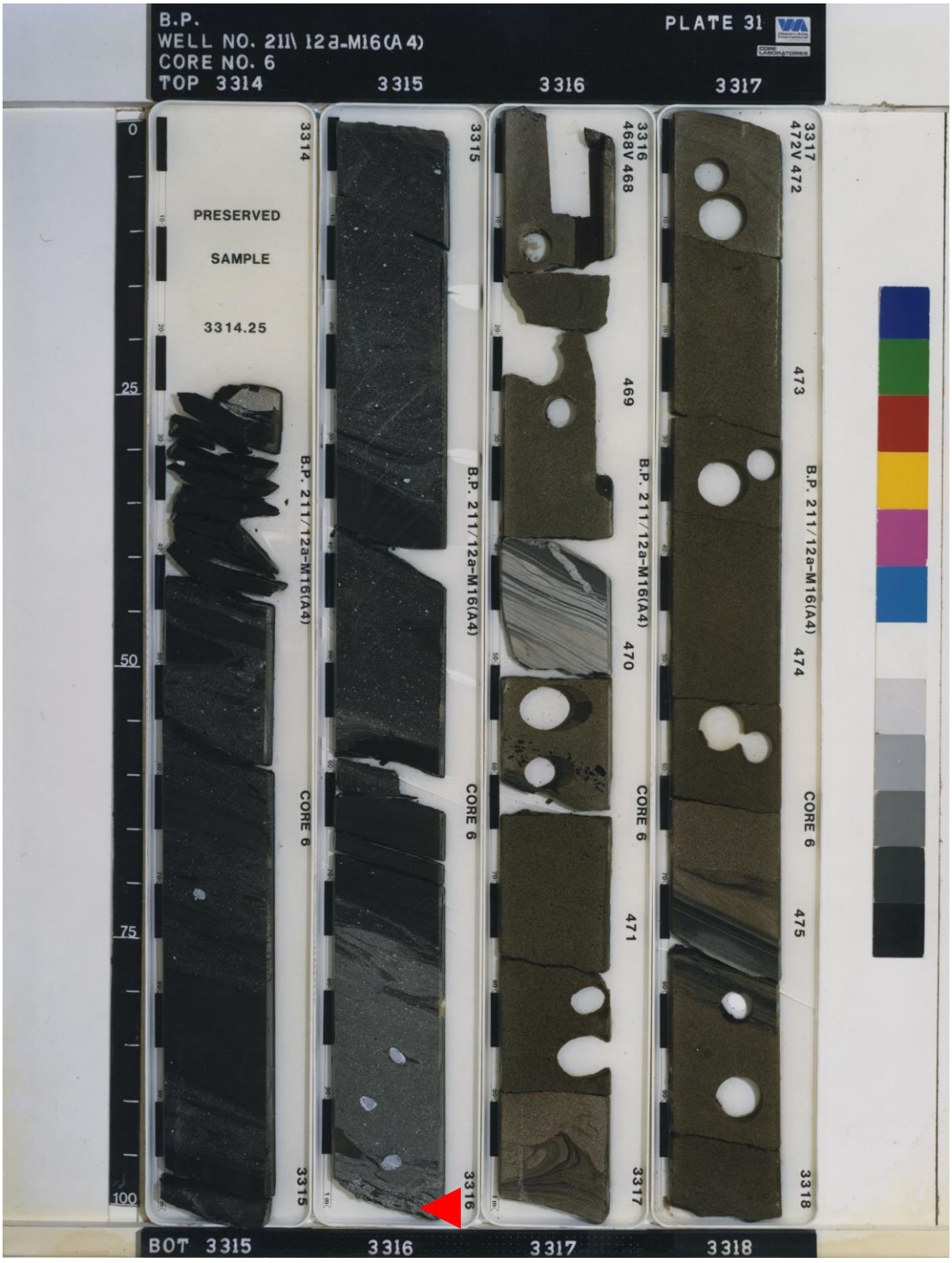

Figure 2: Core photograph from Well M16 in the Magnus Field, Northern North Sea, showing the boundary (c.3316 m) between the lower MSA turbidite reservoir and the B-Shale mass-transport deposit.

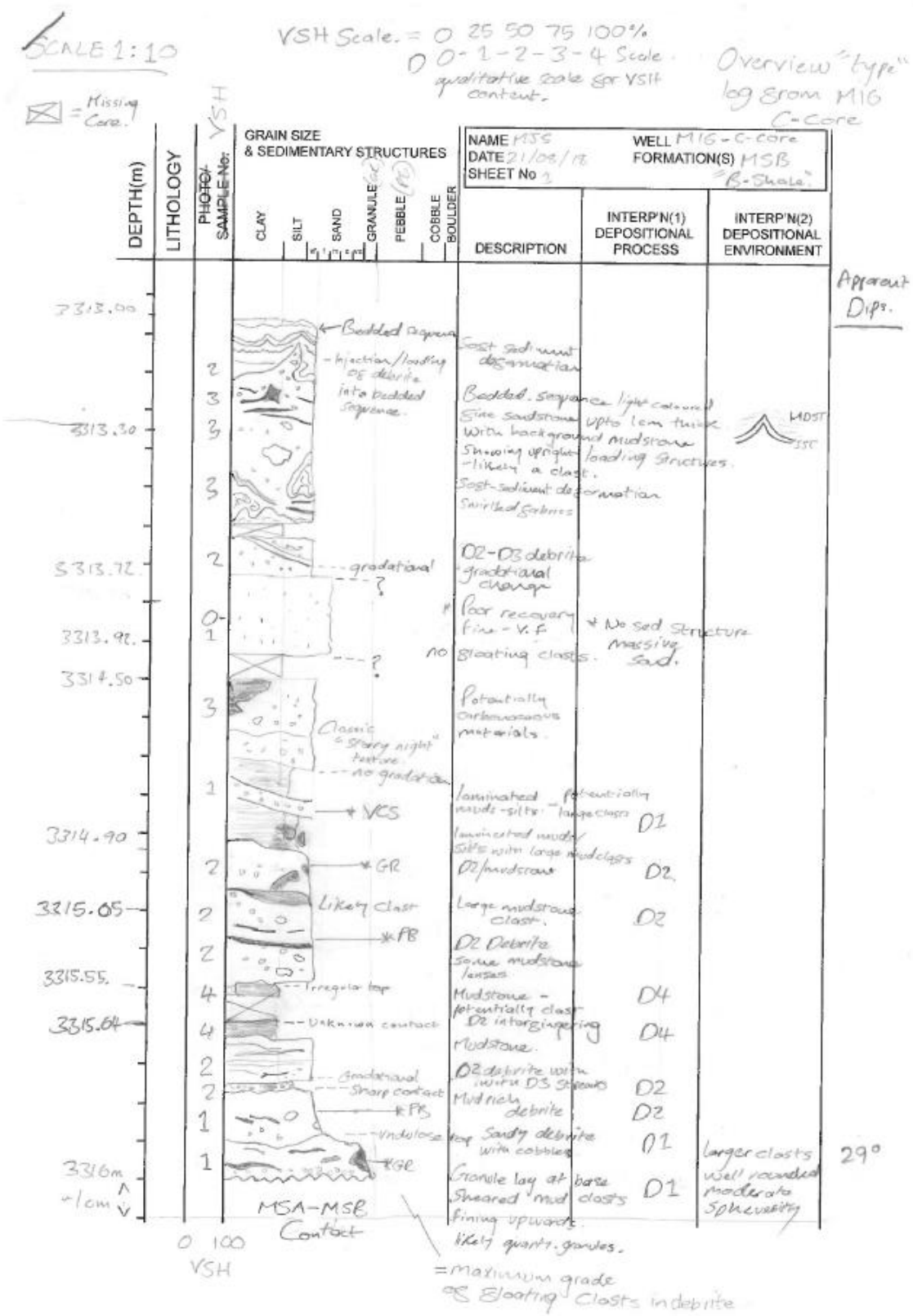

Figure 3: Example of B-Shale core longing detail from well 211/12A-M16.

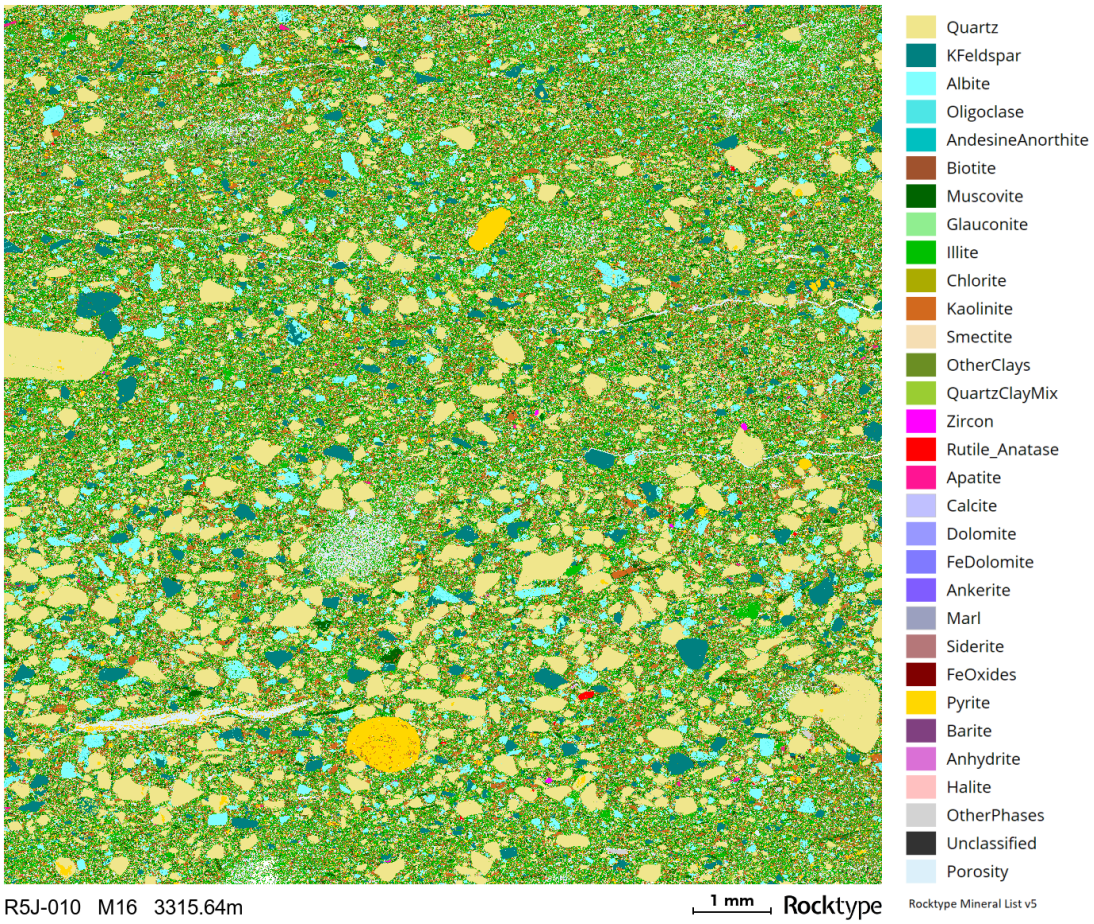

Figure 4: QEMSCAN analysis from B-Shale unit in well 211/12A-M16, highlighting the textural and mineralogical heterogeneity associated with the unit.

References

MacGregor, A., Trussell, P., Lauver, S., Bedrock, M., Bryce, J. & Moulds, T. 2005. The Magnus Field: extending field life through good reservoir management and enhanced oil recovery. *Geological Society, London, Petroleum Geology Conference series*. Geological Society of London, 469-475.

Morris, P., Payne, S. & Richards, D. 1999. Micropalaeontological biostratigraphy of the Magnus Sandstone Member (Kimmeridgian-Early Volgian), Magnus Field, UK North Sea. *Geological Society, London, Special Publications*, 152, 55-73.

Geological Society of London, Research Grant (Joseph Burr Tyrrell Fund 2018): Progress Report

Deciphering the palaeoceanography and temperature structure of Iapetus using conodont oxygen isotopes: temporal variability across the Cambro-Ordovician boundary, Newfoundland, Canada.

Fieldwork in western Newfoundland during summer 2018 (10 days) was undertaken as planned; field logging and conodont sample collection were successful from sections outlined in the application. Work was undertaken collaboratively as set out in the application with Prof. Paul Smith (Director, Oxford University Museum of Natural History) and in the field with support from Prof. Duncan McIlroy (Memorial University, Newfoundland). Conodont samples were shipped from Canada to the UK, arriving winter 2018. The samples will be processed at Oxford, beginning in January 2019 and this part of the work is envisaged to take 3-4 months – once conodonts have been recovered from the acid digestion residues I can then move to making applications in Spring 2019 to NERC for analyses of oxygen isotopes using the Edinburgh ion microprobe. The research grant of £1990 was fully spent on fieldwork and shipping of samples.

James R. Wheeley

17/12/18

Report:
Thermal imaging of a tidewater glacier plume in Svalbard

Recipient of the Robert Scott Memorial award of GBP 2000

Esty Willcox

August 24, 2018

1 Purpose

The fieldwork component of my MSc project was financed by the 'Cambridge Arctic Shelf Programme: Robert Scott Memorial Award' of the Geological Society for the thermal imaging of a Svalbard tidewater glacier. The research is intended to determine whether the detection of a buoyant melt water plume at the surface of a fjord using thermal timelapse imaging is feasible.

Plume dynamics are important to measure because it is extremely difficult to determine the amount of melt taking place on tidewater glaciers since it cannot be measured directly due to logistical impossibility [Truffer and Motyka, 2016].

Currently plume presence, shape, size and dynamics are usually measured by analyzing RGB images from timelapse photography or remote sensing for the suspended sediment concentration (SSC) [Dowdeswell and Cromack, 1991, Schild et al., 2017, How et al., 2017]. However, there have been some indications that fresh water flux and suspended sediment presence are not directly interchangeable [Moskalik et al., 2018].

This project is currently limited by being two-dimensional, and whether the plume penetrates the surface layer of the fjord depends strongly on the density stratification of the fjord water and the velocity and magnitude of the plume(s) at the ice-ocean interface. If this method proves useful, it could be applied in combination with a small mooring, which would allow for a 3 dimensional approximation of a plume at high temporal and spatial resolution.

2 Methods

A small thermal imaging device (Micro Epsilon thermoIMAGER TIM 450) was deployed at the location specified in Figure 1a on 17 August 2018 at 22:43. It recorded one image each 5 minutes for approximately 6 hours. One of the solar panels was damaged in transit so the batteries were not able to charge sufficiently to keep the batteries from discharging.

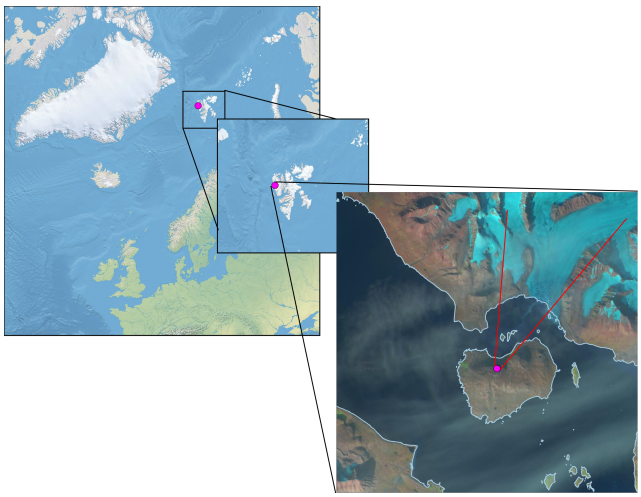

(a) Location of camera placement (pink dot) and the fjord in front of Blomstrandbreen. Red lines denote approximate field of view of the TIR imager.

(b) Placement of equipment overlooking the fjord and Blomstrandbreen

Figure 1: Location and deployment of the field equipment

The TIM 450 was placed inside a length of drainpipe with a 3D printed cap placed at either end to ensure the small computer unit used to record the data was protected from any weather. This was placed on a tripod which was weighted down with rocks. Two charged lithium ion batteries were attached and the remaining solar panel was connected to allow for some recharging. a photograph of the set up at the field location is shown in Figure 1b.

3 Results

The resulting six hours of footage were of good quality, the sum of the emission and reflection spectra between the wavelengths recorded by the sensor seem adequately represented, although further work is neccesary for their validation.

A few unexpected issues did crop up in the field data, examples of which are shown in Figures 2a and 2b. Particularly the issue of reflection from a specular surface will have to be compensated for during any further deployments. I would suggest placing a second camera at a similar angle upwards to normalize the fjord surface data. Placing multiple cameras at

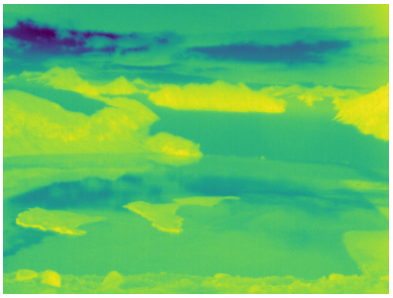

(a) If the surface of the fjord is specular, the sky is perfectly reflected at thermal wavelengths.

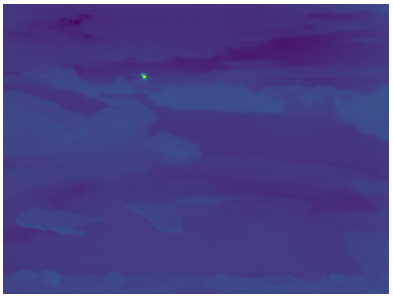

(b) When the sun is directly ahead of the sensor the resulting image is inadquate.

Figure 2: Thermal imagery taken by TIM 450

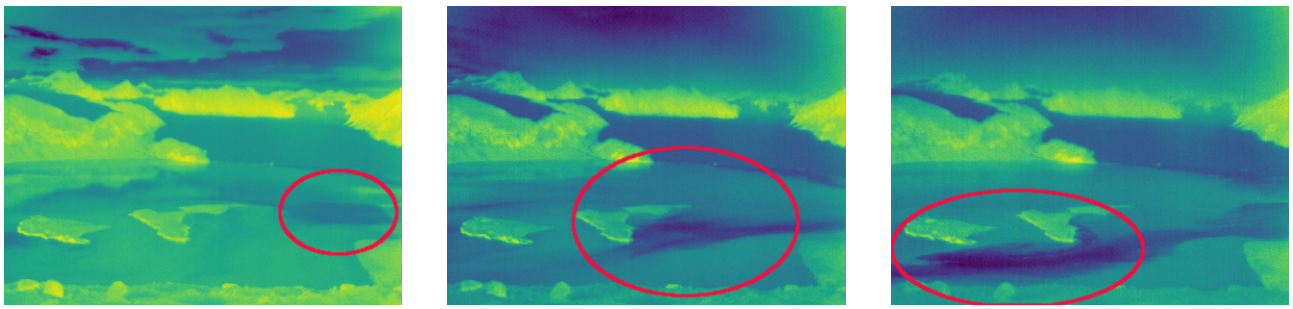

(a) Plume becomes visible at the surface at a distance from the glacier front

(b) Cold water is transported through the fjord and comes to the surface

(c) Cold water from the plume is advected past the small islands

Figure 3: Plume progression using the thermoIMAGER TIM 450. Yellow is warm, dark blue is cold. Currently this is still a relative measure.

different angles around the fjord is also a potential solution. The latter would additionally be useful during those times where the sun is directly ahead of the sensor.

What is interpreted as a buoyant melt water plume does become visible in the footage and is shown in Figures 3a, 3b, and 3c. The cold water becomes apparent in the footage as a roughly elliptical area (shown in the red ellipse in Figure 3a). The plume is transported out of the fjord, past the camera in the successive images. The entire image becomes colder during these three images. It is possible this is due to a reduction in insolation (the sky becomes more diffuse in later images, which would have a direct cooling effect on the surface), or whether this is due to technical or systemic bias. The process currently still requires review.

4 Conclusion

From the fieldwork conducted it looks like it is possible to obtain buoyant meltwater plume data from the deployment of thermal cameras at an oblique angle above a fjord. There are several aspects of the technique which certainly require refinement and review, however the additional information gained at high resolution certainly improves our knowledge of this field.

References

Julian A Dowdeswell and Marianne Cromack. Behavior of a glacier-derived suspended sediment plume in a small Arctic inlet. *The Journal of Geology*, 99(1):111–123, 1991. URL http://www.jstor.org/stable/30068769.

Penelope How, Douglas I. Benn, Nicholas R.J. Hulton, Bryn Hubbard, Adrian Luckman, Heïdi Sevestre, Ward J.J.Van Pelt, Katrin Lindbäck, Jack Kohler, and Wim Boot. Rapidly changing subglacial hydrological pathways at a tidewater glacier revealed through simultaneous observations of water pressure, supraglacial lakes, meltwater plumes and surface velocities. *Cryosphere*, 11(6):2691–2710, nov 2017. ISSN 19940424. doi: 10.5194/tc-11-2691-2017. URL https://www.the-cryosphere.net/11/2691/2017/.

Mateusz Moskalik, Joanna Ćwiąkała, Witold Szczuciński, Aleksander Dominiczak, Oskar Głowacki, Kacper Wojtysiak, and Piotr Zagórski. Spatiotemporal changes in the concentration and composition of suspended particulate matter in front of Hansbreen, a tidewater glacier in Svalbard. *Oceanologia*, 2018. ISSN 23007370. doi: 10.1016/j.oceano.2018.03.001.

Kristin M. Schild, Robert L. Hawley, Jonathan W. Chipman, and Douglas I. Benn. Quantifying suspended sediment concentration in subglacial sediment plumes discharging from two Svalbard tidewater glaciers using Landsat-8 and in situ measurements. *International Journal of Remote Sensing*, 38(23):6865–6881, dec 2017. ISSN 0143-1161. doi: 10.1080/01431161.2017.1365388. URL https://www.tandfonline.com/doi/full/10.1080/01431161.2017.1365388.

Martin Truffer and Roman J. Motyka. Where glaciers meet water: Subaqueous melt and its relevance to glaciers in various settings. *Reviews of Geophysics*, 54(1):220–239, mar 2016. ISSN 19449208. doi: 10.1002/2015RG000494. URL http://doi.wiley.com/10.1002/2015RG000494.

Finally, after months of preparation, in July 2018 I arrived on Tanna island in Vanuatu with all my equipment. As part of an international team, our aim was to measure remotely Yasur's gas emission by using FTIR, MultiGAS and SO_2 cameras to study changes of its volcanic activity. The first time I saw Yasur Volcano (Figure 1 (A)), I was slightly disappointed because I could not imagine that this small and odd-shaped volcano without any sign of visible activity should be one of the most active volcanoes on Earth. At the same day in the in the evening, we climbed Yasur and I knew why it deserved to be called one of the most active volcanoes in the world. Non-stop natural firework is probably the best way to describe it (Figure 1 (B)).

Figure 1 (A) Mount Yasur is a 361 m a.s.l basaltic- andesitic volcano is on Tanna island, in the archipelago of Vanuatu in the Southwest Pacific Ocean. (B) Yasur's spectacular activity. Both of its craters are visible: on the left side of the photo the so-called south crater and next to it the north crater. The photo captured a Strombolian eruption in the north crater that expelled basaltic bombs into the air.

Bubble formation -Volcanic degassing

Magma is a molten rock in the Earth interior that contains gases and minerals. When magma rises towards the Earth surface, the pressure decreases, and gases start to exsolve from it and form tiny bubbles. The first gas to exsolve is CO_2 at around 10 km followed by SO_2, H_2O and many other gas species in the shallow volcanic system. At the beginning, small bubbles are transported in the magma but when bubble merge and reach a sufficient size they can rise on their own. These merging processes are from great interest because bubble size influence the eruption style, the volume of ejected magma and the mass of released gas.

Strombolian activity

My research interest focuses on the formation on large bubbles in volcanic conduits filled with crystal-rich magma and their cyclicity in eruption patterns. This eruptive behaviour is called Strombolian activity. Strombolian eruptions begin with the arrival of a large gas bubble at the top of conduit that is open to the atmosphere. The length of these bubbles varies between 13 and 200 m. Therefore, a gas bubble often increases the height of the magma surface until it bursts and releases a large volume of gas that fragments the melt and ejects molten magma cloths, up to meter sized, and ash into the air. Each violent burst lasts just a few seconds. Among the volcanoes with recognised components of Strombolian behaviour are Stromboli, Pacaya (Guatemala), Erebus (Antartica), Villarica (Chile), Reventador (Ecuador), Arenal (Costa Rica) and Yasur (Vanuatu).

Yasur is volcano is a perfect natural laboratory to study persistent degassing because its degassing rates possibly maintained over the last 1400 years. Yasur's Strombolian activity can be interrupted by Vulcanian eruptions.

Remote volcano and an angry god

The members of our team were Tom Pering, Tehnuka Illanko (University of Sheffield), Roberto D'Aleo (INGV Palermo) and Rodger our local guide. None of us researcher had been to Vanuatu before and we all could not really believe it, that we were there because of the last-minute complications e.g. lack of official permissions, confiscated passport or delay of equipment transport. The flight from Efate, the mean island of Vanuatu, to Tanna takes approximately 40 minutes. At Tanna airport, Kelson, the owner of Jungle Oasis picked us up and from there and it took us more than 2 hours to arrive at our "new home" for the next 2 weeks because we had to do all the shopping, we needed for at least a week. The place we stayed was very close to the volcano that we could even feel the shock waves produced by the volcano during stronger eruptions. One of the first things we did, was to install our solar panel on the roof of our house to charge batteries. Soon we realised that due to the cloudy sky and very early sunsets it was not possible to charge all the batteries with it. In our accommodation we had just 2 hours per day electricity which was powered by a generator but unfortunately, we could not use it for charging batteries. So therefore, I had to arrange a driver who brings me and my six batteries to the main town of the island where only one person could charge batteries and he was not always easy to find. This ride took several hours in the night as we had to drive from one side to the other side of the island, crossing an ash plane and river bed before we were at least on unpaved roads. Because I had to do these trips several times it gave me the opportunity to learn about their daily routine, traditions of clans, relationship between locals and the volcano. Once in the car the driver explained me that Yasur is the bislama word for god because in ancient times they believed that an angry god is living in the volcano causing the eruptions. As the volcano has 4 permanent vents, each vent was dedicated to the 4 villages (Kraesun, Wei Wei, Kaunaung, Kasmiren) close by the volcano for sacrifices to calm the god. Just one person in a village was allowed to make these sacrifices because he could talk to the volcano. They also believed that all the butterflies on Yasur are reincarnated souls. Nowadays, just one village in Tanna believes in this traditional religion and Mormonism took over.

Day in the field

The tasks in the field involved the setting up of the remote sensing instruments to measure the chemistry of gases, install the camera permanently to get information about variable eruptive activity, changes in crater morphology and vulcanological features as well as collecting volcanic bombs for petrological analysis in Cambridge. Setting up FTIR on the volcano rim was far from easy because the continuous eruptions just few meters away were irritating, the plume thickness made it very difficult to align the spectrometer and the artificial light source with each other (Figure 2 (A)). Several times the view was restricted to just 5 m and we always had to take extreme care of flying hot bombs in the air. Sometimes we left the measuring equipment on the crater rim and made our way to more safe areas. We were also aware of the hazardous impact of the volcanic gases itself because everything started to corrode after few hours starting from the light source to safety googles.

First results

In August, I started to process the videos taken during the field work on Yasur to count the number of vents and observe the changing volcanic activity of each vent (Figure 2 (B)). It was very interesting to find out that the number of vents changed nearly daily between 5 and 7 vents. I found out that the frequency of eruptive events (bubble burst per second) varies between 4 and 0.7. There is also a trend indicating that at the number of eruptive events is decreasing with increasing explosive events like Strombolian eruptions. Furthermore, our data

provide results showing that bubble bursts are either SO_2 or HCl rich (Figure 3). Whereas, the CO_2/SO_2 ratios were pretty stable during the whole time in the field with the average value of 1.09 (± 12 %). Our first estimation of Yasurs fluxes are comparable in terms of CO_2 and SO_2 with previous published articles with maximum fluxes of 860 t d^{-1} SO_2 and 936 t d^{-1} of CO_2. Our calculated maximum HCl fluxes are 5 times higher than previous ones with 842 t d^{-1}. Reason for this disagreement could be a change in the volcanic degassing regime itself or could be caused by the methods to measure HCl in the volcanic plume.

Figure 2 (A) Alignment of the FTIR spectrometer and light source (orange arrow) on the south crater rim. The bad visibility made an alignment impossible even for a small distance. Furthermore, the photo shows clearly that bombs in different sizes, ranging from few cm to m, fell down on the crater. (B) South crater activity on 14th July. On this picture vents are marked with numbers. The emerging of a new vent with just ash - rich eruption (vent 6) made it difficult to see the whole crater. Vent 3, 4 and 5 mainly degassed passively and vent 2 and 1 showed powerful Strombolian activity including the release of shockwaves.

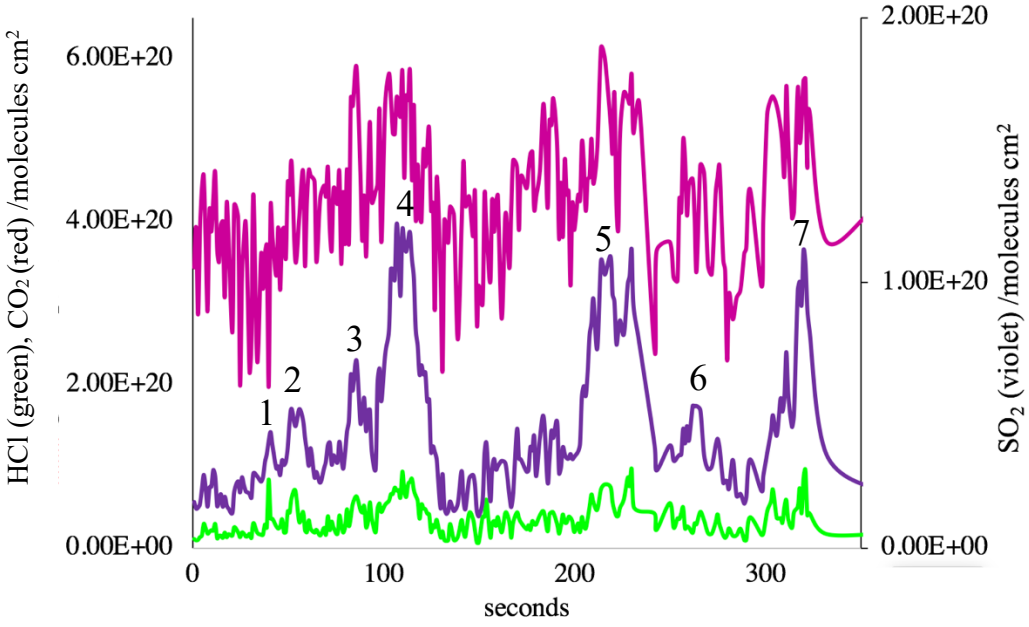

Figure 3 FTIR retrievals for HCl, CO_2 and SO_2 from the southern crater. The record identifies 7 strong explosions in 360 seconds. The explosions were identified by the rapid increase in signal and provides information about changes in gas ratios before and during explosions.

Tracing silicate weathering during the early Tonian using lithium isotopes

Ying Zhou, University College London, £1800

Introduction

The project is based on a high resolution study of several correlative Tonian-age carbonate sections on the North China Craton (NCC), which spans the interval 980 to 920Ma (Zhou et al. in review). The new seawater $^{87}Sr/^{86}Sr$ curve, combined with evidence for a Large Igneous Provence on the NCC at about the same time (Peng et al., 2011), suggest that deposition accompanied initial stages of the break-up of supercontinent Rodinia. The early Tonian has been less studied than both later and earlier times, generally only being mentioned in connection with its position towards the end of the 'boring billion' interval of muted carbon isotope fluctuations.

1 Typical Molar Tooth Structure in carbonate rocks of the Huaibei Group.

The carbonate samples were evaluated using petrological, geochemical and isotopic analysis, and a set of samples, which hold high potential for preserving an original seawater signal, were identified. Throughout the succession on the NCC, a type of early marine, low-Mg calcite cement (Molar Tooth Structure or MTS) is quite abundant. In many cases, MTS geochemistry, including $^{87}Sr/^{86}Sr$, could be compared with the surrounding 'bulk rock matrix', demonstrating in most cases that MTS retains primary C, O and Sr isotope values. Some bulk samples also hold high preservation potential. Therefore, these samples could represent a well preserved material archive for other geochemical tracers, too, such as Li isotopes, which trace silicate weathering processes (Pogge von Strandmann and Henderson, 2015). Because silicate weathering coupled with marine carbonate precipitation is the Earth's primary long-term mechanism for removal of atmospheric CO_2 (Berner, 2003), lithium isotopes show great potential for tracing Earth's long-term carbon cycle (Pogge von Strandmann and Henderson, 2015).

Because lithium isotopes show such promise as useful tracers of silicate weathering processes, the proxy might be able to help us to understand the weathering regimes of the early Tonian.

This project originally aims to answer two questions: 1. Can early marine cements (Molar Tooth Structure) retain the δ^7Li isotopic signature of ambient seawater and so help us to understand the potential of both bulk carbonate rock and carbonate rock components for reconstructing Proterozoic ocean composition; 2. Did weathering intensity or the material undergoing weathering contribute more to the rise in seawater $^{87}Sr/^{86}Sr$ during the early Tonian? This project will result in another two benefits: Firstly, it is the first attempt to measure lithium isotopes for the early Tonian with the best-preserved carbonate from this interval, and so the data will fill a gap in the long-term seawater δ^7Li record of the Precambrian; secondly, the comparison between different sequential leaching methods will help with subsequent Li isotope analysis of other vital geological and biological events, especially for the Precambrian.

Although Li isotopes of carbonate rocks (biogenic or inorganic) were used to trace seawater signals in past studies, it is essential to target the right Li fraction in sedimentary rocks. Because Li isotope fractionation - between the precipitated solid and solution - is greater for Ca-Mg carbonate minerals than for pure Ca carbonates (Taylor et al., 2019), unaltered marine calcite seems best suited to constrain the Li isotopic ratio of seawater but contamination from Li-rich silicate minerals could overprint a primary seawater signal. Moreover, different leaching methods are used in different labs for palaeo-carbonate δ^7Li analysis. Therefore during the analyses another question came to our minds: will sequential leaching techniques, similar to those developed for Sr isotope analysis (Bailey et al., 2000), be able to test which Li fraction will give us the marine Li isotopic composition? Therefore, before measuring the samples from the early Tonian, two pairs of carbonate samples (Tonian samples and modern samples) were to be tested using sequential leaching methods. Three different leaching reagents were used and each sample is going through 5 leaches. Till now one pair of samples (one modern and one ancient) have gone through the sequential leaching, whereby in total 30 leachates were measured for their δ^7Li and elemental composition. Although the carbonate fraction of the Tonian sample was targeted, the seawater δ^7Li value at that time is unknown, and so the modern sample was introduced here to help us to understand the difference between the leachates and marine values. Kosler et al. (2001) reported δ^7Li values for modern foraminifera, with *P. obliquiloculata* yielding 27 to 31‰. The modern seawater δ^7Li value is 31‰. Compared to the growth solution, $^7Li/^6Li$ is ≈ 3‰ lower in calcite in both inorganic calcium carbonate and biogenically produced calcite (foraminifera) (Marriott et al., 2004).

Preliminary results

Below are some of the initial results, which were presented at the 2019 Goldschmidt conference. The results show that sequential leaching attacks isotopically distinct Li sources and so bulk rock values are unlikely to reflect marine signals. 20% to 40% HCl and HAc leachates are mutually consistent and in agreement with expected marine δ^7Li values.

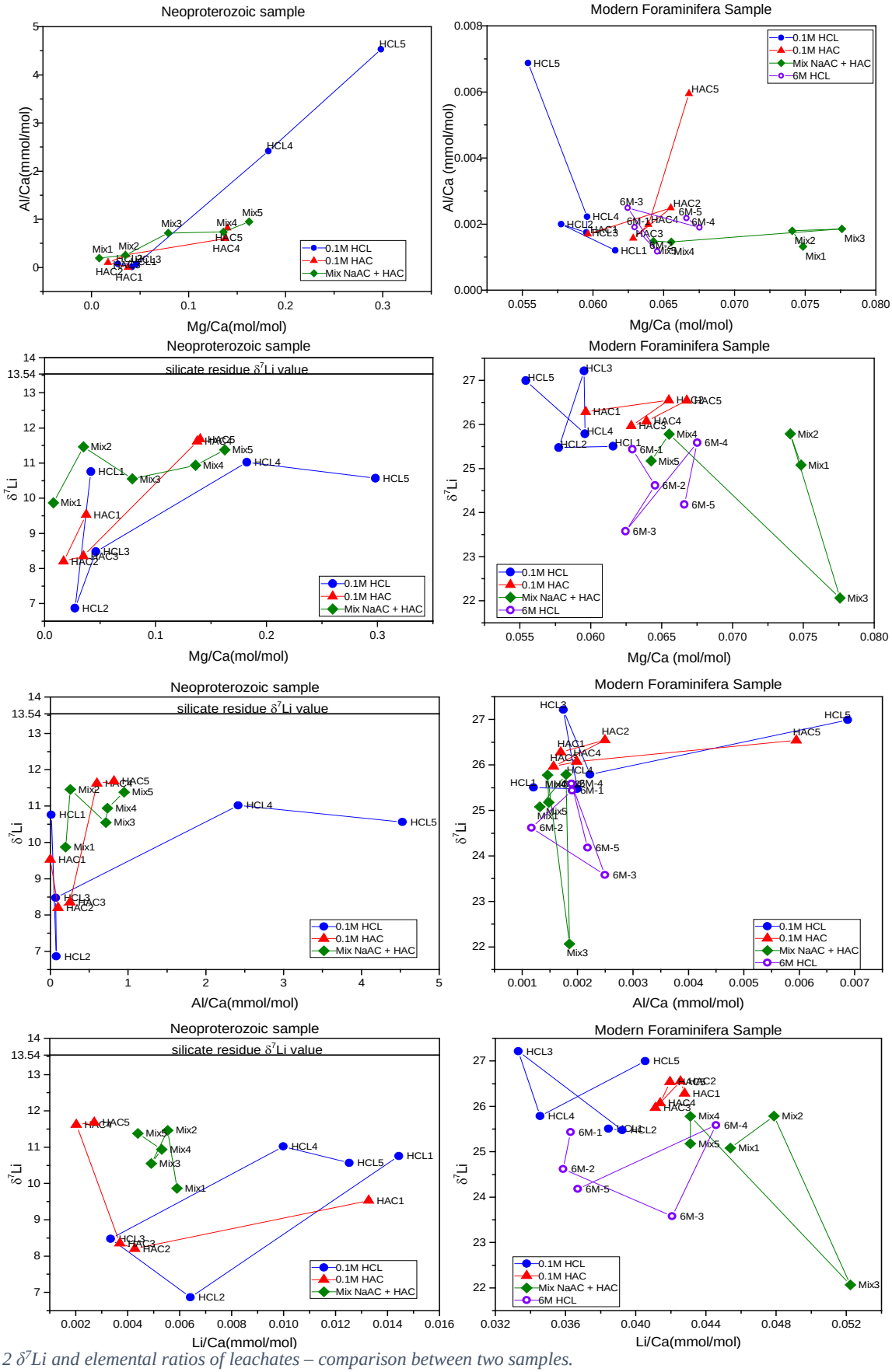

2 δ^7Li and elemental ratios of leachates – comparison between two samples.

Future plan

The next step is to measure the leachates of the second pair of the samples to see if sequential leaching could remove detrital and non-carbonate Li. When the leaching tests are finally finished, we will then be able to use the tested leaching method for targeted Tonian carbonate samples (Molar Tooth Structure and some bulk rocks).

Acknowledgement
This project has been greatly supported by Dr Philip Pogge von Strandmann and Dr Alex Brasier. I thank Dr Mel Murphy, Dr David Wilson and Prof Graham Shields for the great discussions for the leaching tests and I thank GSL to fund this project.

REFERENCE:

Bailey, T.R., McArthur, J.M., Prince, H., and Thirlwall, M.F., 2000, Dissolution methods for strontium isotope stratigraphy: Whole rock analysis: Chemical Geology, v. 167, p. 313–319, doi: 10.1016/S0009-2541(99)00235-1.

Berner, R. a, 2003, Fuels and Atmospheric Composition: Nature, v. 426, p. 323–326, doi: 10.1038/nature02131.

Kosler, J., Kucera, M., and Sylvester, P., 2001, Precise measurement of Li isotopes in planktonic foraminiferal tests by quadrupole ICPMS: , p. 169–179.

Marriott, C.S., Henderson, G.M., Crompton, R., Staubwasser, M., and Shaw, S., 2004, Effect of mineralogy , salinity , and temperature on Li / Ca and Li isotope composition of calcium carbonate: v. 212, p. 5–15, doi: 10.1016/j.chemgeo.2004.08.002.

Peng, P., Zhai, M.G., Li, Q., Wu, F., Hou, Q., Li, Z., Li, T., and Zhang, Y., 2011, Neoproterozoic (~900Ma) Sariwon sills in North Korea: Geochronology, geochemistry and implications for the evolution of the south-eastern margin of the North China Craton: Gondwana Research, v. 20, p. 243–254, doi: 10.1016/j.gr.2010.12.011.

Pogge von Strandmann, P.A.E., and Henderson, G.M., 2015, The Li isotope response to mountain uplift: Geology, v. 43, p. 67–70, doi: 10.1130/G36162.1.

Taylor, H.L., Duivestein, I.J.K., Farkas, J., Dietzel, M., and Dosseto, A., 2019, Technical note : Lithium isotopes in dolostone as a palaeo-environmental proxy – an experimental approach: , p. 635–646.

Zhou, Y., Pogge von Strandmann, P.A.E., Zhu, M., Ling, H., Manning, C., Li, D., He, T., and Shields, G. A. in Review. Reconstructing Tonian sweater $^{87}Sr/^{86}Sr$ using calcite microspar. Geology.